From Gridlocks to Greenways: Analyzing the Network Effects of Computationally Generated Low Traffic Neighborhoods

Von Straßenblockaden zu Grünflächen:
Analyse der Netzwerkeffekte von computergenerierten verkehrsberuhigten Stadtvierteln

Fra trafikkøer til grønne veje:
Analyse af netværkseffekterne af computergenererede lavtrafik-kvarterer

Carlson M. Büth

WWU MÜNSTER

IT UNIVERSITY OF COPENHAGEN

Copenhagen, 2023

WWU MÜNSTER

IT UNIVERSITY OF COPENHAGEN

Master's thesis

From Gridlocks to Greenways: Analyzing the Network Effects of Computationally Generated Low Traffic Neighborhoods

Von Straßenblockaden zu Grünflächen:
Analyse der Netzwerkeffekte von computergenerierten verkehrsberuhigten Stadtvierteln

Carlson M. Büth

Working group Wittkowski
In collaboration with NEtwoRks, Data, and Society (NERDS)

First examiner and co-supervisor:	Jun.-Prof. Dr. Raphael Wittkowski
Second examiner and co-supervisor:	Assoc. Prof. Dr. Michael Szell
Co-supervisor:	Anastassia Vybornova, M. Sc. (PhD fellow)

Institute of Theoretical Physics
University of Münster, Germany
and
IT University of Copenhagen, Denmark

Copenhagen, July 10, 2023

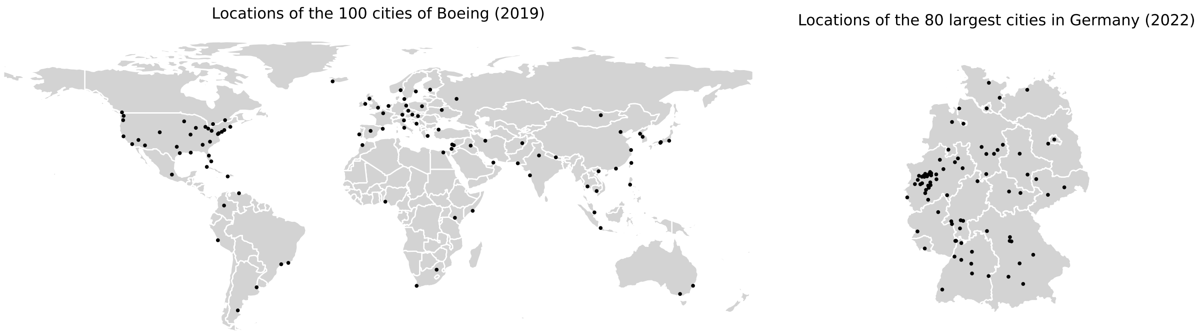

Figure 0.1: Map showing the locations of cities studied in this thesis. A global set of 100 cities and all German cities with more than 100,000 inhabitants.

Abstract

This thesis investigates the impact of the spatial order of cities on the performance of presented, data-driven partitioning approaches. The study addresses two research questions: 1. How does the travel time change if all neighborhoods were Low Traffic Neighborhoods (LTNs)? 2. What LTN configuration can we suggest for different types of cities? We present a framework to analyze the impact of LTNs on travel time that utilizes Open Street Map (OSM) street data, and GHSL population data to calculate network measures, such as directness, global efficiency, average circuity, street orientation order. Central components of this work are the LTN generation, evaluation, and visualization. The evaluation of 100 global cities and 80 cities in Germany reveals that both a residential-based approach and a betweenness-based approach yield positive results, with minimal travel time increases. This research contributes to the understanding of the impact of LTNs on travel time and provides a framework for the simplified generation and evaluation of LTNs.

Contents

Acronyms

LTN Low Traffic Neighborhood

GHG greenhouse gas

OSM Open Street Map

EC European Commission

JRC Joint Research Centre

GHSL Global Human Settlement Layer

GHS-POP R2023A GHS population spatial raster dataset multitemporal (1975-2030)

MAPE mean absolute percentage error

ODR orthogonal distance regression

CI confidence interval

AO Asia and Oceania

EU Europe

LatAm Latin America

MEA Middle East and Africa

NAM North America

Where light traffic
knits a community together,
heavy traffic rips it apart.

— Bruce Appleyard [Sim21]

1. Introduction

Urban planning is a diverse field with continuously evolving guidelines and practices. And they necessarily change, simply because history and the society in which they emerge are reshaping. Additionally, to the general increase in population, the last decades faced us with continuous urbanization; the fraction of people living in rural areas shrinking [RR18]. As urbanization increases, so do greenhouse gas (GHG) emissions [Sat09], with an impressive half of the city's GHG emissions being transport related [Kra+16], placing this issue in the context of the current climate crisis [Rip+20; Rip+22]. Other than that, further interwoven effects connected to urbanization are already intensifying. To name one, the urban heat island effect increasing the risk of heat-related mortality. These mutually related topics need to be dealt with in union if we don't want to risk underestimating their outcome [Cha+17; KVK23; Par+23; Sat08; Xin+22].

Traffic-calming is one way to improve the situation [ZF23]. This way GHGs are reduced by having less speeding cars, less traffic or, at best, fewer cars, optimally in conjunction with public transport expansion and improvement [Ali+21; KR09]. But not all traffic-calming measures are created equal. The road type also plays a role in GHG impact with several factors, one being the material production emissions [Sab+23]. And just to mention it once: this set of issues is furthermore closely linked to and has resonant implications for issues of equity, accessibility, and societal integration [DB23; Mon14; BB21; BB18].

Concepts of changing the land use policy come under various names: Some of the most prominent representatives are Low Traffic Neighborhoods (LTNs), traffic islands, and superblocks. Planning of LTNs is a long an tedious process which encompasses several factors [Nie+19]. Additionally, to the logistics of LTN implementation, governments first need to involve local stakeholders that are directly affected. Urban planning requires knowing traffic patterns and analyzing travel behavior while respecting local neighborhood knowledge. After going over the regulatory considerations and implementing the changes, LTNs are monitored to evaluate their effect [Tra20; Sus]. In the course of this process, decisions can have a political drift despite favorable feasibility studies [Grä23; Sta21].

With this thesis we want to answer two central research questions:

1. How does the travel time change if all neighborhoods were LTNs?
2. What LTN configuration can we suggest for different types of cities?

Our goal is to find a way to create LTNs in a data-driven way, while keeping factors in mind that are important for the success of LTNs. We will measure success with measures from network science, and monitor distribution of LTN generation, e.g. LTN area, population, population density, and demand change by betweenness centrality. To get a grip on this complex topic, there are many factors that need to be simplified or abstracted. This is why for the transportation graph we focus on the drivable street network, as experienced by the private car mode, and assume an all-to-all travel demand. Scoping the problem this way, we can profit from Open Street Map (OSM) data, which is globally available and has enabled a wide variety of research. We will also assume that generated LTN structure is implemented in a way that selected areas are not permeable for private motorized traffic, so the detailed implementations of traffic-calming measures is not to our concern.

Key contributions of our work lie in implementing a framework for LTN generation, the evaluation of the generated LTNs with network science measures, and visualization of the generated partitions. Additionally, we provide a plug-and-play solution, encompassing transport network download, preprocessing, including population approximation on a street level, and population density calculation.

There has been a growing interest in the superblock model in recent years. Mueller et al. estimated the health implications of implementing superblocks in all of Barcelona. They estimated that when implementing 503 superblocks across Barcelona, 667 premature deaths (95 % confidence interval (CI): 235 to 1098) could be prevented annually. They include various factors in their analysis, namely NO_2 reduction, noise reduction, heat reduction, and green space development, and conclude that the superblock model should be implemented consistently across the entire city to achieve an equitable distribution of health benefits [Mue+20]. Eggimann computationally implement the definitions of the Barcelona Superblock model to find areas in cities that satisfy the criteria in Switzerland [Egg22a] and globally [Egg22b]. Only 3 % to 18 % of the current street network in the nine largest Swiss cities were simulated to be potentially suitable for superblock implementation. But this only concerns superblocks by narrow definition to increase green space, notwithstanding other low-traffic formats. A different field of research deals with the analysis of already implemented superblocks. A method of measuring superblocks by their hierarchy matrix of geometry configuration, network, and area is proposed by Song and Pang. They validate their method on the case study of Nanjing, China, and conclude that the hierarchy matrix is potentially a useful method for studying the complex emerging built form of rapidly changing cities, especially in developing countries, such as China [SP23]. Ge and Han do a similar sustainability-oriented configurational analysis of the same case study [GH20]. Studies focusing on very specific aspects of superblocks also exist. Urban ventilation patterns of superblocks are analyzed using numerical methods by Maing. They conclude that the internal architecture is not just affecting the ventilation of the block itself, but also the surrounding ventilation and the wind reaching further into the block, and is a relevant factor in terms of health and comfort [Mai22]. Superblock identification as done by Eggimann [Egg22b] is the closest to come to our proposed goal, but to our knowledge, there has not been an automatized approach to generate LTNs by our problem definition.

Diverse books focus on urban planning, quality of life, sustainability, equity, and health. To name a few, Bruce Appleyard discusses the topic of urban livability and street design [App21], carrying on the legacy of his father Donald Appleyard, also doctor of urban planning [AGL81]. In [Gra23], Grabar explains the state of car-centered mobility and related topics on the example of car parking in the US. Speck points out flaws of Americas urban planning and proposes solutions [Spe13], which he compiled into a list of 101 rules in his book *Walkable City Rules* [Spe18].

The rest of this thesis is structured as follows. Section 2 introduces the necessary background knowledge, including explanation of further LTN concepts, the street graph representation, partitioning requirements, and introduction to important graph metrics in Section 2.3. The methodology is explained in Section 3, with the data sources and main ideas of the road network sparsification algorithms. The developed Python package is outlined in Section 3.3, Section 3.3.1 shows an usage example of the package, and some implementation details are discussed in Section 3.3.2. Section 3.4 explains the experimental configuration, which is then used to obtain the results evaluated in Section 4. Finally, Section 5 concludes the thesis, answering the research questions and sets the work into context.

2. Preliminaries

To understand LTN and how to automatize their generation, we first give an overview of several LTN concepts and recent scientific findings of the impact. Specifically, we present the Barcelona Superblock concept and the idea of traffic islands on the example of Copenhagen. In Section 2.2 the graph representation of a transportation network is introduced, and the formal partition requirements are defined. The several network metrics relevant to answer the research questions are presented in Section 2.3.

2.1. Low Traffic Neighborhoods (LTNs), the Barcelona Superblock Model and Traffic Islands

Influences on traffic-calmed neighborhoods have come from around the globe. For example, the concept of "garden-settlements" (*poselki-sady*) has been developed in the late 19th century in the Soviet Union, inspired by the English Garden City movement [How98], and in the mid 20th century, the idea of "microregions" (*mikroraiony*) followed as a response to the housing crisis [Cra22]. Historically, grid structures similar have also been prevalent in several Asian cities [Che22].

To explain the various terms used in the literature, we will briefly introduce the most common ones. Low Traffic Neighborhood (LTN) is the most general term, symbolizing a concept where neighborhoods are treated with various traffic-calming measures. Traffic islands embrace the idea to specifically introduce zoning with mode filters, disconnecting these traffic islands for private motorized mobility, while knitting the city closer together for bicycles, public transport, and micromobility. This reduces short car trips inside the city, while keeping the regional connection for motorists [Mar21]. Superblocks are a certain format of LTN where plots—parcels with buildings—are grouped to form superblocks with inner streets transformed to pedestrian boulevard, providing urban greenery, and thus reducing motorized transport. The outer streets are kept as the basic road network. The common ground of these is the goal of reducing or eliminating through traffic. In this way, social cohesion can be fostered, while keeping in mind the ecosystem in which we inevitably live [Rue19]. A specific format of superblocks is the Barcelona Superblock model, shown in Fig. 2.1. It builds on the historical grid structure of the city—grouping plots to form superblocks—and draws from the former *Plan Cerdà* (see Fig. 2.2). Each block is $113.3\,\mathrm{m} \times 113.3\,\mathrm{m}$ in size, with some exceptions. The usual group of blocks is 3×3 blocks. Defining the Barcelona Superblock, a superblock usually is between $300\,\mathrm{m} \times 300\,\mathrm{m}$ and $400\,\mathrm{m} \times 400\,\mathrm{m}$ in size. Formerly, the inside of the blocks was used for greenery, some blocks with open sides, but as urbanization progressed, the blocks gradually densified. The superblock model aims to reverse this trend by pedestrianizing the inner streets, and transforming the space to contain more greenery [Rue19]. Several superblocks in Barcelona have been implemented and thoroughly studied, with growing numbers of transformed districts[1].

[1]See an interactive map of the recent accompanying measures at `https://www.barcelona.cat/pla-superilla-barcelona/mapa/en/`.

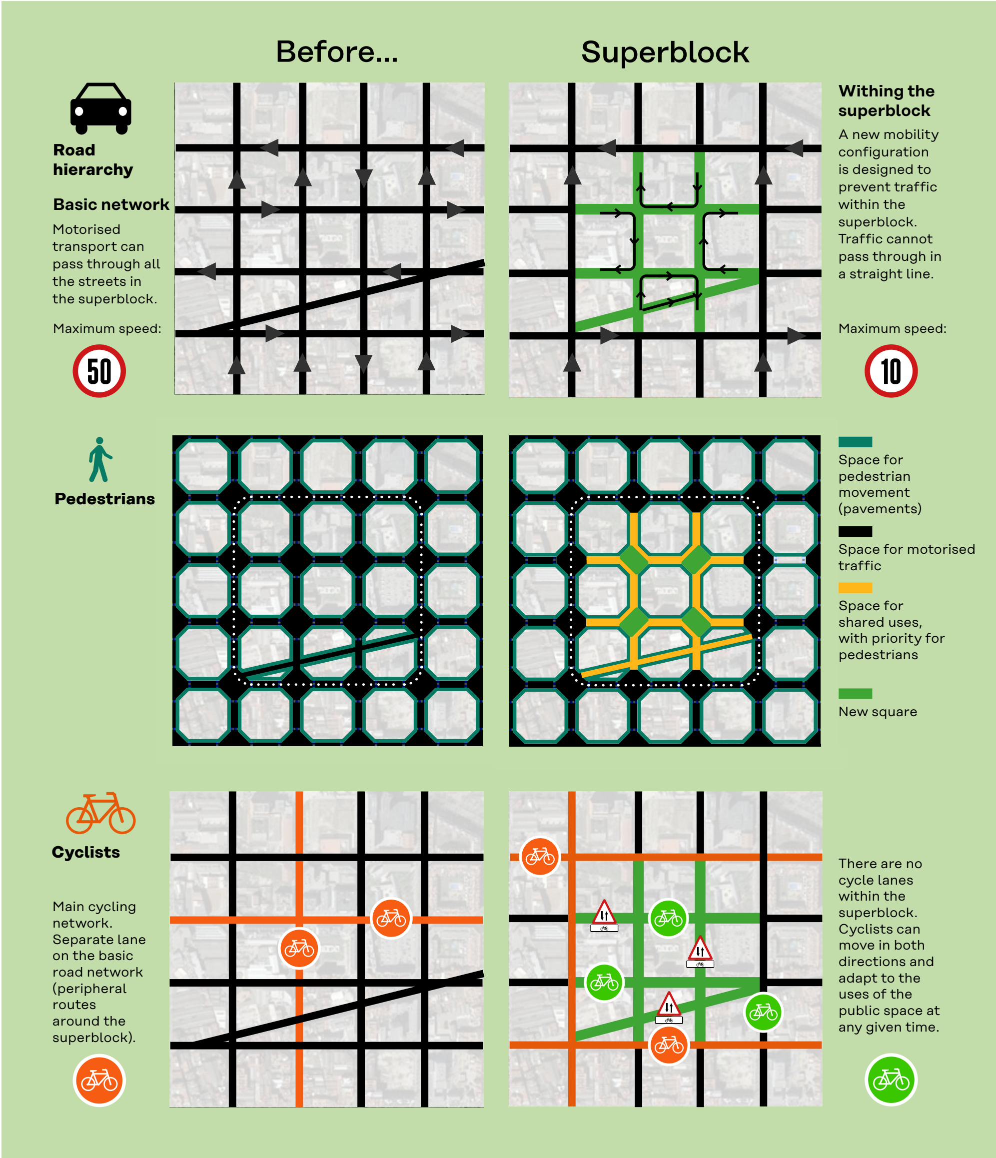

Figure 2.1: Three aspects of the Barcelona Superblock model [ABÀ21]. Using the existing chessboard structure of the city, the superblocks are formed by grouping plots. Inner streets are pedestrianized, while keeping access for residents and deliveries. The space is transformed to contain more greenery, social spaces, and streets on the border elevated to pedestrian level, removing the distinction between sidewalk and street. The cycling network is moved to peripheral routes outside the block, inside it is inherently safe for cycling.

Figure 2.2: The approved *Plànol del projecte Cerdà* for Barcelona from the year 1859. Building footprints are shown in red and green space was reserved as public, green space. [Cer59]

Motivation changing our urban environment, implementing LTNs and superblocks, is manifold. At the same time, it is important to monitor the effects of these interventions, to verify impacts, and mitigate negative side effects. Goodman and Aldred found that LTN introduction resulted in a $(10 \pm 3)\,\%$ reduction of street crime with a $95\,\%$ confidence interval (except bike theft, due to increased number of bicycles), and no evidence of displacement of crime [GA21]. It was also found that there is no evidence for effect on fire service emergency response times [Goo+21]. But there is also an effect on motor-vehicle ownership, which was found to be reduced for residents in LTNs [AG20; GUA20]. The opposite of induced traffic, traffic evaporation, has been found in Barcelona as a result of traffic-calming interventions. In numbers, a reduction of $14.8\,\%$ traffic compared to streets in the remaining city [Rue19]. At times, fears of traffic congestion related to reduced motor vehicle road space are raised, but Nello-Deakin found these to be unfounded [Nel22]. The positive health effects found are not only caused by reduced air pollution, noise reduction, heat reduction, and increased greenery [Mue+20; ABÀ21], but also by safer walking, cycling, and driving. Laverty, Aldred, and Goodman find that data suggests a reduced risk of injury across all travel modes inside LTNs without negative impacts on the boundaries [LAG21]. LTNs show to have the potential to improve equity across citizens, but for this to unleash its full potential LTNs need to be deployed distributed on the whole demography, Aldred et al. stress [Ald+21].

A scaled-up and modified version of the superblock model are traffic islands. The analogue used is isolation of islands that are connected by few or singular connections to the mainland. Traffic islands

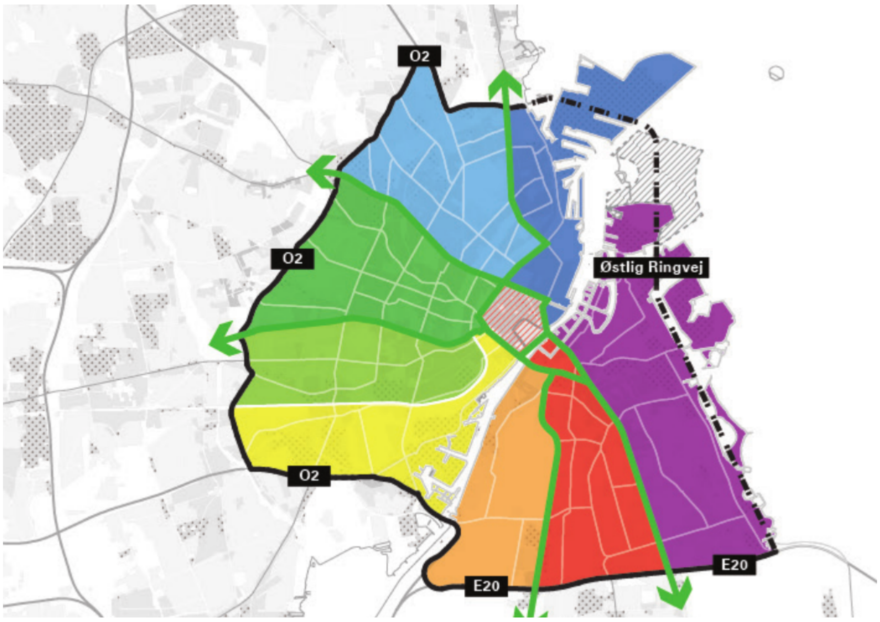

Figure 2.3: Map of Copenhagen with colored traffic islands. The proposed area of intervention is encapsulated by a ring road and a harbor tunnel (planned opening 2035) shown in black. The green paths symbolize *super boulevards* which are dedicated active mobility links, not permissive to the private automobile. The historical center (hatched in red) is proposed to be totally car-free. [Mar21, Figure 8.8]

are areas that connect to the greater traffic network, but have boundaries that are not permeable to the private automobile. Martin propose a plan where the isolation between traffic islands is achieved by a complementary active mobility network, interlocking with the traffic islands. In Fig. 2.3 the proposed traffic islands are shown in color. A clear difference to the superblock model is that the traffic islands are not pedestrianized, possibly partially, but as the direct travel between islands is prohibited for the private automobile, active mobility is motivated. This plan is expected to reduce traffic congestion in the city and excessive car use. If one wants to travel between traffic islands by car, one has to use the ring road or the harbor tunnel. Still, for emergency services and public transport, the boundaries are permeable [Mar21]. Recently, *Enhedslisten*, currently Copenhagen's largest party, has advocated for the traffic island plan by Martin [Hor23; Køb23]. For our use case, we will work with the LTN idea between the described models, not deciding on a specific LTN size, and will not deal with the implementation of traffic interventions, as it would exceed the scope of this thesis. An algorithmic approach only needs to return a set of LTNs containing streets considered to be inside of such an area, and a *sparsified* network of streets that stays open for inter-LTN traffic.

2.2. Transport Network Graph Representation

There are several ways to represent transportation networks, mappings from the real world to another representation, e.g., a visual representation as a hiking map or a graph representation as a network. From application to application, useful representations can differ. We will use a directed multigraph

$G = (V, E, l)$ with edges $e \in E$ and vertices $v \in V$. The edges e are weighted with length l, but can have more attributes, like a type, street geometry, or a name. Also, the vertices v can have attributes, e.g., geographical latitude and longitude. Edges represent streets, and vertices represent intersections, junctions, or dead ends. Streets are specifically not the semantic entity of a road, but a part of a road between exactly two intersections. Another way of dealing with a road network is grouping edges to ways, inspired by the semantics of named roads [ERL22], or a dual construction is defining road sections drivable without turns as nodes and streets connected by a turn as edges [Lag15]. For the street graph, G we require a few more properties:

- Directed: The edges have a direction, e.g., from intersection a to intersection b. In the case of two-way streets are represented by two edges, one from a to b and one from b to a.
- Strongly connected: There is a path from every vertex to every other vertex. In a street graph, this means that every intersection is reachable from every other intersection.
- Loops: An edge can start and end at the same vertex.

As the transportation network can have bridges and tunnels, the graph is not necessarily planar. The Python package `osmnx` [Boe17] implements such functionality to standardizedly retrieve OSM data and simplify the network into a graph representation of the transportation network that satisfies the above requirements after some filtering. It is based on the `networkx` [HSS08] package, which implements graph algorithms and data structures.

Partition Requirements The street graph G will be split into partitions, one for each LTN and one for the sparse network. This can be described by a partitioning $\mathcal{P} : G \mapsto \left(G_{\mathrm{sp}} \cup G_1 \cup \ldots \cup G_k\right)$ returning subgraphs $G_i \subseteq G$, one sparse G_{sp}, and k LTNs G_i. Such a partitioning function $\mathcal{P}$ must satisfy a union property

$$\bigcup_{i=1}^{k} G_i \cup G_{\mathrm{sp}} = G \tag{2.1}$$

and an edge-wise disjoint property

$$\forall i, j \in \{\mathrm{sp}, 1, \ldots, k\} : i \neq j \Rightarrow E_i \cap E_j = \emptyset, \tag{2.2}$$

where E_i is the set of edges of G_i. The union property (2.1) states that the partitioning function $\mathcal{P}$ must return a partitioning of the whole graph G, in other words, no street should be left out. The disjoint property (2.2) states that the partitions must be edge-wise disjoint, i.e., no street should be part of more than one partition. This also means that from the set of edges E_i we can exactly reconstruct the set of vertices V_i. Our goal is to compare performance of automatized $\mathcal{P}$, before any restrictions are applied, to restricting paths to only use edges of the start and, end and sparse network. Such for all paths $p = (e_s, \ldots, e_t)$, where $e_s \in E_{\mathrm{s}}$ and $e_t \in E_{\mathrm{t}}$, the path is a subset

$$p \subseteq E_{\mathrm{s}} \cup E_{\mathrm{sp}} \cup E_{\mathrm{t}}, \tag{2.3}$$

including paths starting or ending in the sparse network. To satisfy connectivity for $\mathcal{P}$, a sufficient condition is that the sparse network is strongly connected and that the LTNs are connected to the sparse network. From anywhere in a neighborhood, it must be possible to reach anywhere else in a city, without passing a foreign LTN. However, it is possible that with a start and end inside the same LTN one must, by car, use the sparse network.

2.3. Network Metrics

To measure the differences in the street networks before and after the introduction of the LTNs, there are a variety of network metrics available. Most central is that when introducing the path restriction of Eq. (2.3) for all shortest paths between two nodes i and j, the shortest path distance on the full network $d_S(i,j)$ changes to $d_N(i,j)$, expected to increase. The following paragraphs introduce relevant metrics and their background.

2.3.1. Global Efficiency

Introduced to the complex network context by Latora and Marchiori in 2001, efficiency measures the average inverse shortest path length in a network. A system considered efficient is one that is well-connected, considering the edge weights. Two types of efficiency are distinguished: local and global. Global efficiency is defined on a connected network

$$E(G) = \frac{\sum_{i\neq j\in G}\epsilon_{ij}}{N(N-1)} = \frac{1}{N(N-1)}\sum_{i\neq j\in G}\frac{1}{d(i,j)}, \tag{2.4}$$

where N is the number of nodes in the network, d_{ij} is the shortest path length between nodes i and j, and ϵ_{ij} is the efficiency between nodes i and j, defined as the inverse distance $\epsilon_{ij} = 1/d(i,j)$. Local efficiency is the "average efficiency of the local subgraphs" [LM01]. Usually this measure is normalized over a fully connected network of the same size, as seen in Fig. 2.4. In our case, we define it as a relative measure between two metrics

$$E_{\mathrm{glob},N/S} = \frac{\sum_{i\neq j}\frac{1}{d_N(i,j)}}{\sum_{i\neq j}\frac{1}{d_S(i,j)}} \tag{2.5}$$

where the normalization takes care of itself, as the number of nodes is the same in both networks. In the case of only increasing distances, $d_N(i,j) \geq d_S(i,j)$, the efficiency is always $0 < E_{\mathrm{glob},N/S} \leq 1$.

2.3.2. Directness

In contrast to efficiency, directness, also called straightness centrality, compares the variation of distances before the summation [CLP06]. Usually in geospatial studies, the link lengths are compared to the Euclidean distance. Instead of the Euclidean distance, we use the shortest path length on the

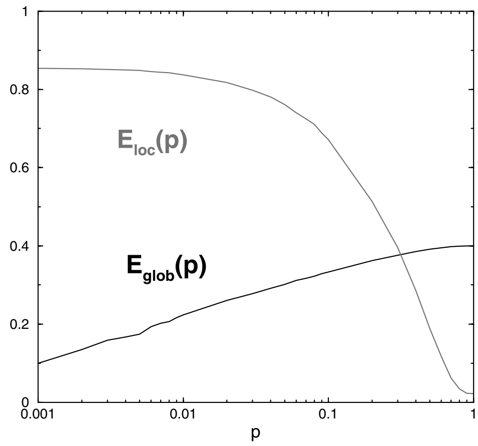

Figure 2.4: In an unweighted small world network, increasing the link probability p, global efficiency increases, while local efficiency decreases. The small world graph is constructed as a regular lattice with $N = 1000$ nodes and node degree $k = 20$, where each edge is rewired with probability p. [LM01, Figure 1]

full network $d_S(i, j)$ as the reference. One can call it the expectation value of the distance change. We use a definition as given in [Sze+22]:

$$D_{S/N} = \langle Q(i, j)\rangle = \left\langle \frac{d_S(i, j)}{d_N(i, j)} \right\rangle_{i\neq j} \tag{2.6}$$

$Q(i, j) = d_S(i, j)/d_N(i, j)$ is called route factor, detour index, stretch, or directness for the node pair (i, j) [Bar11; Bar22]. Vragović, Louis, and Díaz-Guilera proposed this modification of efficiency in the context of informational transfer in complex networks in 2005 [VLD05]. In 2006 Crucitti, Latora, and Porta used it in the context of urban street networks [CLP06].

2.3.3. Low Traffic Neighborhood (LTN) Coverage

As LTN Coverage we define the fraction of street length that is part of LTNs.

$$C_{\text{LTN}} = \frac{L_{\text{LTN}}}{L_{\text{total}}} = \frac{\sum_{e\in E_{\text{LTN}}} l_e}{\sum_{e\in E} l_e} \tag{2.7}$$

Here l_e is the length of edge e. As our motivation is transforming whole cities into traffic-calmed areas, a high LTN Coverage is desirable. At the same time, it needs to be below 100 % for there to be space for the sparsified streets.

2.3.4. Betweenness Centrality

Betweenness centrality is a prominent measure of centrality which tries to measure the importance of a node or edge in a network by counting the number of shortest paths that lead through it. With the geodesics $\sigma(s, t)$ being the number of shortest paths between nodes s and t, and $\sigma(s, t \mid v)$ being

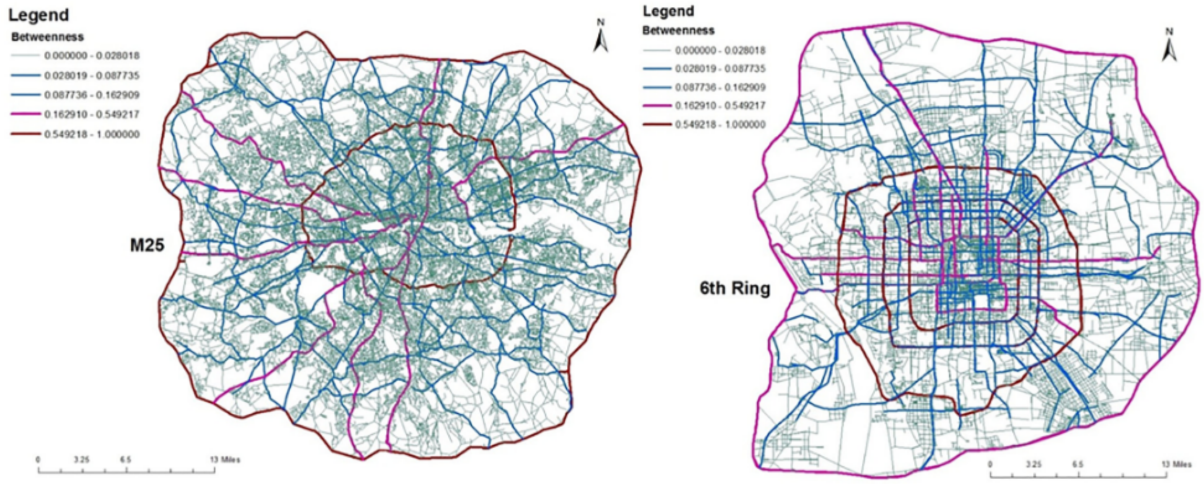

Figure 2.5: Betweenness centrality on street networks, calculated from the dual space. London (left) and Bejing (right) clearly show higher centrality of orbital and long roads, unlikely residential [Kir+18, Figure 3].

the number of those paths that go through node v,

$$C_{\mathrm{B}}(v) = \sum_{s,t \in V} \frac{\sigma(s,t \mid v)}{\sigma(s,t)} \tag{2.8}$$

defines the betweenness centrality of node v. By convention $\sigma(s,s) = 1$ and if $v \in \{s,t\}$, $\sigma(s,t \mid v) = 0$. Edge betweenness centrality is defined analogously

$$C_{\mathrm{B}}(e) = \sum_{s,t \in V} \frac{\sigma(s,t \mid e)}{\sigma(s,t)} \tag{2.9}$$

where the node v is replaced by the edge e. There are two rescaled variants of betweenness centrality. Length-scaled betweenness introduces the prefactor $1/d(s,t)$ in the summands of Eqs. (2.8) and (2.9), linearly-scaled betweeness the prefactor $d(s,v)/d(s,t)$. The rationale of length-scaled betweenness is dampening the effect of long paths, while linearly-scaled betweenness tries to account for the fact that long paths are more likely to go through nodes that are in the middle of the path. The nearer a node v to the target t, the more influential it becomes [Bra08].

C_B has been shown to be able to capture the hierarchical structure of street networks, especially on the dual-graph representation, see Fig. 2.5 [Wan15]. We are especially interested in edges with low betweenness centrality, as they make a good candidate to be residential streets and thus considered to be inside LTNs.

2.3.5. Spatial Clustering and Anisotropy of High C_B Nodes

The distribution of the previously introduced betweenness centrality C_B can hint the structure of relevant streets. Fig. 2.6 shows the distribution of C_B for three metropolitan areas. This is a relevant

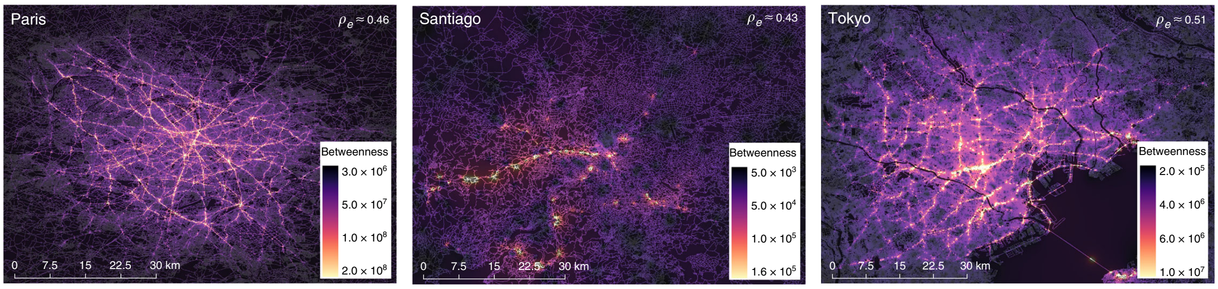

(a) Paris (b) Santiago (c) Tokyo

Figure 2.6: Distribution of C_B for nodes in Paris, Santiago and Tokyo [Wan15, Figure 3].

measure for the resilience of a transport network. The distributed character of Paris, as seen in Fig. 2.6a, enables it to withstand the loss of relevant nodes, and keeping the traffic in the city center low. Fig. 2.6b in contrast, shows a more centralized structure, due to its rather sparse network. Tokyo exhibits a lattice-like structure with roads of high betweenness centrality. High betweenness centrality nodes are defined through a percentile threshold $\theta \in [0, 1]$. The shape of the high C_B node distribution is measured in terms of clustering and anisotropy as follows:

$$C_\theta = \frac{1}{N_\theta \langle X \rangle} \sum_{i=1}^{N_\theta} \left\| x_i - x_{\mathrm{cm},\theta} \right\| \tag{2.10}$$

N and the average distance to the high C_B node center of mass $\langle X \rangle_{\mathrm{cm},\theta}$ normalize this measure for comparison between networks of different sizes. $\| \dots \|$ denotes the Euclidean norm. A maximally distributed, or unclustered network has $C_\theta = 1$. In case, the network collapses to a single node $C_\theta = 0$. For Anisotropy, the ratio of the two high C_B node eigenvalues λ_1 and λ_2 are used:

$$A_\theta = \frac{\lambda_1}{\lambda_2}, \quad \lambda_1 \geq \lambda_2 \tag{2.11}$$

A perfectly isotropic network has $A_\theta = 1$, like any point symmetric shape or other uniform distribution. The more anisotropic the network, the higher A_θ, diverging to infinity for a line. Both C_θ and A_θ realize values between the given extremes for real-world networks [Kir+18].

2.3.6. Street Orientation-Order

The order of a street network can be measured using the distribution street segment directionality. Based on Shannon entropy, the orientation-order ϕ is defined as

$$\phi = 1 - \left(\frac{H_o - H_g}{H_{\max} - H_g} \right)^2, \tag{2.12}$$

where H_o is the observed entropy, H_g is the entropy of a grid network and $H_{\max}$ is the maximum entropy of a network, assumed to be a two-dimensional grid. Numerically, the entropy values are dependent on the number of bins k used to discretize the distribution. For 36 bins, the maximum

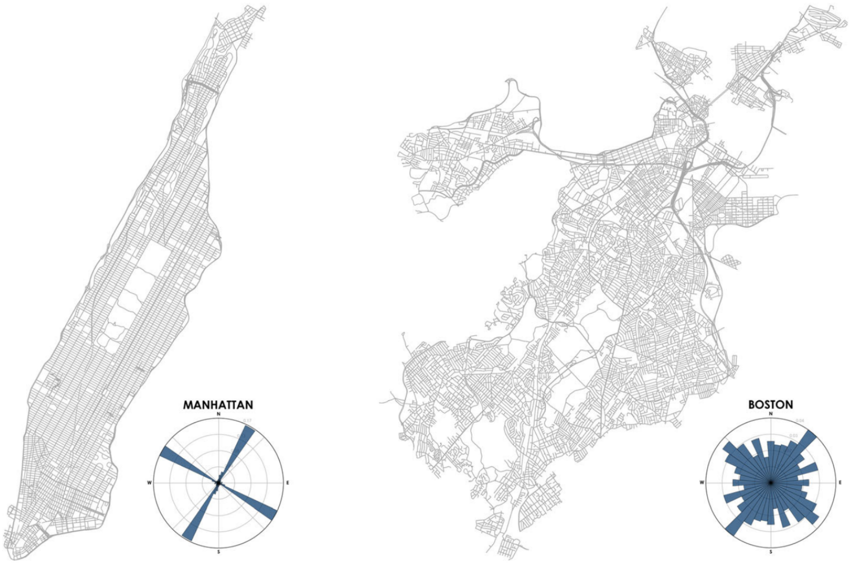

Figure 2.7: Two examples for the polar distributions of street patterns. Manhattan, NY, USA (left) has a higher street orientation-order ϕ than Boston, MA, USA (right). Manhattan's street network is almost exclusively distributed in four cardinal directions, i.e. two-dimensional, except for isolated symmetry breaks. Boston, on the other hand, represents one of the least grid-like cities in the USA. [Boe19b, Figure 3]

entropy is $H_{\max} = -\log(36^{-1}) \approx 3.5835$ nats and the entropy of a grid network where the directions fall into four bins—one for each cardinal direction—is $H_g = -\log(4^{-1}) \approx 1.3863$ nats. The orientation-order ϕ is thus monotonic in H_o and bounded between 0 and 1. Fig. 2.7 shows two examples for the polar distributions of street patterns [Boe19b].

2.3.7. Average Circuity

The average circuity ς is the ratio of the network's total edge length L_{net} and the Euclidean distance (how the crow flies) between all node pairs L_{gc}. It relates to directness (Eq. (2.6)), in the sense that the distances between two distance measures are compared. But in this case, we compare edge lengths to straight-line distances and the summation is done before the division.

$$\varsigma = \frac{L_{\text{net}}}{L_{\text{gc}}} = \frac{\sum_{i=1}^{E} l_i}{\sum_{e=\{i,j\}\in E} \|x_i - x_j\|} \tag{2.13}$$

A network with intersections connected by perfectly straight streets has $\varsigma = 1$. The more the network edges deviate from straight lines, the higher ς. For a place with many serpentine roads, ς is higher than for a place with straight roads [Boe19a].

Figure 2.8: Morphological classification (left) and seven identified block types (right) by Song and Pang for Nanjing, China. The four dimensions are (a) configuration of network (Con N), (b) configuration of area (Con A), (c) geometry of network (Geo N), and (d) geometry of area (Geo A) [SP23, Figure 3].

2.3.8. Hierarchy Matrix

Song and Pang propose a hierarchy matrix to classify types of superblocks, and identify seven superblock types for the case study of Nanjing, China. It consists of four dimensions: configuration of network, configuration of area, network connectivity and area connectivity. Configuration of network uses the network depth as a proxy of connectivity (Fig. 2.8 (a)). They define the depth of a street as the number of steps of adjacency to the main road. With increasing depth of a street, its connectivity decreases. Analogously, this means the deeper one is in a neighborhood, the more difficult it is to reach the main road. Such main roads are being used as a basic date (baseline) to determine the depth of the other streets. The configuration of the area is based on the (Con N) level value of the street where the main access is located. This way the level of embeddedness is defined, see Figure Fig. 2.8 (b). Song, Zhang, and Han study the access structure of plots and streets earlier in detail [SZH21]. The geometry of the network is based on the width and length of the streets (Fig. 2.8 (c)). Street length and width are used to describe importance of a street. “The greater the width and length of a street, the higher its Geo N level, and vice versa.” Finally, building footprints and residual space are used to determine the geometry of the area (Fig. 2.8 (d)). Urban density is measured using the floor space index (FSI) and ground space index (GSI). Both are compiled into one index using a cluster analysis determining the level of the plot. A higher level indicated a denser area [SP23].

Figure 2.9: Orthogonality indicator ort. (w_{ref}) for Paris, France. In this case the operator is applied to the lanes of the road network, not just the roads [Lag15, Figure 3.15].

2.3.9. Orthogonality

Orthogonality is a measure of the connection angle of a street to its direct neighborhood [Lag15]. It measures the orthogonal fraction of the connecting streets by summation of the sine values of the connection's angles between the reference way and the arcs it intersects.

$$\text{ort.}\left(w_{\text{ref}}\right) = \frac{\sum_{n \in w_{\text{ref}}} \sum_{a_i \cap n \wedge a_j \notin w_{\text{ref}}} \min\left(\sin\left(\theta_{a_i} a_j\right)\right) / \left(a_j \cap n \wedge \in a_j \in w_{\text{ref}}\right)}{\text{con.}\left(w_{\text{ref}}\right)} \tag{2.14}$$

$$\text{con.}\left(w_{\text{ref}}\right) = \sum_{n \in w_{\text{ref}}} \text{Card}\left(a \mid \left[(n \in a) \wedge \left(a \notin w_{\text{ref}}\right)\right]\right) \tag{2.15}$$

In this nomenclature, w_{ref} is the path in question and a are the adjacent connections with the intersection angle θ. The orthogonality is normalized by the number of connections, ergo the number of arcs intersecting the reference way. In their thesis Lagesse focus on the analysis of semantic roads and historic evolution of the road network [Lag15; ERL22]. Fig. 2.9 shows that the indicator reveals local structures, but no global, city-wide patterns, but it shows a close relation to the speed limit of the street. High-speed traffic arteries with flexible connections and old or residential areas are pronounced [Lag15].

2.3.10. Morphometrics

Furthermore, there are many other approaches trying to measure urban form with various terminology which would exceed the scope of this thesis [FRP21]. The elements studied go beyond the road network and analyze buildings, their imprints, building height or the forms enclosed between the

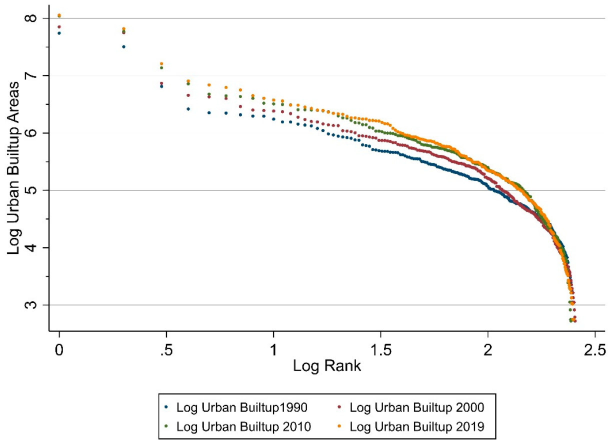

Figure 2.10: Zipfian plot showing all built-up areas by rank of all cities and municipalities in Bangladesh. Colors indicate the year of the used satellite imagery [BS20, Figure 8]. If the distribution followed a Zipfian distribution, the scatter plot would form a straight line. For all four years, a characteristical deviation at the first three ranks can be observed, also the slope decreases with rank, the effect Gibrat's law tries to capture.

streets [LB14; Shp22]. A deciding difference for morphometrics is the focus on built form, in contrast to the morphology of streets we focus on. Fleischmann, Romice, and Porta identify six categories of measures: Dimension, Shape, Spatial Distribution, Intensity, Connectivity and Diversity. Using further indicators, as population, accessibility to parks, restaurants and other amenities, spatial signatures can be determined at the building lot level, giving policymakers a tool to better grasp local similarities, or compare across cities. With this technology it is possible to obtain from building footprints and contextual data a morphometric taxonomy, represented by a dendrogram, able to uncover meaningful spatial patterns, i.e. the historical city center or different types of residential housing [AF22]. Dibble et al. also identify a *bifurcation* in the context of historical changes in urban trends whose influences can still be measured today [Dib+19]. A similar approach, using Shannon entropy of 2D matrices, has also been taken on an inter-city level. Cellular configurations were used to characterize the degree of disorder in various metropolitan areas, reinforcing the hypothesis that proximity of built form is related to cultural proximity [NBC23].

2.3.11. Rank-Size Distributions

Useful to investigate rank-size rules, the rank-size distribution is able to give a visual queue of the size distribution of a city. But when including a wider range of cities, the rank-size distribution is not able to capture the full picture, then a rule of proportionate effect, called Gibrat's *law* [Gib31], can be used to describe the population distribution [Eec04]. Usually applied to the population of cities, it can also be applied to the area and total street length of cities [Mas+15]. In our case, we are interested in the distribution of LTN block sizes inside a city for qualitative analysis of the LTN block size distribution, but no quantitative analysis. A related distribution showing Bangladeshi built-up areas is shown in Fig. 2.10 [BS20].

As explained, all the above metrics have their own advantages and disadvantages in capturing the urban form or graph structure, depending on the choice of representation. We will use all of them, except the hierarchy matrix, orthogonality and morphometrics measures, which could still be interesting for future extensions, but exceed project scope. For the LTN analysis, we use further fundamental graph quantities, e.g., the number of edges, nodes, intersections, the node degree, street length. Especially, approximating population densities for arbitrary LTN is a key measure for urban planning. Directness and global efficiency serve as key determinants for the performance of city LTN configuration. LTN coverage reassures the fraction of street length affected of traffic calming measures, in terms of routing restrictions (Eq. (2.3)), while the betweenness measures can be used to show the change of street usage, and thus LTN usage, in the city. Clustering and anisotropy coefficients at the same time give insights into the actually used network shape when LTN restrictions are applied. The rank-size distribution is used to show the distribution of LTN block sizes inside a specific city when partitioned. Finally, as street orientation order and average circuity are deeply intertwined measures of city graph geometry, they are calculated to see if especially oriented or curved streets facilitate or complicate the use of LTNs.

Our need for nature, and our need for sociability and culture, can be served all together if we let them. Cities should be the conservation sites of the twenty-first century. They are ecosystems deserving of our protection and nurture. Miracles happen on our doorsteps.

— Ben Wilson [Wil23]

3. Methods

First, we describe the data sources used in this study. Namely OSM, the GHS population spatial raster dataset multitemporal (1975-2030) (GHS-POP R2023A), and the cities analyzed in this study. Second, we describe the sparsification of the road network, the practices of how to partition a road network into LTNs and the sparse graph G_{sp}. Third, we overview the framework produced for this study, give a short example of its usage, and highlight relevant implementation details. Finally, in Section 3.4, we describe the experiments conducted in this study, before we present the results in Section 4.

3.1. Data Sources

In the following, we describe the data sources used in this study. Our intention is to use as few data sources as possible, with a coverage as big as possible. This is to ensure reproducibility of the study and to make it easy to apply the methods to other cities.

3.1.1. Open Street Map (OSM)

The study is based on the Volunteered Geographic Information (VGI) data Open Street Map (OSM) [Ope23]. As OSM spans the whole world, we can analyze cities from all over the world, which we posed as a requirement for this study. OSM is a collaborative project to create a free and open map of the world, but it is not only used and mapped by volunteers, also regional governments and other groups of interest take part. Especially, large parts of the road network have been imported from governmental data [ZHN13]. OSM data are widely used in research [Jok+15] and data quality has been assessed extensively. Building footprint data quality varies across countries, but the street data are much more reliable [BCL23]. The OSM car road network has been widely used and the data quality well studied [Fon+17]. To such extent that every urban region in the world has been studied using OSM, with some of the metrics we use in the present study [Boe22]. In some instances, e.g., bicycle related data, it has an even better quality than the official data [VVS23; HZN15]. OSM is also used in citizen science projects, where volunteers can contribute with the Open Street Map surveyor app *StreetComplete* in a gamified way [ZC]. As mentioned before, `osmnx` implements the interface to OSM, to download and preprocess the data [Boe17].

3.1.2. Set of Cities

There are two lists of cities used in this study. The first list is 100 cities, distributed across all continents (except Antarctica), which have been used in a study by Boeing [Boe19b]. The global distribution of the cities is shown in Figure 3.1. This set of cities includes a large variety of geographic and demographic characteristics. By analyzing the cities in this set, our approaches are be exposed to a wide range of different conditions. The general characteristics are first summarized in Section 4.1.

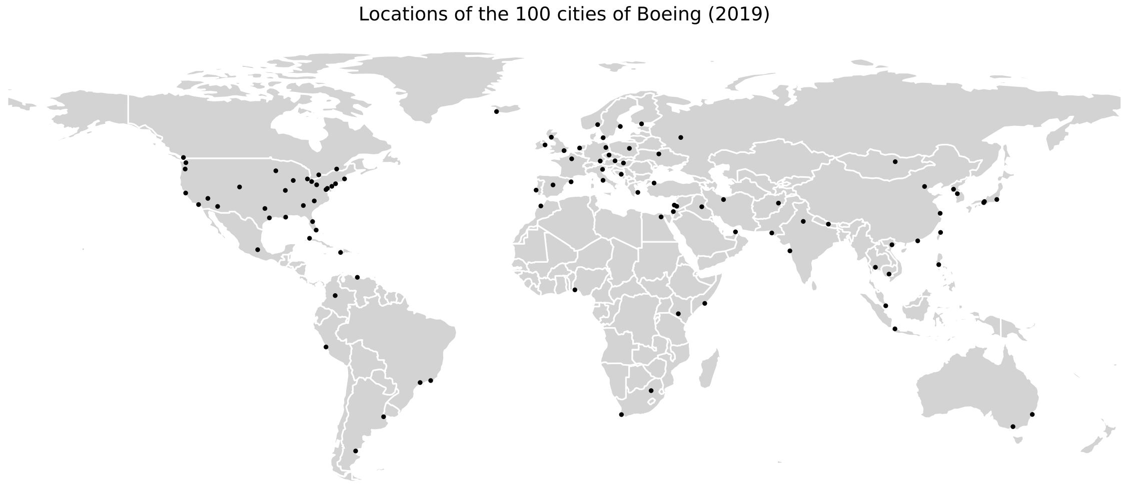

Figure 3.1: Distribution of the 100 cities as used in the study by Boeing [Boe19b].

The second list consists of the 80 most populated German cities, as of the 2021 census [Sta22]. These 80 cities are all *Großstädte* (literally: big cities), which are defined as cities with more than 100 000 inhabitants. In 3.2 the distribution of the cities is shown. This set of cities is a supplement to the first set, with cities lighter in size.

3.1.3. Population Counts — GHS-POP R2023A

The Joint Research Centre (JRC) is an institution under the European Commission (EC) and provides independent knowledge and scientific services to the European Union. One of the commissioned projects is the Global Human Settlement Layer (GHSL) dataset, which is a global raster dataset of several characteristics. It centers around a dataset of built-up areas (GHS-BUILT-S), based on satellite imagery, used to infer a variety of other datasets [PP23]. Regularly, new releases of the dataset are published, which improve the quality of the data. One of those datasets is the GHS-POP R2023A population dataset. The dataset consists of a population raster, with a resolution of 100m x 100m, and a population count for each cell. Mollweide projection is used, with the origin at the equator and the prime meridian, which means the cells are not square, but the area of the cells is invariant. Each updated GHS-POP R2023A release updates the population raster for several epochs, starting in 1975 with an 5 year interval up until 2030. For our study, we use the 2025 epoch. Furthermore, there are other resolutions available, 1 km and 3″ or 30″ in WGS 84 projection, which is an earth-centered, earth-fixed coordinate system [SFM23]. For our application, the 100m x 100m raster is the most suitable, as it is the highest resolution available, which is needed to detect variations at LTN level.

Satellite and census data are both used to infer the population raster, but still raw census data are inherently more accurate than the inferred population raster. Nonetheless, the resolution of the raster is much higher than census data, as administrative units usually bound the areas of

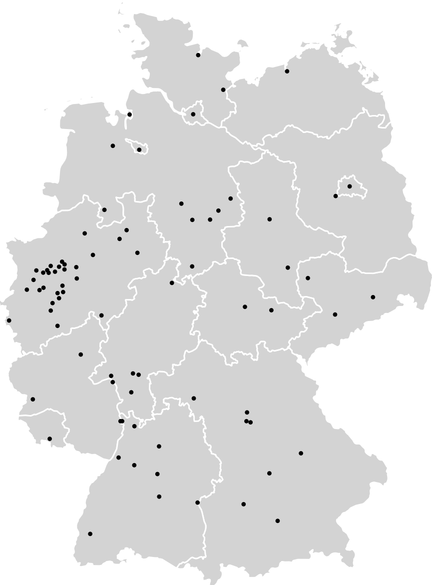

Figure 3.2: Map of the 80 most populated German cities by 2021 census [Sta22]. The East-West divide is visible in the distribution of the cities, with the Rhine-Ruhr area being the significantly more populated area in the West.

consideration which can be much larger than the 100 m raster cells. To make sure the data quality of the GHS-POP R2023A dataset is sufficient for our application, we estimate the uncertainty of the data. The GHSL datasheet does not give an explicit error estimation for the population values. However, it gives expected errors of the new GHS-BUILT-S R2023A release at 10m for the various area types, see Table 6 in the report [PP23]. For the urban and built-up areas the root mean square error (RMSE) is 29.6 % and the mean absolute percentage error (MAPE) is 21.8 %. Because the population data are inferred from this data, we assume the error is of the same magnitude. As the used GHS-POP R2023A data compiles down to a lower resolution than the original built-up data, we estimate the error for our 100m x 100m cells is lower, or at least bounded by the error of the original data. For each population cell, we estimate the uncertainty by a symmetric triangle distribution of the width $p \cdot \mathrm{MAPE}_{\mathrm{urban}}$, where p is the population of each raster cell. From this we get a standard deviation of $u(p) = 6^{-1/2} p \cdot \mathrm{MAPE}_{\mathrm{urban}}$ [KV04].

For Poland and Portugal case studies Calka and Bielecka estimate MAPEs from 1.0 % to 5.71 % for the 250m resolution of the 2019 data [CB20], while Kuffer et al. stress that overestimation in low-density or sparsely populated outskirts of cities can be even bigger. Underestimation can happen for high-density residential areas. Crucial is also, there is no one accepted standard for the uncertainty estimation of population data [Kuf+22; Ley+18]. This means while our population estimates are not perfect, still we can expect them to show differences between the LTN estimates.

In our calculation we do not need to keep track of a separate numerical uncertainty estimate, as the mathematical operations we do are only additive and multiplicative. For the cell area A_i we do not add an uncertainty. Due to this choice, the final uncertainty estimate of each LTNs aggregated population density ρ_{LTN} has a standard deviation

$$u(\rho_{\mathrm{LTN}}) = \sqrt{\sum_{i=1}^{N} \left(\frac{u(p_i)}{A_i}\right)^2} = \frac{\rho_{\mathrm{LTN}} \cdot \mathrm{MAPE}_{\mathrm{urban}}}{\sqrt{6}}, \tag{3.1}$$

where N is the number of cells in the LTN, and A_i is the area of the i-th cell. The same holds true if a LTN partially intersects cells, then population p_i and area A_i are linearly scaled.

3.2. Road Network Sparsification

Task is to partition arbitrary street network graphs G into subgraphs G_i and the sparse graph G_{sp} holding the given restrictions Eq. (2.3). We do this twofold: one approach depending on the street attribute `highway` and one depending on the betweenness centrality of the streets. One simplification we lay out beforehand is the important distinction that for our purposes we search solutions where none of the subgraphs G_i are connected to each other. If this is the case, it is sufficient to find the sparse graph G_{sp} and the subgraphs G_i fall out of it as the connected components of $G \setminus G_{\mathrm{sp}}$. This works because the subgraphs G_i are not allowed to be connected to each other, so they are not allowed to share any edges. The procedure for this common step is shown in Algorithm 1.

Algorithm 1 Partitions from Sparse Graph

Require: $G = (V, E)$, $G_{\mathrm{sp}} = (V_{\mathrm{sp}}, E_{\mathrm{sp}})$
Ensure: $G_i = (V_i, E_i)$, $G_{\mathrm{sp}} = (V_{\mathrm{sp}}, E_{\mathrm{sp}})$
1: $C \leftarrow \mathrm{scc}(G_{\mathrm{sp}})$ ▷ scc: strongly connected components
2: $G_{\mathrm{sp}} \leftarrow \mathrm{argmax}_{c \in C} |c|$ ▷ select largest component
3: $G \leftarrow G \setminus G_{\mathrm{sp}}$ ▷ cut off residuals
4: $G_i \leftarrow \mathrm{wcc}(G)$ ▷ wcc: weakly connected components

The highway tag describes common use and importance of a street. One possible value is `residential` which is used for streets in residential areas. All streets that do not have this tag will be considered as `non-residential`, they are included in the sparse graph G_{sp}. The pseudo-code for this approach is shown in Algorithm 2.

Because tagging of streets is not always consistent, even the proportion of residential streets can vary between different cities, we also want to have a more general approach. We use the betweenness centrality of the streets, defined in Eq. (2.9), to determine their importance. As rule of thumb, the higher the betweenness centrality of a street, the more important it is for the connectivity of the graph. Residential areas should have a lower betweenness centrality than the rest of the graph. This also means that when implementing such LTN configuration, the status quo will not be changed, as streets more important for the connectivity will be kept and only the less important ones will be calmed down. The pseudo-code for this approach is shown in Algorithm 3. First, the betweenness centrality of all edges is calculated. Then, the edges are sorted by their betweenness centrality,

Algorithm 2 Residential Partitioner

Require: $G = (V, E)$
Ensure: $G_i = (V_i, E_i)$, $G_{\text{sp}} = (V_{\text{sp}}, E_{\text{sp}})$
$E_{\text{sp}} \leftarrow \emptyset$
for $e \in E$ **do** ▷ loop over all edges
  if `residential` $\notin e$.highway **then** ▷ check if `residential` is in highway tag
    $E_{\text{sp}} \leftarrow E_{\text{sp}} \cup \{e\}$ ▷ add edge to sparse graph
  end if
end for
$G_{\text{sp}} \leftarrow (\text{nodes}(E_{\text{sp}}), E_{\text{sp}})$
PARTITIONS FROM SPARSE GRAPH(G, G_{sp})

so the edges with the highest betweenness centrality are at the beginning of the list. Edges with betweenness centrality above than a given threshold percentile p are added to the sparse graph G_{sp}. r is the maximum path length included in the betweenness centrality calculation. For $r = \infty$, all paths are included. Another parameter Algorithm 3 takes is the type t of betweenness centrality to use. For simplicity, we only use the unscaled, normal betweenness centrality.

Algorithm 3 Betweenness Partitioner

Require: $G = (V, E)$, $t \in [\text{normal}, \text{length}, \text{linear}]$, $p \in [0, 1]$ $r \in [0, \infty)$
Ensure: $G_i = (V_i, E_i)$, $G_{\text{sp}} = (V_{\text{sp}}, E_{\text{sp}})$
$E_{\text{sp}} \leftarrow \emptyset$
$b \leftarrow \text{betweenness}(G, t, r)$ ▷ betweenness: Eq. (2.9)
$E_{\text{sorted}} \leftarrow \text{sort}(E, b, t)$ ▷ sort edges by betweenness centrality
$b_{\text{p}} \leftarrow \text{percentile}(E_{\text{sorted}}, p)$ ▷ minimum betweenness centrality for percentile p
$E_{\text{sp}} \leftarrow \{e \in E_{\text{sorted}} \mid b(e) \geq b_{\text{p}}\}$ ▷ select edges with high C_B edges
$G_{\text{sp}} \leftarrow (\text{nodes}(E_{\text{sp}}), E_{\text{sp}})$
PARTITIONS FROM SPARSE GRAPH(G, G_{sp})

3.3. Implementation: `superblockify`

For this study, we developed the `superblockify` package in Python, available on GitHub `cbueth/Superblockify` [Büt23]. The package provides a set of functions to calculate the superblocks of a street network, analyze all the metrics presented in this work and more, simplified visualization functions, and a GeoPackage export function to be used in GIS software for interactive analysis and urban planning. No additional download is necessary, as the package automatically downloads and caches all the required OSM and GHS-POP R2023A data of the study areas. The code uses Python 3.10, is linted with `black` [Łc], and tested with `pytest` [Kre+04] having a test coverage of 100 %.

Central code dependencies are the `osmnx` [Boe17] and `networkx` [HSS08] packages for network analysis, and the `geopandas` [Bos+23] package for spatial analysis. Runtime relevant code is JIT compiled using `numba` [Lam+23] for performance reasons. `numba` uses the LLVM compiler infrastructure to translate Python code into optimized machine code at runtime [LA04]. Simple, repetitive, and

```python
"""New Partitioning Approach"""
from .attribute import AttributePartitioner

class NewPartitioner(AttributePartitioner):
    """Documentation..."""

    def write_attribute(self, *args, **kwargs):
        """Description..."""
        self.attribute_label = "new_descriptive_label"
        set_edge_attributes(
            self.graph,  # graph given by parent class
            {
                (u, v, k): True  # Write True to edge to include in sparse graph
                if my_deciding_condition(u, v, k, data)
                else False
                for u, v, k, data in self.graph.edges(keys=True, data=True)
            },
            name=self.attribute_label,
        )
```

Listing 1: Extending the `superblockify` package by adding a new partitioning approach. Any Python functionality can be used to define the sparse graph G_{sp}.

computationally intensive code is thus executed at speeds comparable to C or Fortran, without sacrificing the flexibility of Python.

The design philosophy of the package is mainly object-oriented, with a focus on modularity and extensibility. A central characteristic of the package is inheritance, this way, the user can easily add further partitioning approaches. A child class of the `BasePartitioner` class only needs to define the abstract method `partition_graph` to partition the graph into LTNs, set G_{sp} and the LTNs G_i. Calculating metrics, plots, saving, loading, and exporting are handled by the parent class. Another useful function is the partition check before calculating metrics. If any of the partition requirements from Section 2.2 are not met, the user is notified in the program log or console, and reports the violated requirement. An even simpler approach to adding a new partitioning approach is to use the meta-class `AttributePartitioner` and only overwrite the abstract `write_attribute` method. In this case, the user only needs to define the sparse graph G_{sp} by assigning each edge an attribute. An example of this is shown in Listing 1. The parent class then takes care of the LTNs, as described in Algorithm 1.

3.3.1. Example Usage — Nancy, France

A minimal working example is only as short as seven lines of code, as shown in Listing 2. It partitions the city of Nancy, France into superblocks using the residential street tags, and saves the resulting LTNs as a GeoPackage file and key metrics as a human-readable YAML file all to a dedicated folder. Population density is determined for every LTN and the aforementioned metrics are calculated. Further details on the usage of the package are provided in the documentation available online [Büt23].

```python
import superblockify as sb
part = sb.ResidentialPartitioner(
    name="Nancy_test", city_name="Nancy", search_str="Nancy, France"
)
part.run(calculate_metrics=True, make_plots=True)
part.save(key_figures=True)
sb.save_to_gpkg(part, save_path=None)
```

Listing 2: Minimal working example of the `superblockify` package to partition the city of Nancy, France into superblocks using the residential street tags. To change to the approach using the betweenness centrality C_B, the only change necessary is replacing the constructor call with `sb.BetweennessPartitioner(...)`, or the new approach from Listing 1 with `sb.NewPartitioner(...)`.

This example produces the results shown in Fig. 3.3. Each LTN is colored in an own color in Fig. 3.3a, marked by a larger dot, so small and similar colored LTNs can be distinguished. The black lines symbolize the sparse street network. The component rank-size distribution in Fig. 3.3b shows the LTN size distribution by accumulating the street length of each LTN in descending order. If one only wants to create the superblocks but not calculate the metrics, the `calculate_metrics` parameter can be set to `False`. Then only Figs. 3.3a and 3.3b are produced. When looking into the key figures file, one can see the general stats of the city graph, e.g., number of nodes $n = 1379$, number of edges $m = 1997$, the total area $A = 1.496 \times 10^7\,\mathrm{m}^2$, total street length[2] $L = 1.841 \times 10^5\,\mathrm{m}$, average circuity $\varsigma = 1.034$, street orientation order $\phi = 0.196$, and more. These statistics are also saved for every LTN. Finally, accumulated performance metrics are given. For this example, the LTN Coverage[3] is 61.1 %, directness D is 96.3 %, global efficiency E_{glob} is 96.4 %, and the high betweenness nodes distribution characterized by the clustering coefficient C_θ is 0.823 and the anisotropy A_θ is 2.876. We use a percentile characterizing high C_B nodes set to $\theta = 90\,\%$, which is parametrized in the central configuration file of the package. To summarize, converting all residential streets of Nancy into superblocks, which is 61.1 % by length, the increase in travel time for motorized private transport can be expected to be only 3.7 % on average. E_{glob} shows that the efficiency is predicted to change similarly little.

3.3.2. Calculation of Metrics

This section touches on a few deciding aspects of the implementation details. All the following methods and more are illustrated in detail online as interactive code notebooks in the Reference Section[4] of the documentation.

[2]While total *edge* length counts every length of the directed graph, the total *street* length L takes the undirected graph into account.

[3]The LTN Coverage is calculated on the directed graph, by *edge* length.

[4]`https://cbueth.github.io/Superblockify/guide/`

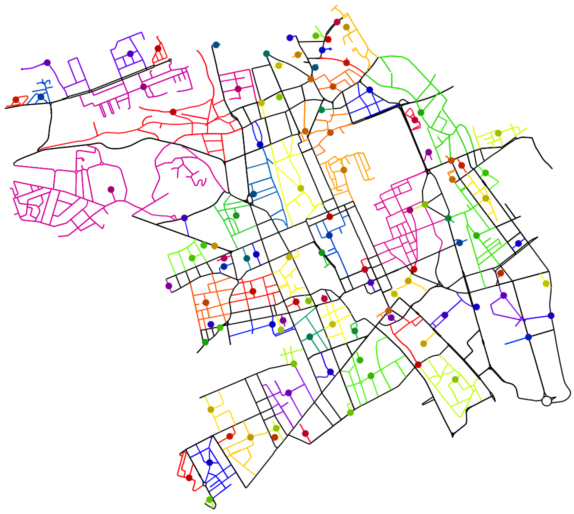

(a) LTNs of Nancy, France using the residential street tags through Algorithm 2.

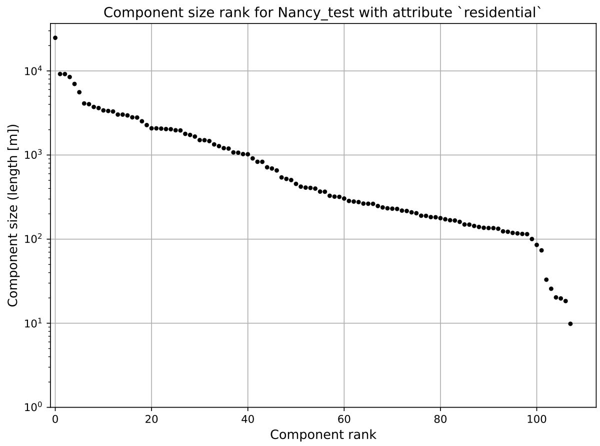

(b) Component rank-size distribution of the superblocks. For each LTN the street length sum is calculated and sorted in descending order. For clarity and easier comparison, we only plot the component size logarithmically, but the rank is still linear.

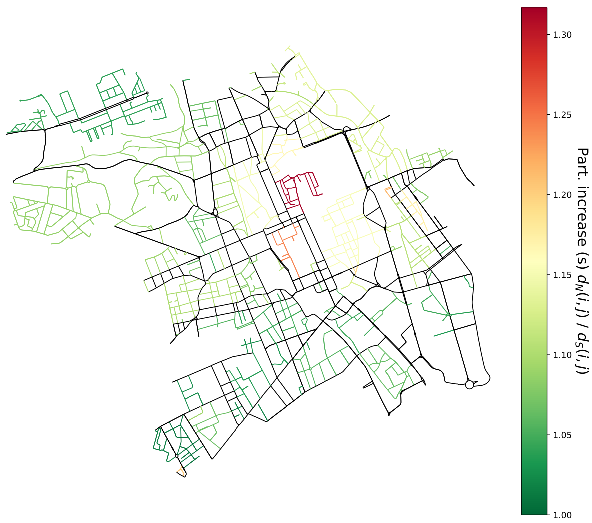

(c) Travel time increase of the superblocks compared to the original street network. The colorbar indicates the relative increase in travel time d_{LTN}/d_S. Black edges are not part of the superblocks.

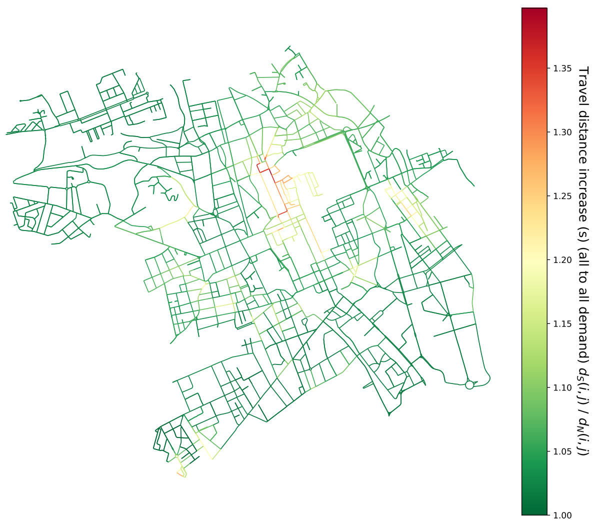

(d) Travel time increase of each edge in the superblocks compared to the original street network. The colorbar indicates the relative increase in travel time d_{LTN}/d_S. Traffic circulation in the city center and the restricted short cutting through the superblocks results in higher travel time for the reachability on small parts of the sparse street network.

Figure 3.3: Partitioning of Nancy, France into LTNs using the residential street tags. The shortest paths are determined using the travel time metric. A part of the historical city center has the highest travel time increase, this is due to partial traffic calming of one way streets on the connecting sparse street network.

Restricted Distance Calculation Directness D, global efficiency E_{glob}, and betweenness C_B are calculated using the shortest paths on the unrestricted street network G and the restricted one. Directness and global efficiency only need the distances, while for betweenness the paths themselves are needed. Finding all shortest paths on a graph is a well-known problem in graph theory. Depending on the graph structure, different algorithms are more efficient. We use *Dijkstra's algorithm* with a Fibonacci heap, which has a runtime of $O(|E| + |V| \log |V|)$. This works well for the street networks we are dealing with, as the number of edges scales roughly linearly with the number of nodes (see for our cities Fig. A.7), and not quadratically as in a complete graph. For the complete, unrestricted graph distance d_S, we can use a simple cythonized implementation of Dijkstra's algorithm from one of the dependency packages to obtain all shortest distances and paths. In the case of the restricted graph G_{sp}, we need to construct the distances and paths ourselves. If one naively calculated the distances for each combination of LTNs separately, this would scale quadratically with the number of LTNs and produce a lot of redundant calculations for the sparse subgraph. Instead, we can use the fact that the shortest path between two nodes in a subgraph is a subset of the shortest path between the same two nodes in the original graph. In other words, it is possible to construct a bare-bones version of the restricted graph, where the nodes in G_{sp} function as intermediate nodes between the nodes in G_i. The proposed solution to determine d_N and the paths comes down to two Dijkstra passes. One pass to dertermine all distances from all nodes in G_i to all nodes in G_{sp} (see Fig. 3.4a), and one pass to determine all distances from all nodes in G_{sp} to all nodes in G_i (see Fig. 3.4b). The final step is to find the shortest paths between all V_i and V_j, which only scales with the number of nodes intersecting the boundaries $V_i \cap V_{\text{sp}}$ or $V_j \cap V_{\text{sp}}$.

$$d_{ij} = \min_{k_n \in V_{\text{sp}} \cup V_n, l_m \in V_{\text{sp}} \cup V_m} \left(d_{ik} + d_{kl} + d_{lj}\right), \quad i \in V_n \Leftrightarrow j \in V_m \tag{3.2}$$

An implementation can search over either $k_n \in V_{\text{sp}} \cup V_n$ or $l_m \in V_{\text{sp}} \cup V_m$, as we already know $d_{ik} + d_{kl}$ from from the first, and $d_{kl} + d_{lj}$ from the second pass. In the same time all shortest distances inside G_{sp} are found, and all shortest distances inside G_i or departing to the sparse graph and returning to G_i.

This distance calculation works regardless of the chosen weight for the edges. In other words, the shortest path can be calculated either using the geographical distance, the travel time, number of steps, or any other metric. The third distance metric we introduce is travel time with modified speed limits. This speed limit can be set in the configuration file. By default, a speed limit of 15.0 km/h is used for the LTNs, and 50.0 km/h for the rest of the street network.

Betweenness Centrality Betweenness centrality C_B is part of most network analysis toolkits. But we found no library that can work with predefined paths. Most implementations use Dijsktra's algorithm under the hood. For the application to only save betweenness centrality and with enough processing power, this is a viable option even for large graphs. Another escape is the limitation through a maximum path length. But in our case, this is not an option. This is why we took the implementation of betweenness centrality from the *NetworkX* library and modified it to work

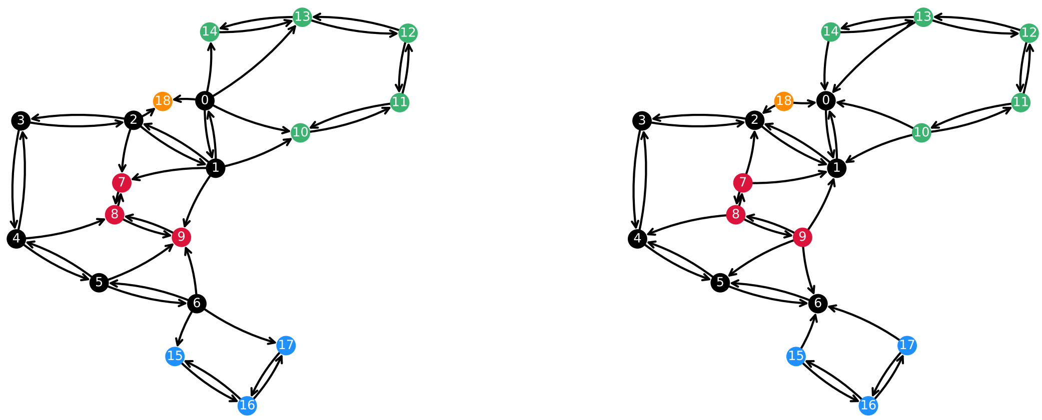

(a) Edges leading into G_{sp} filtered out. (b) Edges leading out of G_{sp} filtered out.

Figure 3.4: Visualization of the two distance calculation passes for a toy graph. The colored nodes constitute the G_i, while the black nodes are the sparse subgraph G_{sp}.

with predefined paths. This had simplification benefits, and we optimized the code to work with `numba` while calculating all six types of betweenness centrality (edge and node, with the three scaling options) in one pass. The main idea of effective C_B calculation comes from Brandes [Bra08], stating "the cubic number of pair-wise dependencies $\delta(s, t \mid v) = \sigma(s, t \mid v)/\sigma(s, t)$ can be aggregated without computing all of the explicitly." To not iterate over all possible paths, the algorithm accumulates the number of shortest paths along all paths to a node, in the form of a dependency tree of one-sided dependencies $\delta(s \mid v) = \sum_{t \in V} \delta(s, t \mid v)$.

In our case we are interested in the change of betweenness centrality C_B for the street network. Ergo, we need to determine the betweenness centrality C_B two times, for the street network before and after the introduction of LTNs. To illustrate the difference, we show the node and edge betweenness centrality C_B for the toy graph from before in Fig. 3.5. For larger node C_B values, the node is drawn larger. The edge C_B values are shown as the color of the edge, with darker edges having a higher C_B value. When comparing the two figures Figs. 3.5a and 3.5b, the introduction of restrictions has a significant impact on the distribution of betweenness centrality C_B. Before, shortest paths could shortcut through the LTNs, but after the introduction of restrictions, the shortest paths have to go around the LTNs, and the sparse subgraph (black nodes) increases in importance.

Street Population Density For each LTN, we want to calculate the population density for arbitrary geographical areas. To accomplish this task in a manner that can be scaled up to large areas, we propose to precalculate the population density for each street segment. By doing so, only one expensive calculation is needed to split up the population onto the streets, and doing this step only once in the graph preparation before caching the graph, lets us save time and resources when trying out different LTN configurations.

As we have the GHS-POP R2023A population raster data, it is our task to redistribute the population

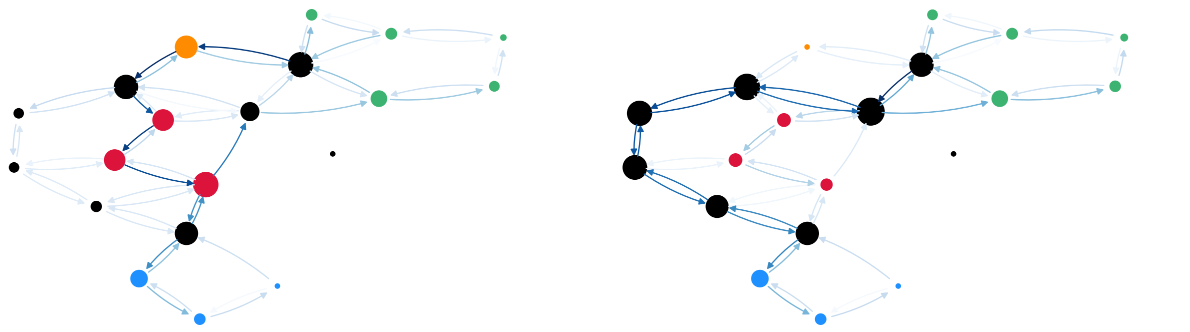

(a) Without restrictions. (b) With restrictions, combined paths from Fig. 3.4.

Figure 3.5: Edge and node betweenness centrality C_B for the toy graph with and without routing restrictions.

of the 2d raster onto all the streets while conserving the total population. The first step is to find a tessellation of the streets. A tesselation is a division of a plane into polygons, in our case, the plane is the street network, and each street corresponds to a polygon. The idea is to construct polygons that include all points in space that are closer to a street than to any other street. There is a solution satisfying our requirements. Okabe and Sugihara define the line Network Voronoi Diagram (line N-VD) [Equation 4.7]. It is basically a Voronoi diagram (also called Thiessen polygons in some fields) where lines are made up of multiple points instead of only one [OS12]. Araldi and Fusco use this idea to do geostatistical analysis [AF19]. Fleischmann et al. implement this idea in the `momepy` package for building footprints [Fle+20; Fle+23].

In Fig. 3.6, we show the tessellation of the drivable street network of Scheveningen, The Netherlands. Every street has been interpolated by equidistant points, and a Voronoi diagram has been constructed, see Fig. 3.6a. The polygons are then dissolved to the street level, see Fig. 3.6b.

In Fig. 3.7, we show the population raster and the corresponding population cells for Scheveningen, The Netherlands. The 10 000 m^2 large population cells each have a population density value assigned to them counting the number of inhabitants inside the cell. To map the population to our street tessellation there are two approaches. Classically, one would use a rasterstats approach, the street geometries "collect" the population values of all the cells they intersect, but by their center points. This approach works well if the raster resolution is sufficiently high, but it is not very accurate for low resolutions, as the population is not distributed evenly across the cells. To keep the approximation as accurate as possible, we use a weighted sum of the intersecting cells, where the weight is the fraction of the cell area that is inside the street geometry. To find each possibly intersecting paris of raster cell and street geometry, we use a spatial index `shapely.STRtree` [Gil+23]. The uncertainty is taken as described in the GHS-POP R2023A data description of Section 3.1.3. For the cell area, we do not introduce any uncertainty because it works as a normalization factor after intersecting over it, and the quantity arises from a synthetic construction. Floating point inaccuracy is not considered to be a relevant factor, due to the character of the executed operations. A visualization of the input

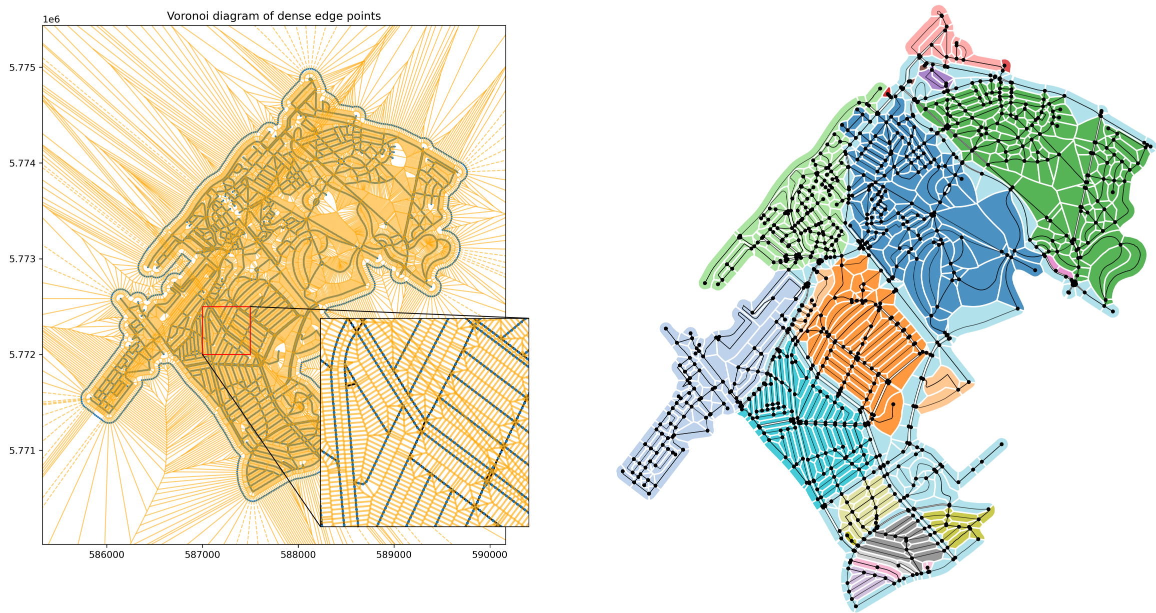

(a) Dense edge point voronoi cells before dissolving to street level.

(b) Dissolved edge cells, colored by the LTN they belong to using the `ResidentialPartitioner`. The light blue cells belong to the sparse graph in this case.

Figure 3.6: Street tessellation cells of the Scheveningen, The Netherlands drivable street network, near The Hague.

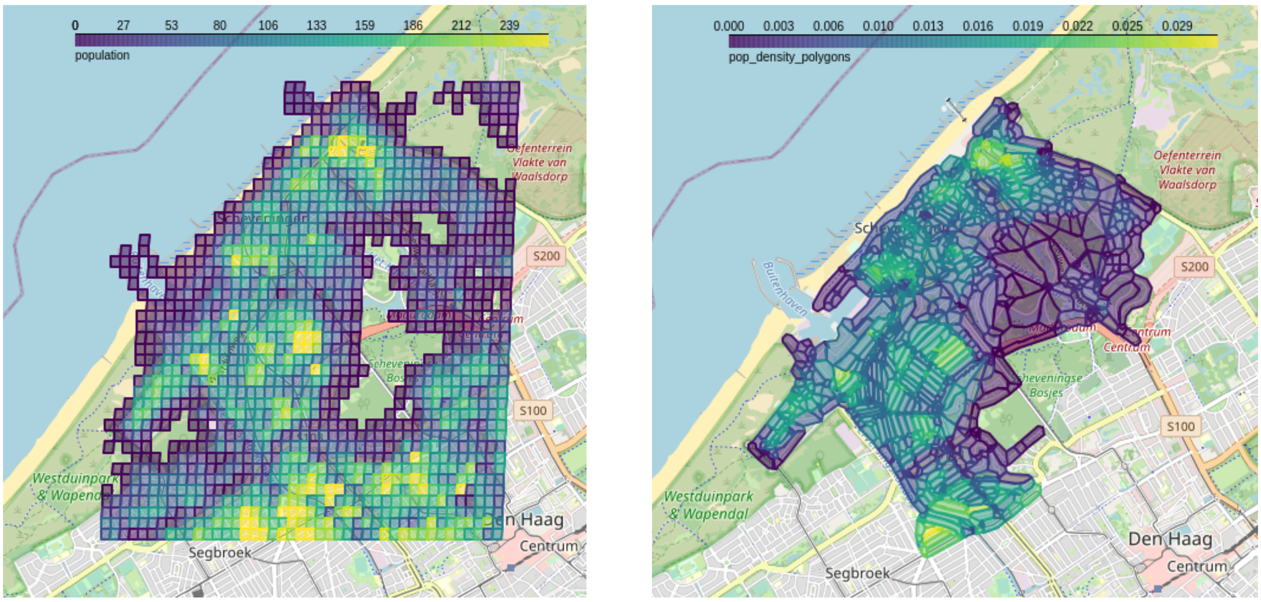

(a) Raw population raster (inh.) for the extent of Scheveningen, The Netherlands. As The Netherlands is near the meridian, the raster is barely slanted.

(b) Population density (inh./m^2) polygons for each edge.

Figure 3.7: GHS-POP R2023A population raster and the corresponding population cells for Scheveningen, The Netherlands.

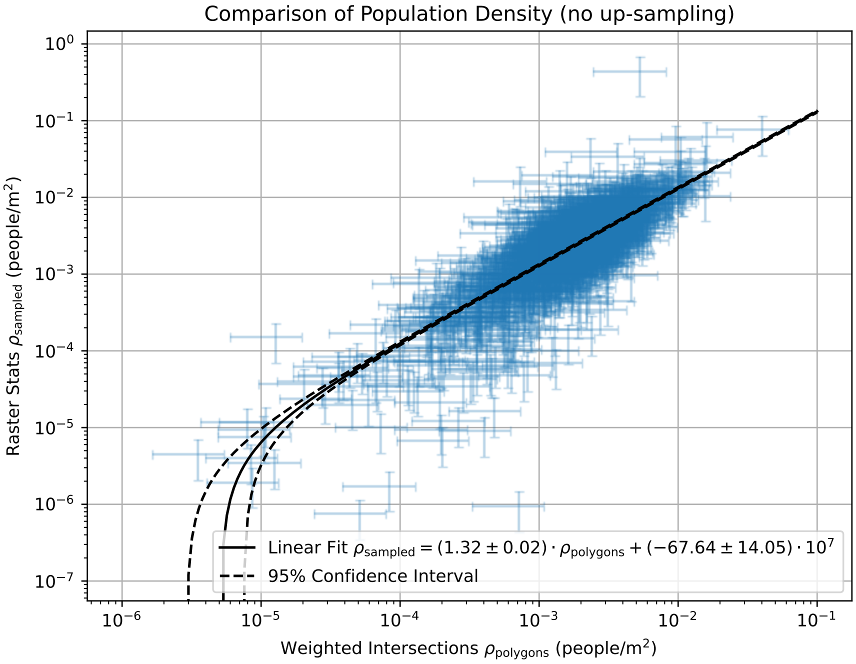

Figure 3.8: Comparison of the cell population results from our result to using the rasterstats approach, for the case study of La Crosse, Wisconsin, USA. The rasterstats approach overestimates the population density by (32 ± 2) %, using a linear orthogonal distance regression (ODR) between the two densities for each cell, and 95 % CI. Upsampling the rasterstats approach reduces the overestimation to about (4 ± 1) %, see Fig. A.1.

raster and the resulting population density is shown in Fig. 3.7. Fig. 3.7b is able to reproduce the population distribution of the input raster in Fig. 3.7a. Interactive maps for another example can be found in the corresponding notebook and the actual optimized calculation code in the source.

As a comparison, we also use the rasterstats approach to calculate the population density for each street. The result is shown in Fig. 3.8. We see that the rasterstats approach overestimates the population density by (32 ± 2) %. This was calculated using a ODR between the two densities for each cell, respecting the standard deviation of both population densities. A CI of 95 % for this linear ODR is also shown. A possible explanation is that the rasterstats approach counts the population of the cells double for multiple street geometries, which leads to an overestimation of the population density. Overestimation shrinks, when we up-sample the raster to a higher resolution, see Fig. A.1. Up-sampling is a good solution for small areas, but as the number of cells scales with the square of the resolution, it is not practical for large areas to maintain two large lists of geometries.

3.4. Experiments

Finally, to investigate the behavior of the LTN framework, our approaches, and patterns in the data, we conduct a series of experiments. We start by describing the general statistics of the analyzed cities, to get a sense of the data, and to compare the global regions in the set of 100 cities. Then, we investigate the behavior of the LTN framework, starting with the simple `ResidentialPartitioner`, and the three kinds of distance metrics: geographic distance, travel time, and travel time with introduced speed limit (15 km/h inside LTNs, 50 km/h outside). The behavior of directness D, global efficiency E_{glob}, and the high C_B node distribution shape are investigated dependent on the LTN coverage. For the `ResidentialPartitioner` the parameters percentile p, and maximal path length r are varied. Eleven values of p are chosen, ranging from 50 % to 95 % in steps between 2.5 % to 10 %, and for the radius r we choose 3000 m and ∞, i.e., no limit. Some cities only have metropolitan boundary polygons, due to this and limited memory, the package implements an option to set a maximum node count n. When preprocessing the street graph, the package will only consider the n nodes, starting from a representative, central node. This is done by constructing an ego graph by breadth-first search (BFS). For cities that have been reduced, the city tables in Appendix B show the graph statistics before and after the reduction. In summary, for the `ResidentialPartitioner`, we have 178 distinct cities and three different distance metrics, resulting in 534 experiments. For the `ResidentialPartitioner`, we have 178 distinct cities and $11 \times 2 = 66$ parameter combinations, resulting in 3916 experiments. That are 4450 experiments in total. To answer the question if there is a relation of directness D and global efficiency E_{glob} to street orientation order ϕ or average circuity ς, we take all 4450 experiments and plot these values against each other. Scripts used to conduct the experiments are available in the repository under `scripts/analysis/` and HPC (High Performance Computing) scripts are available under `scripts/slurm/`. The HPC scripts are batch scripts compatible with the SLURM workload manager, so several experiments can be run in parallel on a cluster. For a subset of all experiments, we plot the partitioning maps, and add them in the separate Appendix C, which can be used as a flipbook—per experiment one page—to get a sense of the partitioning behavior varying the parameters. Plotting all maps would exceed the scope of the appendix.

4. Evaluation

In this section, the results of the application of our framework to the two sets of cities, the 100 global cities of [Boe19b] and the most populous 80 German cities, are presented. We first give a comprehensive overview including the general characteristics of the street graphs, highlighting the commonalities and differences between the two sets of cities, and inside the sets. Then we group the spatial order by global regions and german states, to compare average circuity and street orientation order. As the first batch of results, we present the results of the residential partitioner, using different distance metrics, e.g., the geographical distance, the travel time, and the travel time with speed limits. Dependent on the LTN coverage, we present the performance results and high betweenness node distribution. Furthermore, LTN area and the three betweenness centrality scaling types are shortly compared. The second batch of results is the analysis of the betweenness partitioning approach, analogous and compared to the residential partitioner. Finally, we try to answer whether LTN partitioning performance is dependent on the spatial order of the underlying city, before giving the limitations of the study.

4.1. City Overview

Fig. 4.1 and Fig. 4.2 show histograms of the most important metrics for the 100 global cities and the 80 German cities, respectively. The full lists of metrics are given in Tables 3 and 5 in Appendix B. The cities in the two sets span multiple orders of magnitude in population p_{GHSL}, area A, and number of nodes n, edges m, total length L, population density ρ, and street orientation order ϕ. For the set of 100 cities, the number of nodes peaks around 15 000 nodes, the number of edges around 30 000 edges, while the area has a wider distribution. For the circuity, most cities have a ς from 1.01 to 1.07, with a few outliers reaching up to above 1.15. Street orientation order reaches from nearly 1 down to below 10^{-2}. The wide range of cultural and geographical backgrounds of the cities in the set of 100 global cities is reflected in the wide range of values for the metrics. The population density reaches from a few 500 inh./km^2, to about 50 000 inh./km^2. The variance of population density spans a wider range than could be possible from the variance of the area or population data alone.

Germany reaches fewer orders of magnitude in population, area, and number of nodes and edges, as shown in Fig. 4.2, compared to the global cities in Fig. 4.1. Still, the street orientation order spans from less than 10^{-2} up to 10^{-1}. Population density ρ is in the lower half of the range of the global cities.

For a quick overview of the street graphs, the Pearson correlation coefficients between the metrics are shown in Fig. 4.3. Immediately clear are the correlations in the upper left corner of the correlation matrix The number of nodes n, edges m, and intersections[5] n_{int} are highly correlated. This linear connection is shown in two scatter plots in Fig. A.7. The total street length L also correlates with this group by 89 %. Graph area A and population approximation p_{GHSL} correlate with this group

[5] The number of intersections is the number of nodes with degree greater than 2, not counting dead ends.

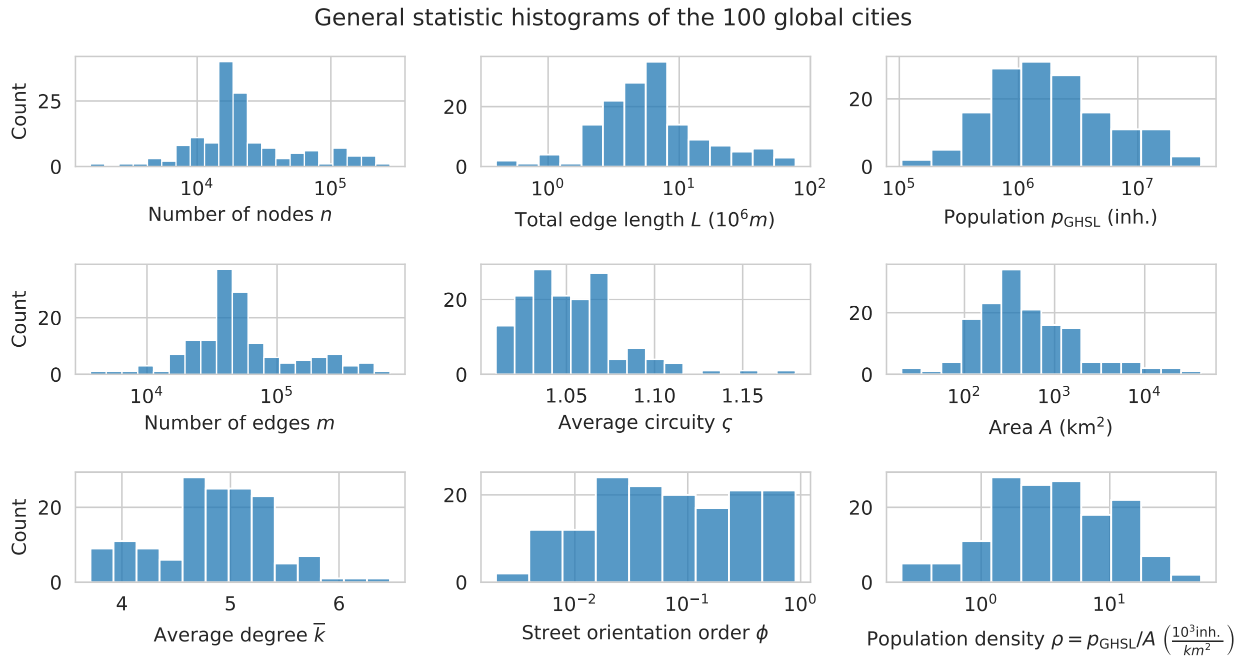

Figure 4.1: Histograms of the most important metrics for the 100 global cities. The cities in this set span multiple continents and countries, as well as multiple orders of mangitude in sizes population p_{GHSL}, area A, and number of nodes n and edges m. Except for average degree $\bar{k}$, and average circuity ς, the abscissa is logarithmic.

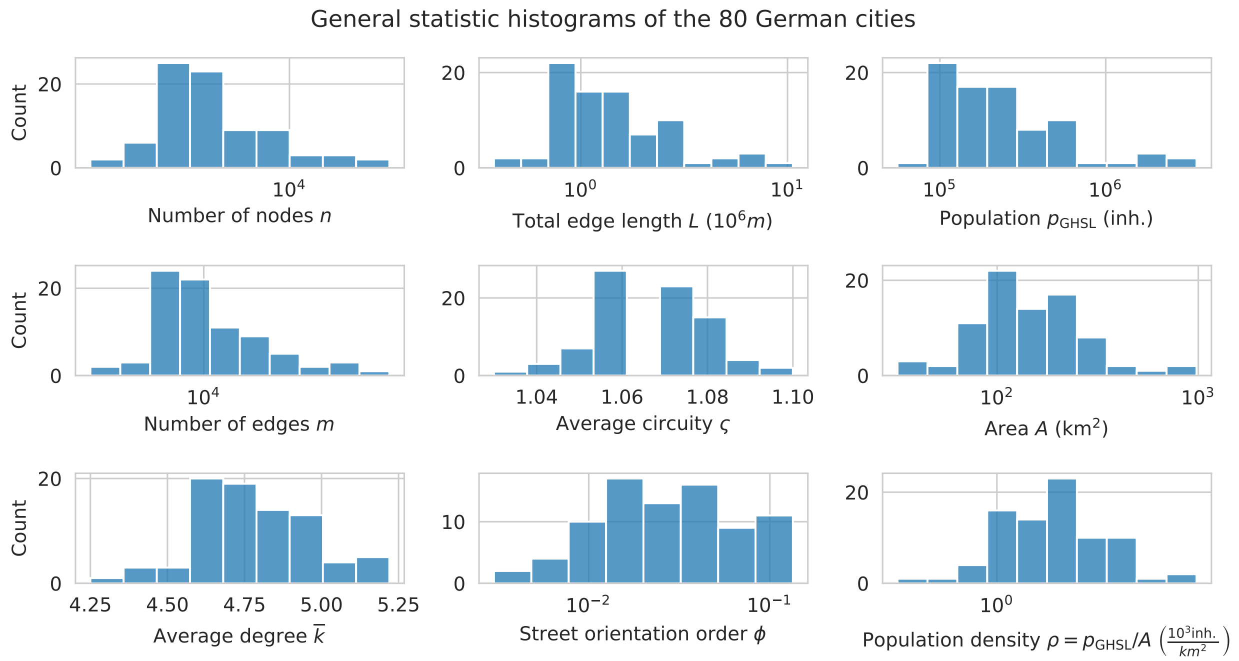

Figure 4.2: Histograms of the most important metrics for the 80 German cities. The cities in this set are distributed all around Germany, and span fewer orders of mangitude, compared to the global cities in Fig. 4.1. Still, street orientation oder ϕ span from less than 10^{-2} to more than 10^{-1}.

with around 72 %. For the German cities, this block is even more pronounced, with correlations of 95 % to 100 %, seen in the left matrix of Fig. 4.4. The average street length is slightly anticorrelated with the number of nodes and edges with a correlation coefficient of −21 %. This fits the observation that when the number of nodes and edges increases, the average street length decreases if the total street length stays constant. For the german cities, this anticorrelation alone vanished, which might be due to more homogenous data in this set. But in this case, there is a correlation of around 45 % between this block and the average streets per node, and an anticorrelation of −38 % with the average circuity. For both sets of cities the average circuity is anticorrelated with the average streets per node, −54 % for the German cities, and −60 % for the global cities. This can be explained with the detail of mapping and the dependence of the circuity on the simplified graph. A graph with fewer streets per node might have a larger average circuity, compared to a graph that has more detail with more nodes, where the great circle distance is more similar to the street length, resulting in a lower average circuity. Finally, the categorical variable of the region shows a correlation of around 44 % for the upper left block, in the global cities, but only a slight anticorrelation of around −10 % for the German cities. For the global cities in Fig. 4.3, the region (as seen in Table 3) is given as the continent. This is one of Asia and Oceania (AO), Europe (EU), Latin America (LatAm), Middle East and Africa (MEA), or North America (NAM). For the German cities, the region is given as the state, as seen in Table 5. The higher correlation for the global cities might be due to the larger differences in mapping styles between continents, compared to the mapping styles between states in Germany.

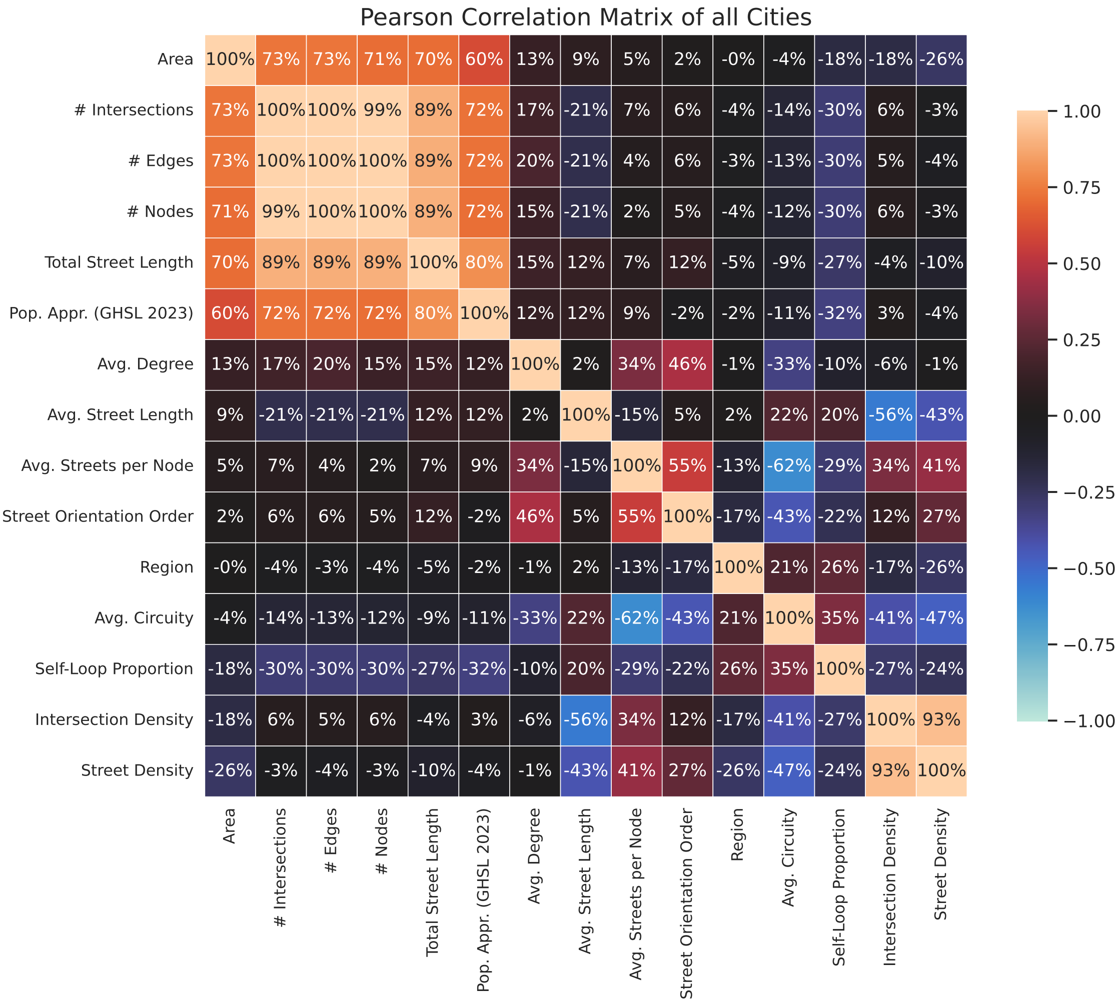

Figure 4.3: Pearson correlation coefficients for graph metrics of both sets of cities. A colorbar indicates the correlation coefficient from −1 to 1.

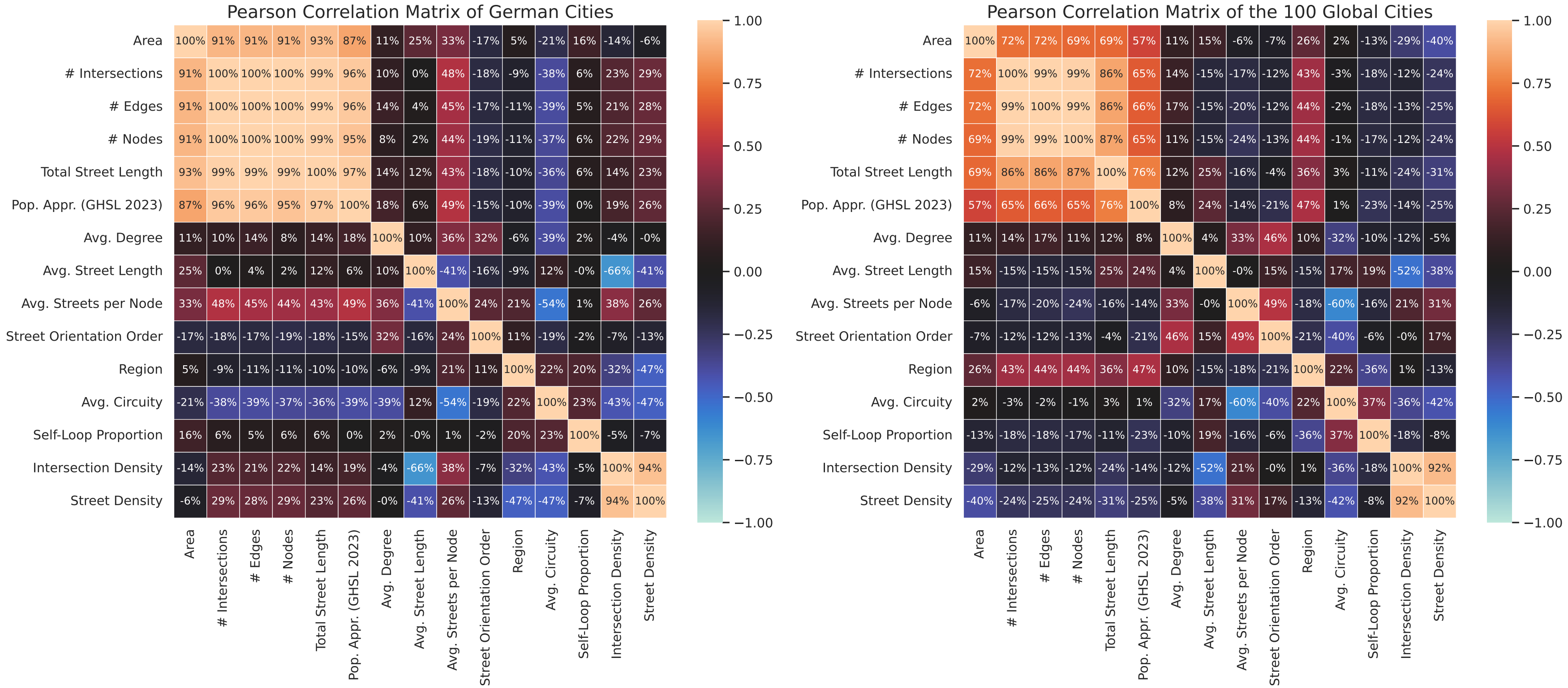

Figure 4.4: Separate Pearson correlation coefficients for graph metrics of the two sets of cities. The left matrix shows the correlation coefficients for the 100 global cities, the right matrix for the 80 German cities. Differences between the two sets can be seen which cancel out in the combined matrix in Fig. 4.3.

The total population of the cities is approximated using the GHS-POP R2023A data set, which is described in Section 3.1.3. For each global city, population is plotted against the graph area in Fig. 4.5. The uncertainty of the population approximation is shown as error bars, but is barely visible behind the data points. For the German cities, the same plot is shown in Fig. 4.6. The black line shows a ODR fit in log-log space, including the uncertainty of the population approximation. An error band of two standard deviations is shown as a gray area around the fit. The linear fit results in a slope of 0.671 ± 0.064 for the global cities, which corresponds to the exponent of a power law. The exponent for the German cities is steeper, and nearly linear with 1.004 ± 0.085. Find all absolute values in the appended Tables 3 and 5.

4.2. Urban Spatial Order

For all cities we calculated the average circuity ς and the street orientation order ϕ. Some examples are shown in Fig. 4.7. When comparing the average circuity ς for all cities, we see that the cities in NAM have the lowest average circuity by median, followed by the cities in LatAm, EU, and finally AO and MEA. By far the highest average circuity is exhibited by the outlier Caracas, Venezuela, with ς over 1.175. Caracas is also shown in the top left of Fig. 4.7. Also in LatAm is Buenos Aires, Argentina, with the lowest ς, also depicted in the top right of the same figure. In Germany, the lowest average circuity is exhibited by the city of Berlin, with ς of 1.04, the highest by the city of Wolfsburg, with ς of 1.10, both shown in the middle row of Fig. 4.7. Generally, the German circuity falls into the 1.5 interquartile range of the EU circuity boxplot. For the street orientation order ϕ (see Fig. 4.9), immediately obvious is the relatively high median of about 0.46 for NAM, which is still higher than the most ordered city outlier outside NAM: Kyoto, Japan, with ϕ of less than 0.4. By median, AO has the next highest street orientation order ϕ of nearyl 0.1, followed by MEA, EU, and lowest LatAm. Buenos Aires, Argentina, has the highest street orientation order ϕ of all cities in LatAm. Both the low average circuity ς and the high street orientation order ϕ of Buenos Aires are due to its grid-like street network. The same can be seen for Beirut, Lebanon, in MEA. The opposite is the case for Berlin, Germany. While it exhibits the lowest average circuity ς of all German cities, it also has a relatively low street orientation order ϕ of about 0.12. Reasons for this can be suspected in Fig. 4.7, where the street network of Berlin is shown. Clear straight streets are prominent and many right angles, but also many defects in the grid can be seen. In the example, the street orientation order is with 0.326 higher than the city wide average of 0.12. This means the rest of the city exhibits even less order.

4.3. Residential Partitioner

With the residential partitioner, we tested with 534 configurations the three distance metrics, geographical distance, travel time, and travel time with slowed LTNs. Fig. 4.10 shows the results of the different distance metrics. For each distance metric, a boxplot is shown for directness $\boldsymbol{D}$, global efficiency $\boldsymbol{E}_{\text{glob}}$, high $\boldsymbol{C_B}$ anisotropy $\boldsymbol{A_\theta}$, and high $\boldsymbol{C_B}$ clustering $\boldsymbol{C_\theta}$. The results for the distance and

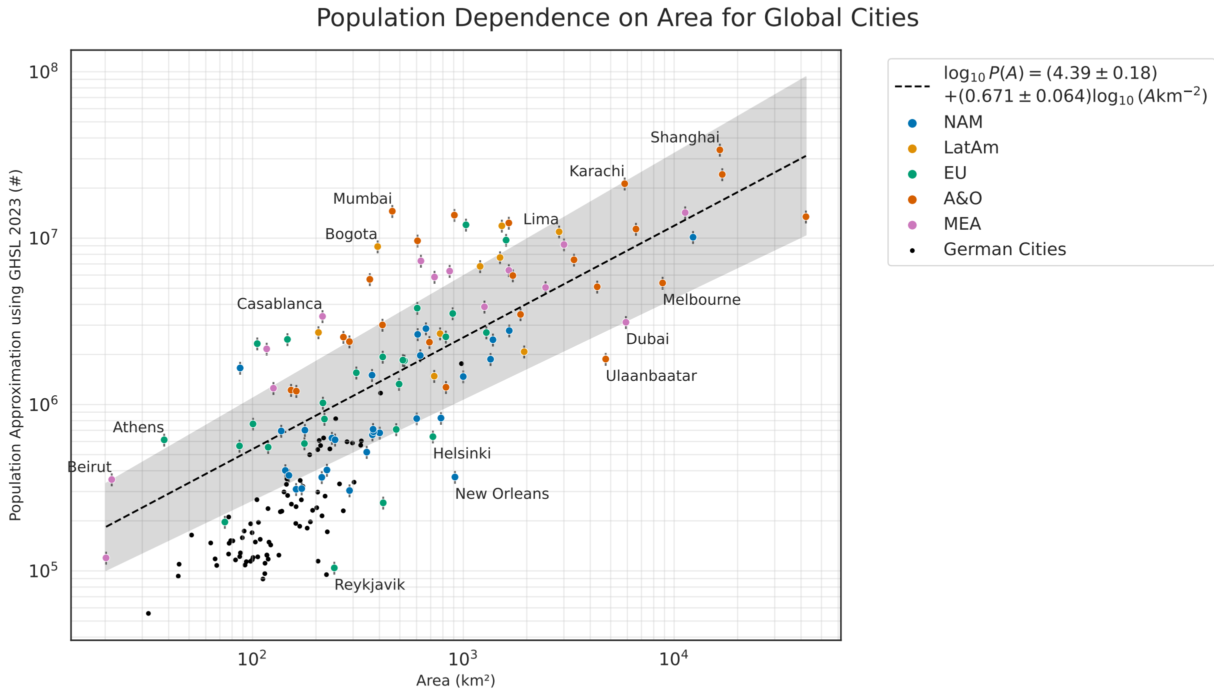

Figure 4.5: Population approximation using the GHS-POP R2023A data set. Plotted by region and area for the 100 global cities, the uncertainty is shown as error bars, barely showing behind the data points. The black line shows the orthogonal regression line in log-log space. The small black scatter points hint the German cities, which are plotted in more detail in Fig. 4.6. North American (blue) and European (green) cities tend to be less populated than the Latin American (yellow), Asian and Oceanian (red) cities.

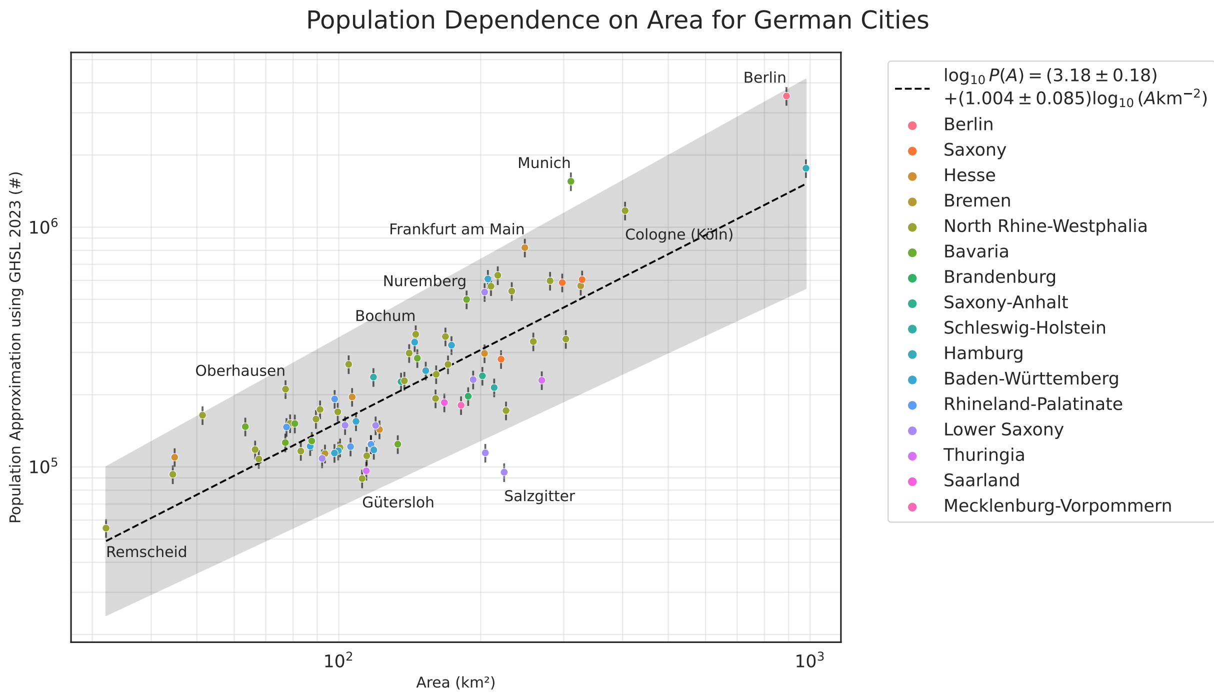

Figure 4.6: German cities from Fig. 4.5 plotted in more detail.

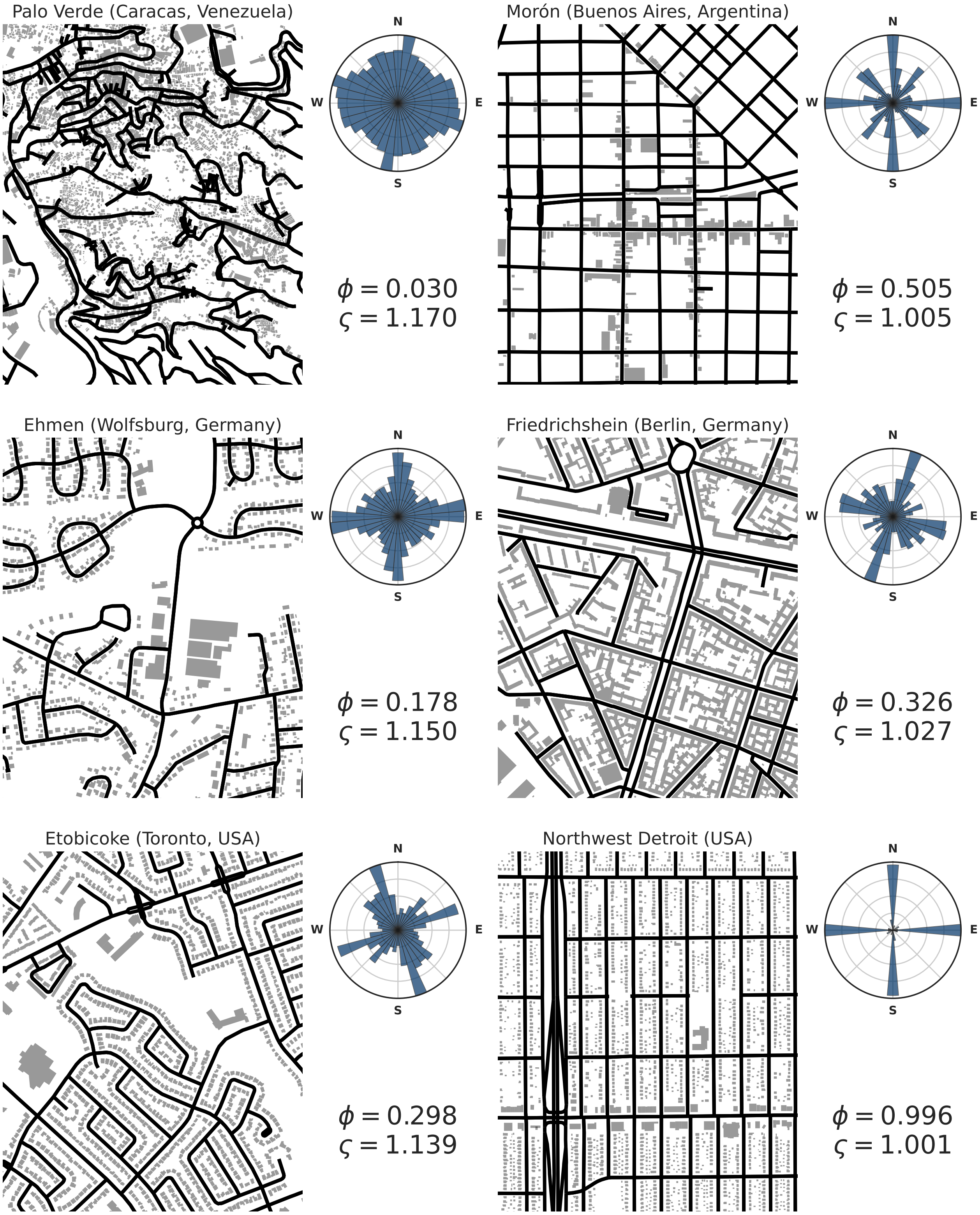

Figure 4.7: Six selected street graph examples of 1000 m×1200 m, and the street direction distribution. Average circuity ς and street orientation order ϕ are calculated for exactly the shown area. The first row shows the two extremes of ς in LatAm, the second one inside Germany, and the third one in NAM. The examples also show great variance in the street orientation order ϕ.

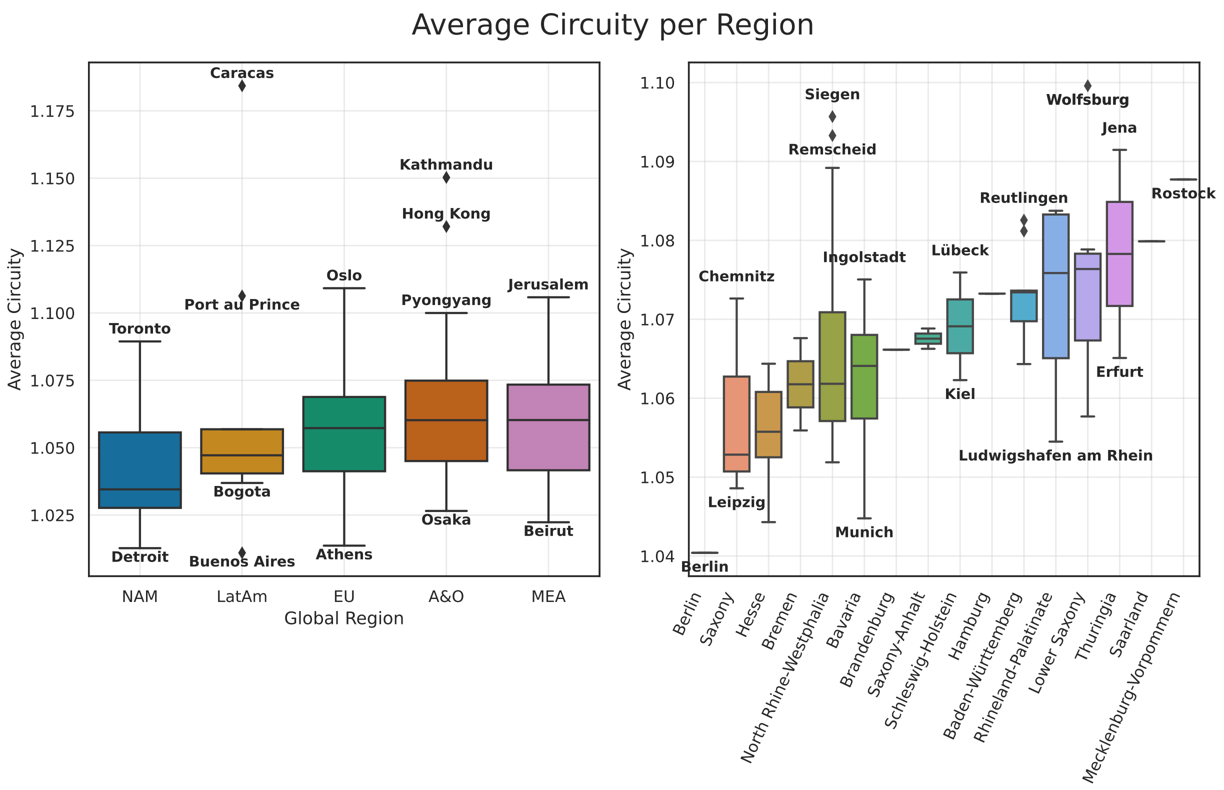

Figure 4.8: Boxplots of the average circuity ς for all cities in the five regions (left), and for the 80 German cities (right). The regions and states are sorted by the median of the average circuity ς.

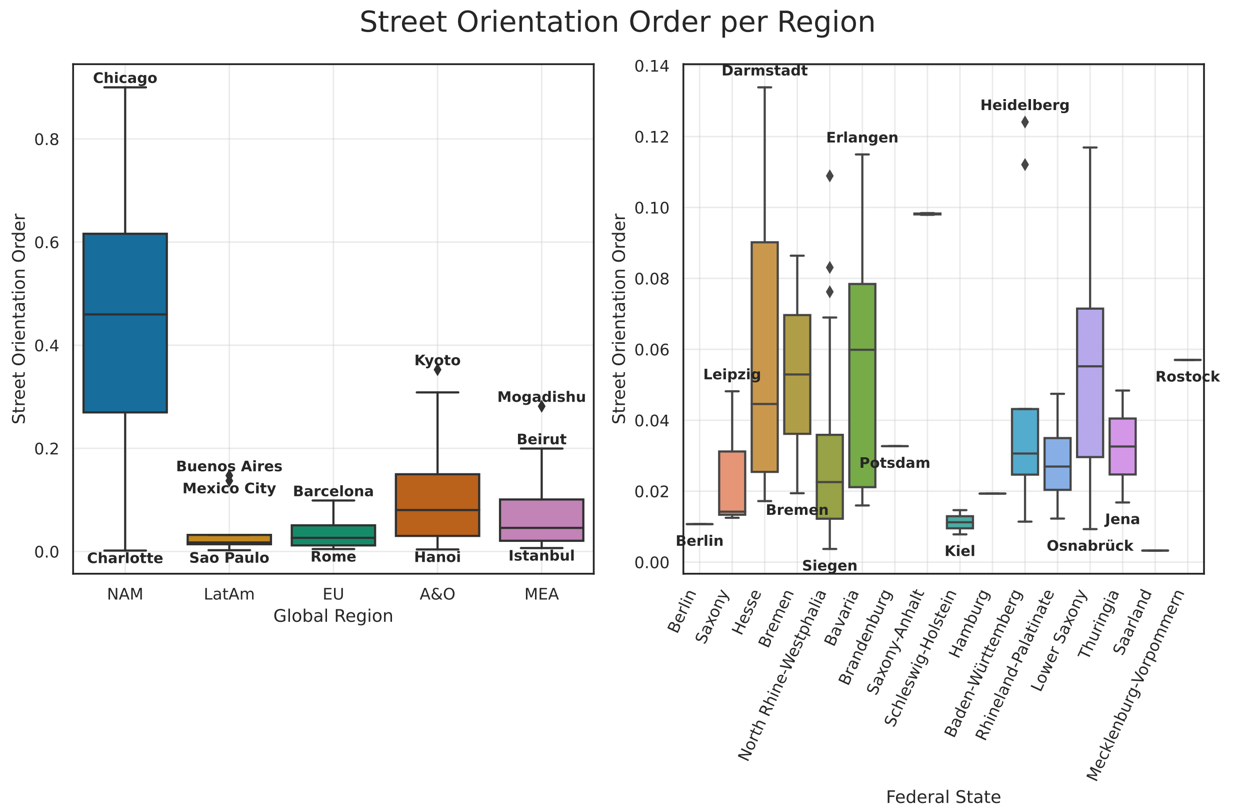

Figure 4.9: Boxplots of the street orientation order ϕ for all cities in the five regions (left), and for the 80 German cities (right). The regions and states are sorted the same as in Fig. 4.8, by the median of the average circuity ς.

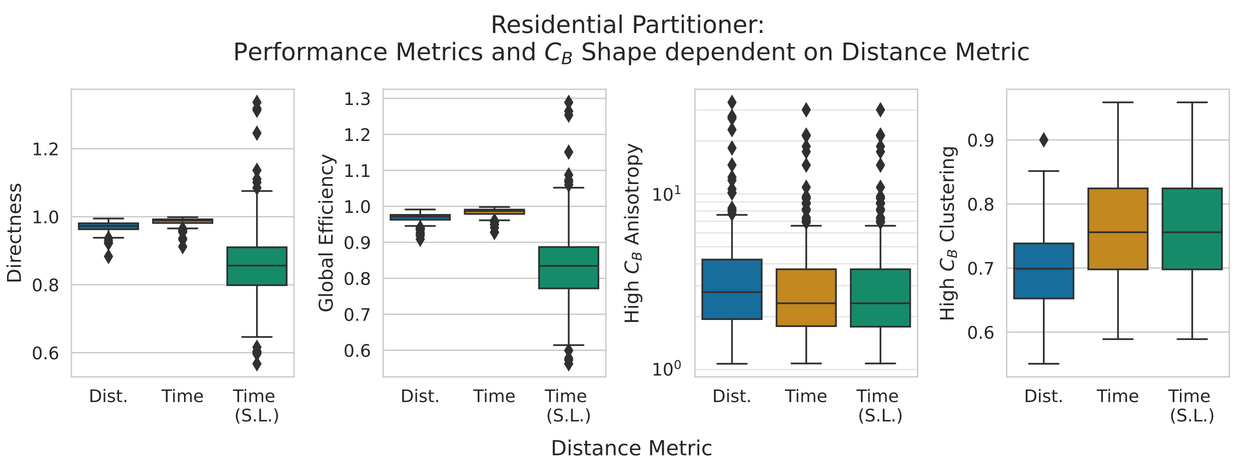

Figure 4.10: Comparison of the different distance metric configurations using the Residential Partitioner. Directness, Global Efficiency, High C_B Anisotropy and High C_B Clusttering.

travel time with unchanged speed limits are all under 1 for the performance measures D and E_{glob}, but above 90 %, except of one outlier. This means that the increase in travel distance and travel time is not higher than 10 %. When changing the speed limits, the results scatter much wider by the 1.5 interquartile range of 20 %. There are also cases of over 100 %. This is possible for places where the speed limit is already low, or the higher speed network is normally capped by a lower speed limit. For specific cities and point-wise application, the distance metric by travel time with changed speed limits might be useful, but for the global application, we cannot generalize, as the speed limits are not consistent across the globe. Another way to implement a similar feature could be to scale the existing speed limits, possible for future work. Due to this, we only compare the geographical distance and travel time metrics with unchanged speed limits in the following. For the high C_B shape, we can observe that the distance metric results in a slightly higher A_θ and lower C_θ. When using the distance metric, the geographical shortest paths tend do be spatially more centered, resulting in a more compact shape. Travel time paths are more likely to follow the road network, resulting in a less compact and isotropic shape.

As every city has different proportions of residential streets, we compare the four aforementioned performance measures by the LTN coverage. For the two distance metrics, the results are shown in Fig. 4.11. LTN coverages reach from low 20 % to high 80 %. Directness and global efficiency behave qualitatively the same, this can also be seen from their correlation in Fig. A.2. They are 97.5 % correlated with each other. The binned medians are highest around 23 %, but as thera are only very little cities with low LTN coverage, the median is not representative. Up to 65 %, the D and E_{glob} are stable around 99 %, before showing a slight decline. For the distance metric, both D and E_{glob} are 1 % to 2 % lower than for the travel time metric. This speaks for the travel time metric, as taking the quickest path regarding slower and faster roads is more realistic than plainly searching the shortest path. For the anisotropy we cannot observe a clear trend in LTN coverage, neither for the metrics. Again, as seen in Fig. 4.10, the distance metric results in higher C_θ.

The larger the cities are, the more LTN area is available. Fig. 4.12 shows that the LTN do not just grow with the city area, but they stay roughly the same size absolutely. The fractional LTN area $a_{\mathrm{LTN}} = \frac{A_{\mathrm{LTN}}}{A_{\mathrm{city}}}$ exhibits a power law with the exponent -1.018 ± 0.025 when using the residential partitioner approach. If the LTNs would stay exactly the same size, the exponent would be -1. This value is covered by the uncertainty of the exponent.

For the population densities, we have not found a specific trend related to the total city area A, as shown in Fig. A.4. Different regions exhibit different characteristical population densities. When aggregating the population densities of Table 3 by region, we find the following values in Table 1.

Analyzing the betweenness centrality C_B, we start by comparing the three types of edge betweenness centrality in Fig. 4.13. Here we analyze the median values of the aggregated C_B of all LTNs in each city. Then we compare C_B before and after restricting the LTN to the residential streets. We will concentrate on the edge betweenness centrality, as the node betweenness centrality behaves analogously, and the edge C_B is more interesting for the LTN finding procedure. The linear scaled edge C_B seems to show an offset of about a magnitude in size for the geographical distance metric.

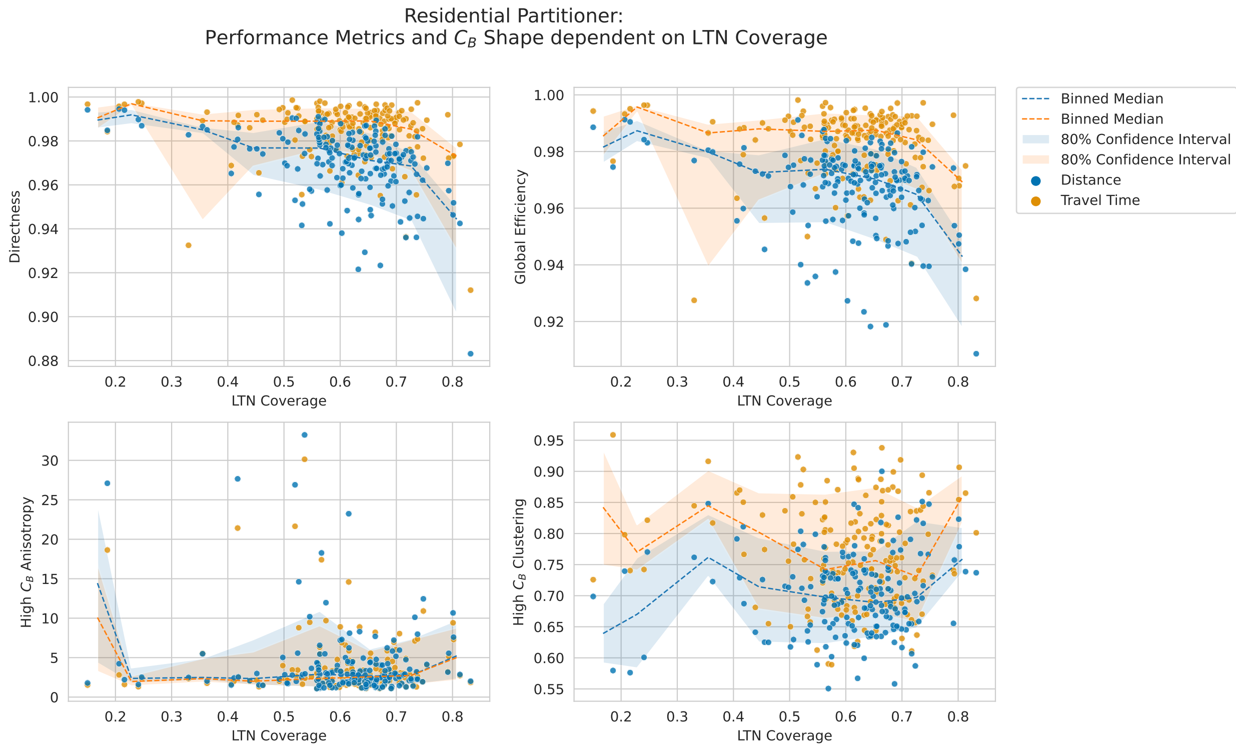

Figure 4.11: Directness D, Global Efficiency E_{glob}, High C_B Anisotropy A_θ, and High C_B Clusttering C_θ by LTN coverage, using the distance metric (blue) and travel time metric (orange). Scatter plot with overlayed median and 80 % CI, binned in 10 % LTN coverage bins.

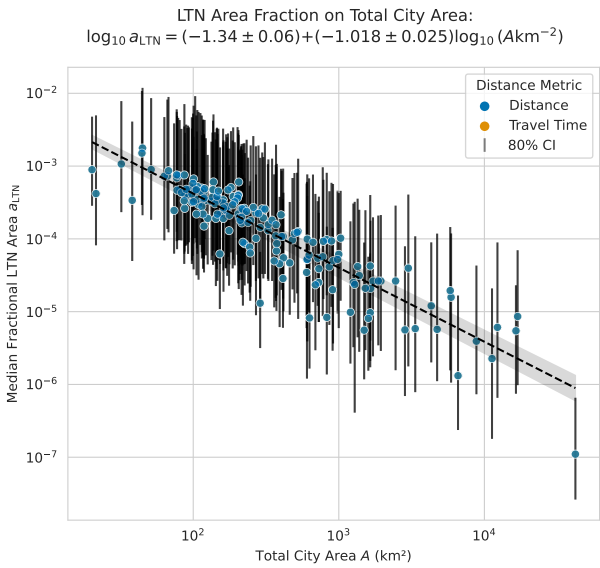

Figure 4.12: The fractional LTN area $a_{\text{LTN}} = \frac{A_{\text{LTN}}}{A_{\text{city}}}$ exhibits a power law with the exponent -1.018 ± 0.025 when using the residential partitioner approach. Both distance metrics are shown, but lay on top of each other, as the LTN finding procedure is independent of the distance metric. The error bars give the 80 % CI of all LTNs for each city.

Table 1: Overview of the population densities of the cities in Table 3 by region, aggregated for LTNs found by the residential partitioner approach.

Region	Population density [inh./km^2]	Lower 80 % CI	Upper 80 % CI
MEA	16 089	3952	35 717
AO	15 383	3843	37 195
LatAm	11 525	3981	23 921
EU	9826	2880	20 089
NAM	4170	377	10 215
GER	3350	773	7595

A power law C_B might govern dependence between the normal and linear edge. A clearer, nearly linear dependence is observed for the length scaled edge C_B, the exponent for both distance metrics is nominally identical with 1.024 ± 0.007 for the geographical distance metric and 1.024 ± 0.006 for the travel time metric.

Comparing C_B for each LTN before, and after restricting the LTN to the residential streets, we can se a clear decrease in C_B when restricting passing through residential areas (see Fig. 4.14). When averaging the effect with a linear fit, we find a decrease of (7 ± 2) % for the geographical distance metric, and (26 ± 3) % for the travel time metric. This is the general trend, but when comparing this across the regions, we cannot say that one distance metric is better than the other for all regions. Generally, inside all LTNs the street usage decreases, except for one outlier, and up to cases of −60 % for cases in NAM, MEA, and EU.

4.4. Betweenness Partitioner

3916 experiments are conducted with the betweenness partitioner. We will analyze the results analogously to the residential partitioner in the previous section. This time we only use plain travel time as the distance metric. The betweenness partitioner tries to imitate the residential partitioner by using the edge betweenness centrality as a proxy. A parameter given to the betweenness partitioner is the percentile θ inclusion criteria, determining the threshold for the edge betweenness centrality. But the percentile does not directly translate to the LTN coverage, as the partitioning approach only uses the largest strongly connected component of these high C_B edges. Another parameter is the maximal path length. The goal of this parameter is to counteract the effect of the high C_B edges being concentrated in the city center.

The directness D of the unbounded approach results in similar outcomes as the residential partitioner, but is slightly less efficient by E_{glob} (Fig. 4.15). When setting C_B range to 3 km, the directness D is slightly higher with lower 1.5 interquartile range at about 99 %, but the global efficiency E_{glob} is not noticeably better than the residential partitioner. For the high C_B node shape, we do not see a significant change, even between the two path ranges seen in Fig. 4.15.

When splitting the results by LTN coverage, we see a similar, but much rounder distribution of the

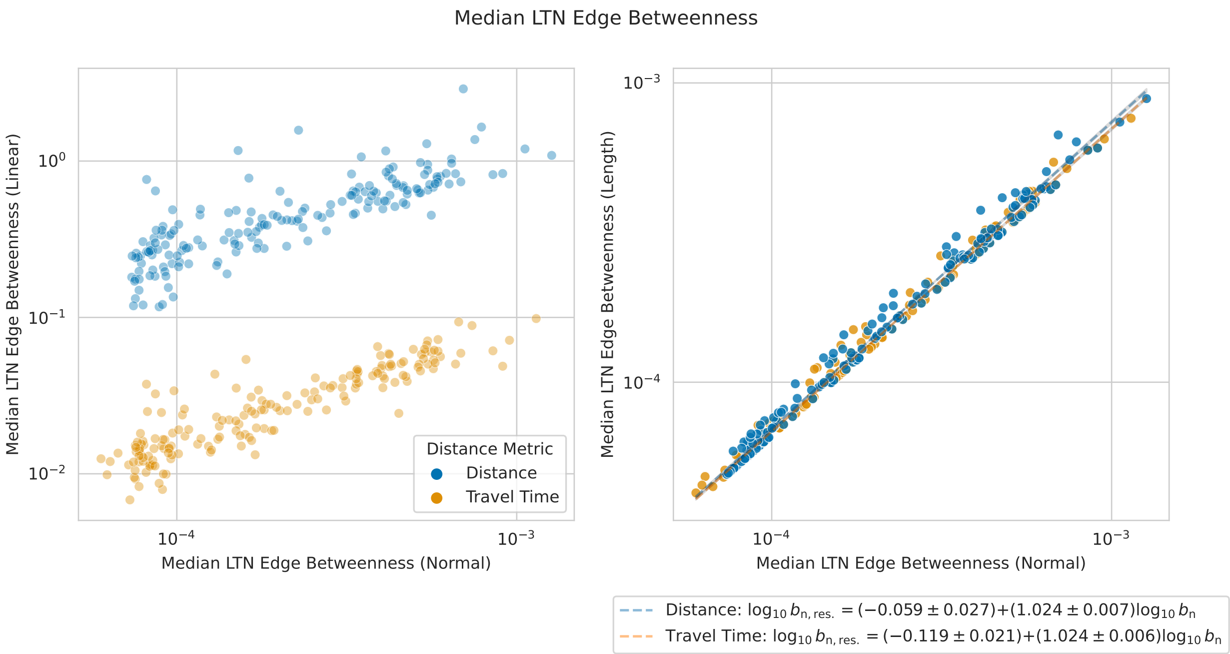

Figure 4.13: Comparison of the three edge betweenness centrality C_B types for both the geographical distance metric (blue) and the travel time metric (orange). These are the aggregated C_B of all LTNs in each city. The left scatter plot shows the normal, un-scaled edge C_B and the *linealy* scaled edge C_B. The right scatter plot shows the normal, un-scaled edge C_B and the *length* scaled edge C_B, additionally two ODR fits with uncertainties are shown.

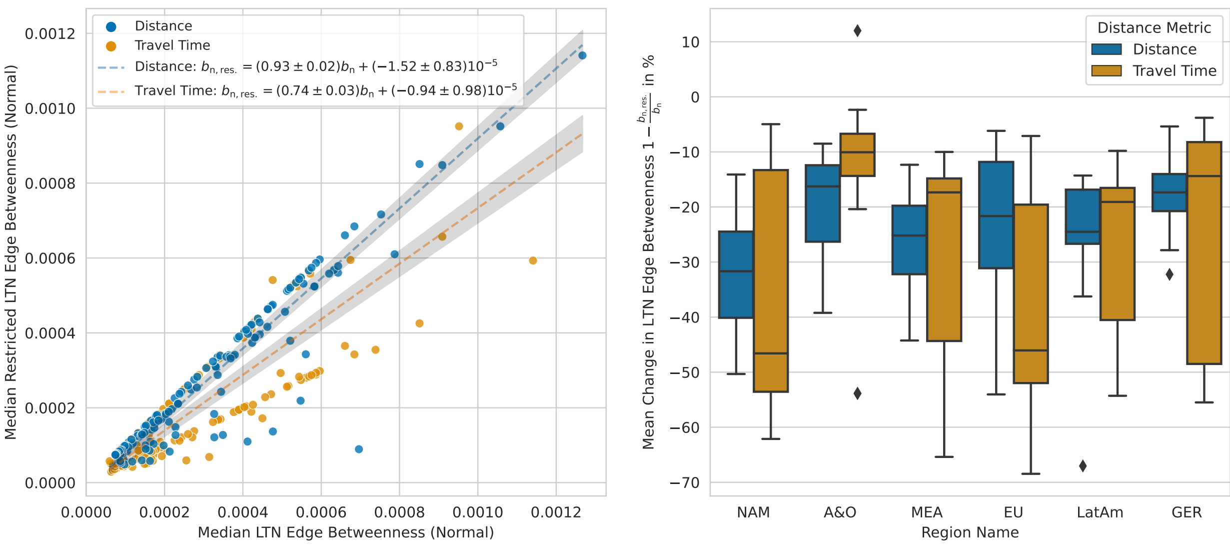

Figure 4.14: Comparison of the normal edge C_B before and after restricting the LTN to the residential streets (left), and a linear fit with uncertainties for each distance metric. Averaged percentual change of edge betweenness in the LTNs (right) by region and distance metric.

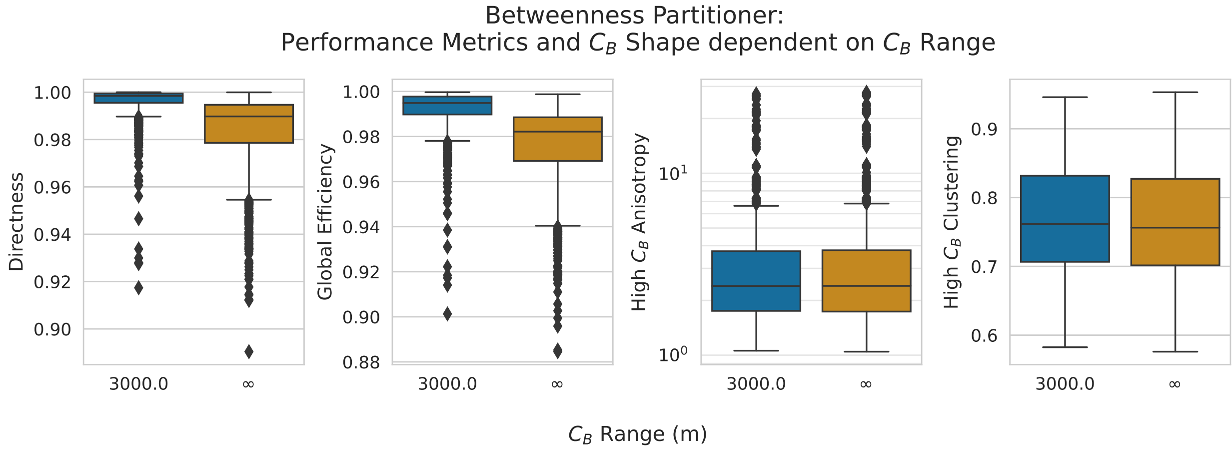

Figure 4.15: Performance metric comparison for the betweenness partitioning approach with unbounded and 3 km maximal path length.

directness D to the residential partitioner (Fig. 4.16). The median directness D and global efficiency E_{glob} are larger than the residential partitioner, up til a coverage of 70 % and similar until 80 %. For coverage larger than 80 %, the performance metrics do not change significantly, but at this high coverage, the idea of LTNs is more of one like traffic islands, as some LTNs can grow significantly large. The anisotropy A_θ does not change significantly with coverage, neither to the residential partitioner nor between the two path ranges. But with growing LTN coverage clustering increases, with the 3 km path range having a slightly lower nominal value, but a wide range 25 % of 80 % CI.

Again, the correlation between the performance metrics D and E_{glob} is 96.5 % (Fig. A.3).

The difference between the percentile and the LTN coverage was mentioned before, and could slightly be seen in Fig. 4.16. In Fig. 4.17 we plot this effect more clearly. The same parametrized experiments result in consistently lower LTN coverage when decreasing the maximal path length for the C_B range. This is because the betweenness centrality depends on identifying relevant edges by their inclusion of many shortest paths. If the range is decreased, the result gets more local and homogeneous, which in turn leads to less strongly connected components. This is not a problem in itself, but important to factor in when one wants to use the betweenness partitioner.

To substantiate the claim that the components clump together for especially high LTN coverage, we plot the number of LTNs by LTN coverage, compared to the residential partitioner. Fig. 4.18 gives clear insight into the number of LTNs. The distribution is formed like a pyramid, with the lowest number of LTNs for the lowest and highest LTN coverage. In green, we see the residential partitioner, with LTN coverage given by the data and maximally 2300 components. In blue, a bunch of range pruned results below a LTN coverage of 20 % clump up. Here the few LTNs are very small, which is not the aim of the LTN concept. Around 40 % LTN coverage, the number of LTNs is highest, still the coverage can be improved while keeping directness and global efficiency high. With growing LTN coverage, the number of LTNs decreases again, as the components grow larger. When the coverage would reach 100 %, the number of LTNs would be 1. A compromise between the 3 km and

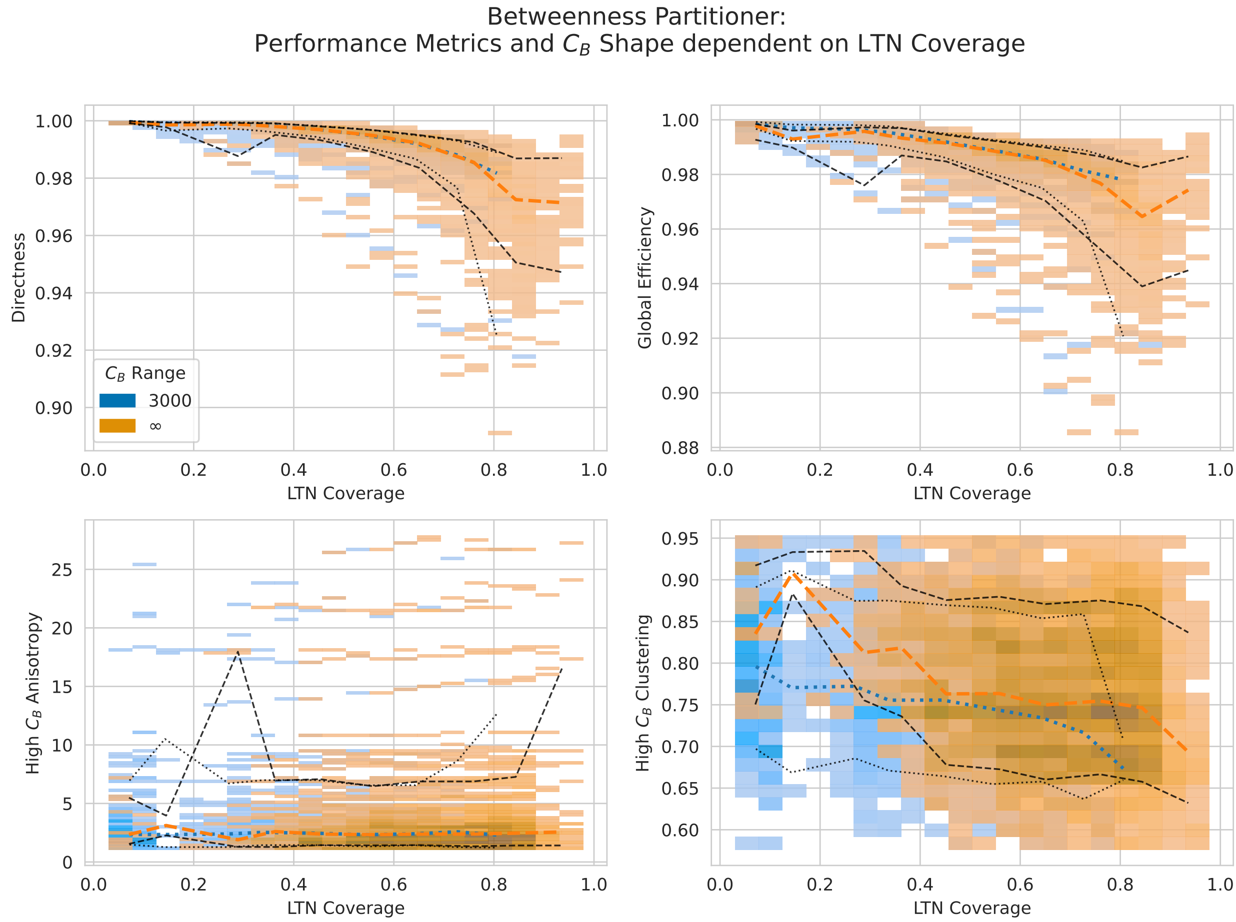

Figure 4.16: Histograms of for the betweenness partitioner results with median and 80 % CI, binned in 10 % LTN coverage bins like Fig. 4.11. Directness $\boldsymbol{D}$, global efficiency $\boldsymbol{E}_{\text{glob}}$ and high $\boldsymbol{C_B}$ node shape by LTN coverage for the betweenness partitioner. The 3 km maximal path length is shown in blue, the unbounded approach in orange.

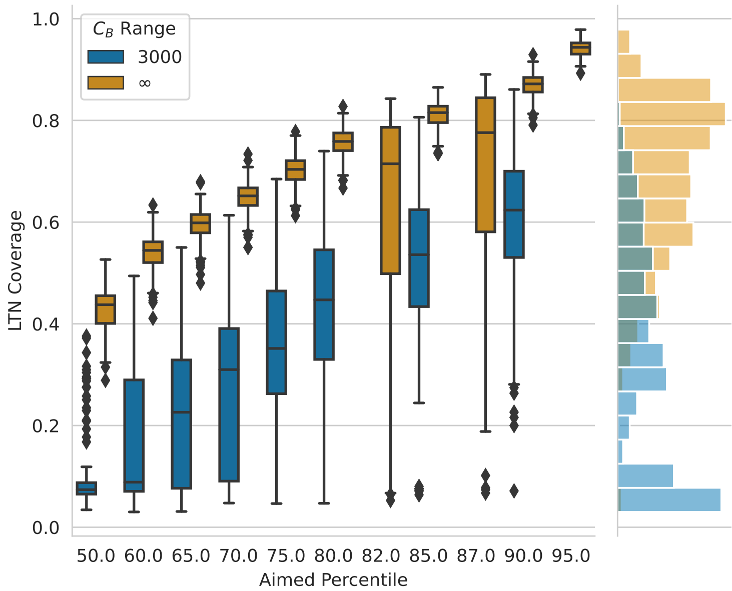

Figure 4.17: Aimed and actual LTN coverage for the betweenness partitioner. With decreasing C_B range, the actual LTN coverage decreases.

Table 2: Overview of the population densities of the cities in Table 3 by region, aggregated for LTNs found by the betweenness partitioner.

Region	Population density [inh./km^2]	Lower 80 % CI	Upper 80 % CI
MEA	15 672	2874	34 955
AO	14 182	3179	35 369
LatAm	11 354	2976	25 140
EU	9070	2056	19 930
NAM	3546	121	9777
GER	3567	679	7916

∞ maximal path length, one could select a higher C_B range. This way higher LTN coverage can be achieved, while avoiding high C_B clustering.

The relative LTN size compared to the total area is shown in Fig. 4.19. Here both C_B ranges split up, confirming that introducing a maximal path length results in smaller LTNs. The scaling is again governed by a power law exponent. For the 3 km maximal path length, the exponent is -1.20 ± 0.02, for the unbounded approach -1.10 ± 0.02. To sum up, the residential partitioner has an exponent of -1.018 ± 0.025, which means the betweenness approach generally results in smaller LTNs.

For the population densities, aggregated over the LTN population densities created by the betweenness partitioner, we find distributions similar to using residential partitioner, see Fig. A.5. The population might overlap by the 80 % CI, but the betweenness partitioner approach generally results in slightly lower population densities. All nominal values, except for GER, are each about 10 % lower than the residential partitioner from Table 1.

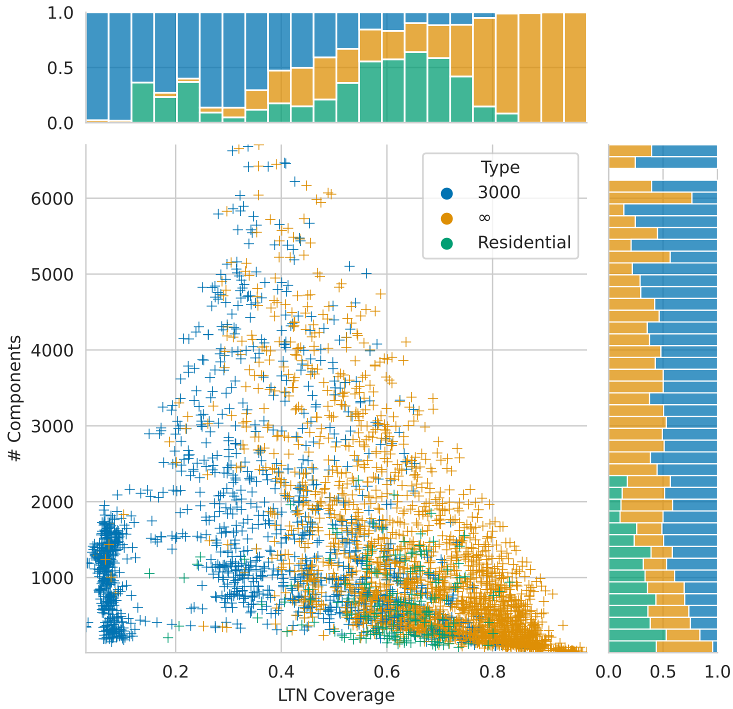

Figure 4.18: Distribution of the number of LTNs by LTN coverage and maximal path length, compared to the residential partitioner. For especially low and high LTN coverage, the number of LTNs is lowest. The marginal stacked bars are normalized to the number of experiments and converted to a relative frequency.

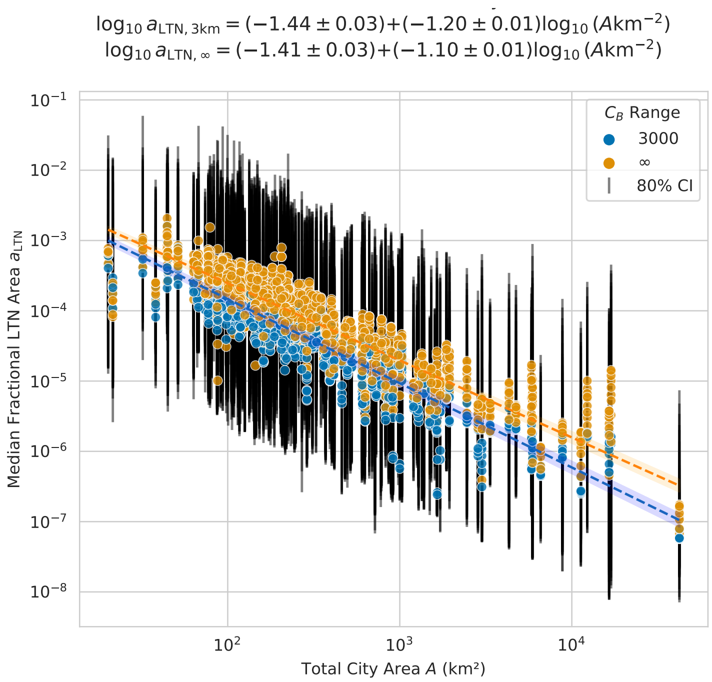

Figure 4.19: The fractional LTN area $a_{\mathrm{LTN}} = \frac{A_{\mathrm{LTN}}}{A_{\mathrm{city}}}$ again exhibits a power law when using the betweenness partitioner approach. The different colors represent the maximal path length. The error bars give the 80 % CI of all LTNs for each city.

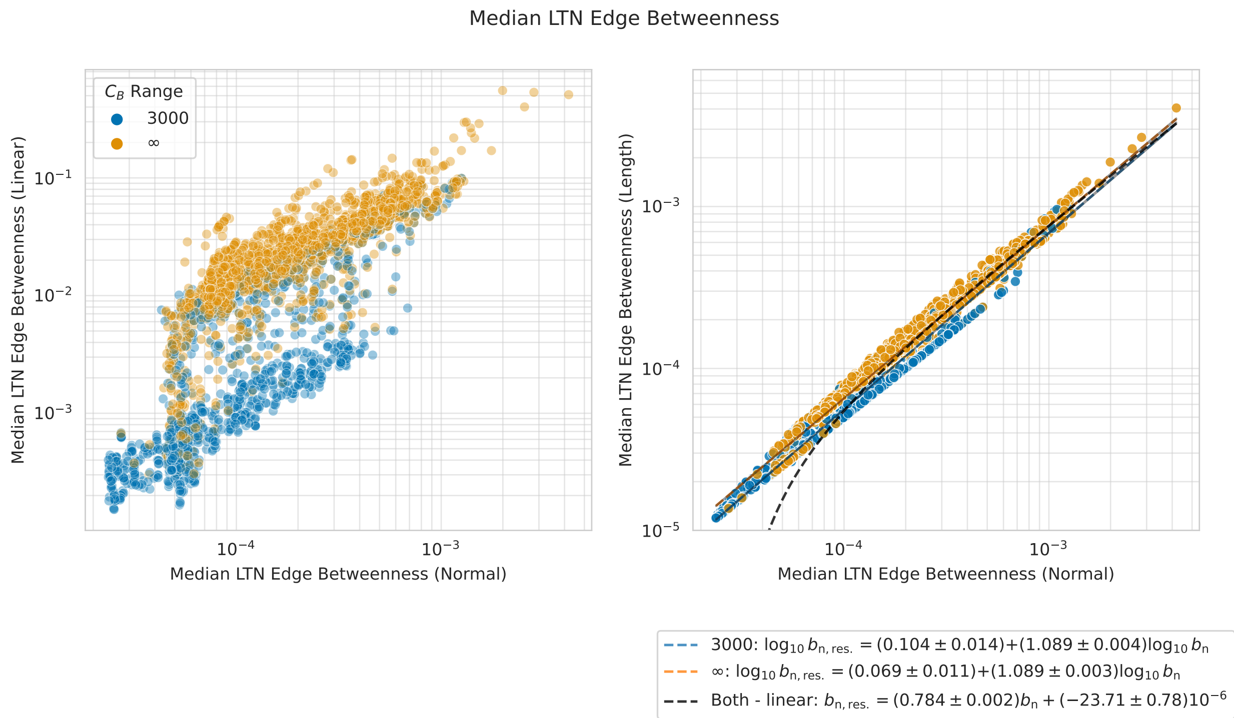

Figure 4.20: Comparison of the edge betweenness centrality types for the betweenness partitioner with the maximal path length set to 3 km and unbounded. The left scatter plot shows the normal, un-scaled edge C_B and the *linealy* scaled edge C_B. The right scatter plot shows the normal, un-scaled edge C_B and the *length* scaled edge C_B, additionally two ODR fits with uncertainties are shown.

The connection between the length scaled edge betweenness gets clearer. The exponent using the maximal path length of 3 km is 1.089 ± 0.004, for the unbounded approach 1.089 ± 0.003. To visualize this, a linear fit is shown in Fig. 4.20. Linerly scaled C_B values still show no clear connection to the normal C_B values for this construction of LTNs, and the resulting shortest paths.

By comparison of the linear fit, the average decrease of betweenness centrality to introducing the LTN restrictions are $(33 \pm 1)\,\%$ for the maximal path length of 3 km, and $(39 \pm 1)\,\%$ for the unbounded approach. This is a slightly larger improvement than the residential partitioner, which had an average decrease of $(26 \pm 3)\,\%$. In Fig. 4.21 we also show the averaged percentual change of edge betweenness in the LTNs by region and distance metric. Compared to the residential approach, there are more outliers of the boxplots. This might be due to the boundary cases introduced through the varied percentile p and C_B range, which was highlighted in the pyramid-like distribution of number of LTNs in Fig. 4.18. But generally, the unbounded approach results in a larger median decrease of betweenness centrality across all regions.

One central question of this thesis is whether LTN partitioning performance is dependent on the spatial order of the underlying city, namely average circuity ς and street orientation order ϕ. The correlation matrix in Fig. 4.22 shows no clear correlation between the performance metrics D and E_{glob} and the spatial order of the city. The largest cofficients are found for the residential partitioner

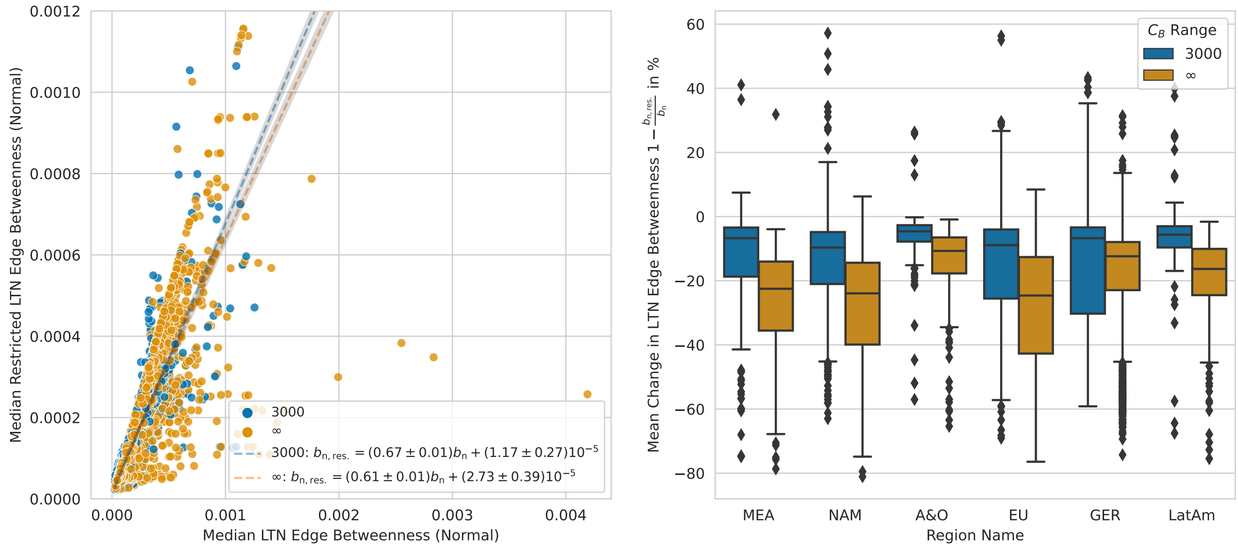

Figure 4.21: Comparison of the normal edge C_B before and after restricting the LTN of the betweenness partitioner (left), and a linear fit with uncertainties for each distance metric. Averaged percentual change of edge betweenness in the LTNs (right) by region and distance metric.

and the street orientation order ϕ with 24 % for the 100 global cities. The correlation is still weak, and from the actual distributions in Fig. 4.23 we can see that the correlation is not monotonic, and thus probably an artifact of the selection of cities. A full pairwise distribution plot of all metrics and spatial orders is shown in Fig. A.6.

4.5. Limitations

There are a few, but important limitations to this study. First, the residential partitioner approach uses the OpenStreetMap tags to identify residential streets. The completeness of the metadata is not given everywhere, or mapping is not consistent sometimes, and thus the residential partitioner approach is not applicable everywhere, but large cities are usually well mapped. But in this case, the approach using the betweenness centrality is still useful. Second, the circuity measure ς is dependent on the simplification algorithm. As the circuity is defined dependent on the graph representation, having nodes and edges, the simplification algorithm is decisive for the result. A simplification algorithm that removes many nodes and edges will result in a higher circuity. Optimally, there would be a quantity like the circuity that is independent of the simplification algorithm, or even better, independent of the graph representation. Another factor one should consider is the quality of the GHS-POP R2023A population dataset. We emphasize that the population density estimate is an approximation useful to gain insight of the population distribution inside a city and their LTNs. But it is not a tool to determine exact population densities. For the case of a city that wants to use this tool to get a first LTN partitioning, they can add more accurate raster data and use this tool without any problems, as the procedures under the hood are as exact as possible. Then, when calculating the metrics, we used an all-to-all demand, which is not realistic. To get more exact results, one

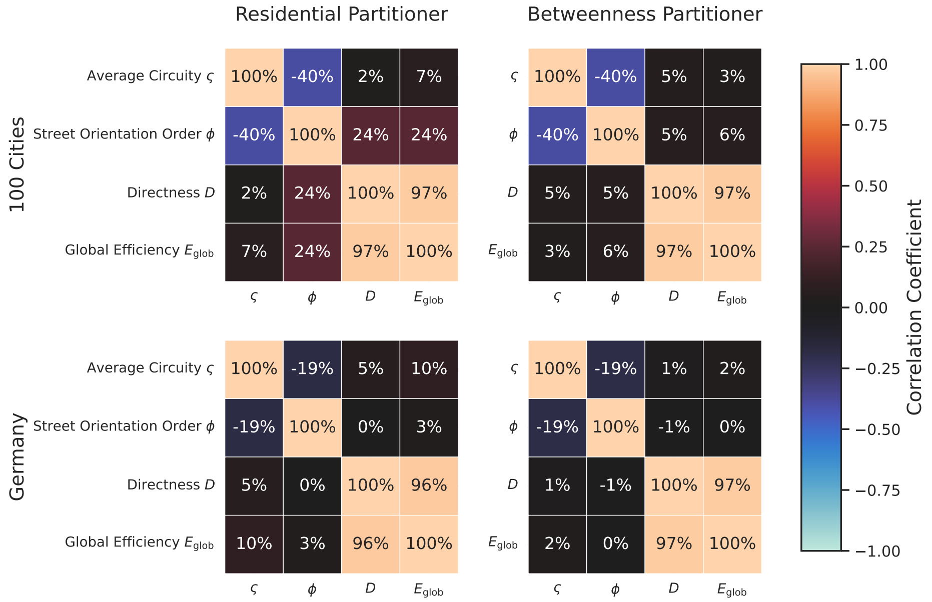

Figure 4.22: Pearson correlation coefficients between the performance metrics D and E_{glob} for the different partitioners and the different city sets. For all four combinations directness and global efficiency are highly correlated, but no special correlation with the spatial order of the city.

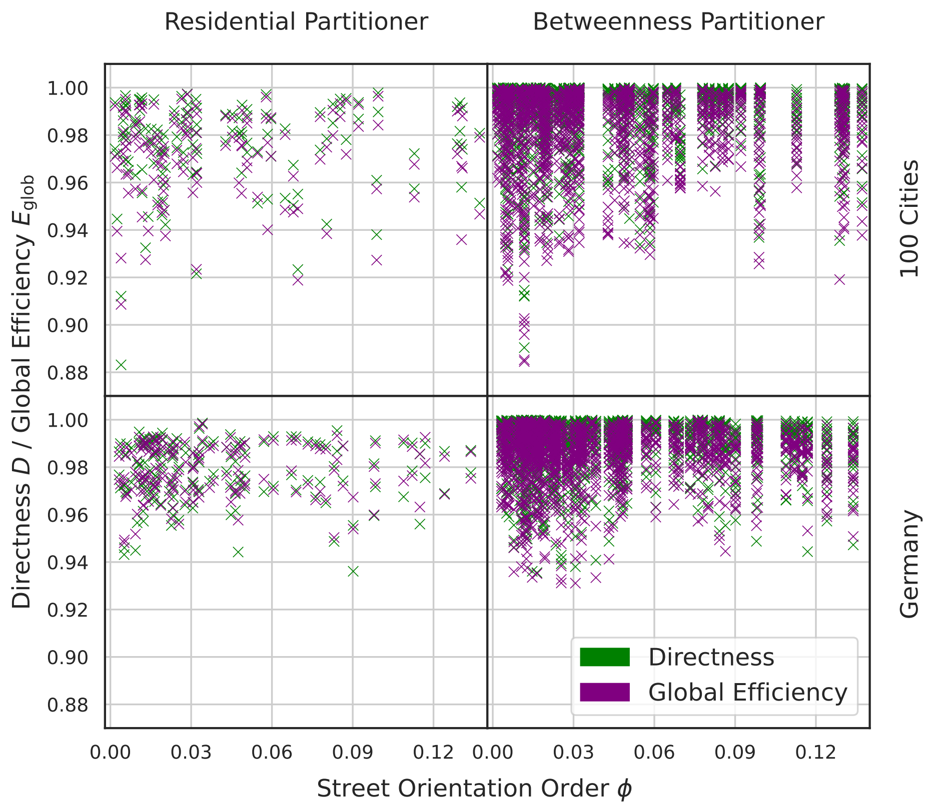

Figure 4.23: Distribution of directness D and global efficiency E_{glob} dependent on the street orientation order ϕ for the two approaches and the two city sets.

could weight the performance metrics (directness and global efficiency) with a concrete demand. The same can be done with the missing street capacities. In this study, we treated all streets with infinite capacity, as the distance metric disregarded any effect of congestion or higher order effects able to see with traffic modeling including the temporal dimension. Such street capacity can be integrated by rescaling the distance metric. A short street with small capacity can be rescaled to a longer street, this way our framework can be used to find LTNs that are more robust to congestion. Finally, we focused on private motorized traffic, but not everyone uses only the car to get around. Shared mobility, public transport and active mobility modes are not considered in this study, but must be included in coherent transport plans.

Nuestro lema era: "No vueles bajo, crea pensando en una ciudad donde no hay ninguna norma escrita". A partir de ahí se abre la creación y la generación en mayúsculas.

Our motto was: "Don't aim low. Create for a city where no rules are set in stone". This opens up a world of opportunities for creation and generation.

— Moisès Morató [ABÀ21]

5. Conclusion

The goal of this thesis was to investigate the potential of LTNs in cities, centered around the drivable road network. Two research questions were posed:

1. How does the travel time change if all neighborhoods were LTNs?
2. What LTN configuration can we suggest for different types of cities?

To answer these questions, we developed two methods to partition cities into LTNs. In that context, we mathematically defined requirements for LTNs, introduced a wide variety of relevant graph metrics, and developed an out-of-the-box solution for the LTN partitioning problem, called `cbueth/Superblockify`. With this tool, city planners can easily partition their city into LTNs and evaluate the results.

After evaluating the performance of the two partitioning methods on 100 global cities, and additionally, the largest 80 cities in Germany, we found a median directness $D = 97.3\,\%$ (80 % CI from 99.3 % to 81.4 %), and a median global efficiency $E_{\text{glob}} = 97.0\,\%$ (99.1 % to 78.8 %) for the approach using OSM residential tagged roads as LTNs. The betweenness-based approach performed slightly better with a median directness $D = 99.4\,\%$ (99.9 % to 97.1 %), and a median global efficiency $E_{\text{glob}} = 98.8\,\%$ (99.8 % to 96.2 %). More specifically, when implementing LTNs where the OSM map data already has residential roads, the median travel time would increase by only 2.7 % (0.7 % to 18.6 %) for the representative set of 100 global cities. This increase is if the LTN restrictions are respected by all road users. This answers question one.

We were able to achieve similar and even better results with the betweenness-based approach, without using the residential tag. For the actual implementation, this is an advantage if street use can be changed when implementing LTNs. But the cheaper LTN configurations are returned by the residential-based approach, as streets do not need to change their use. We were not able to find a dependency of the results on the spatial order of a city, especially the average circuity ς and street orientation order ϕ showed no correlation with the directness D or global efficiency E_{glob}. Answer for question two is, that any of the two approaches can be used, depending on the city's needs and the available resources. For some configurations of the betweenness-based approach, very large LTNs can be achieved, similar to large traffic islands. These might be impractical to implement for some cities, but also have their use in the context of other LTN concepts. In the flipbook appendix Appendix C, we show the LTN of a few experiments conducted. To get an idea of the partitioning behavior of the two approaches, we recommend navigating through the flipbook.

One functionality of the tool is to implement speed limits on the LTNs. During the analysis we discarded this functionality, as it does not return comparable performance results with as little influence as possible on the status quo. To give an opposing way of thinking, even with a coherent and dense bicycle network as Amsterdam already has, the city does not stop there. Amsterdam is implementing a city wide speed limit of 30 km/h which will be in effect by November 2023 [Gem21]. This is a important puzzle piece in many ways. It is not only safer for all road users, mitigates climate change. This fundamental approach to urban planning is necessary, as the city is expecting 250 000 new residents by 2050 [Jac23]. We also predict that having more LTNs will also increase the demand for cycling [Fos+23], even if the routes for cycling are not as direct as before, because such routes might be more pleasant to ride, which is shown to be as important as directness for route choice [Cho+23]. A possible extension of the tool is to analize each LTN for its included or reachable amenities. This would be a step towards the "15-minute city" concept [Mor+21; Mor; Alv22], where all amenities are reachable within 15 min by foot or bicycle.

References

[ABÀ21] Agència d'Ecologia Urbana de Barcelona, Barcelona Regional Agència de Desenvolupament Urbà, S.A., and Àrea Metropolitana de Barcelona. *BCNecologia: 20 años de la Agencia de Ecología Urbana de Barcelona*. Barcelona: Ajuntament de Barcelona, 2021. ISBN: 978-84-9156-349-5. URL: `http://hdl.handle.net/11703/122998`.

[AF19] Alessandro Araldi and Giovanni Fusco. "From the Street to the Metropolitan Region: Pedestrian Perspective in Urban Fabric Analysis". In: *Environ. Plan. B Urban Anal. City Sci.* 46.7 (Sept. 1, 2019), pp. 1243–1263. ISSN: 2399-8083. DOI: `10.1177/2399808319832612`.

[AF22] Daniel Arribas-Bel and Martin Fleischmann. "Spatial Signatures - Understanding (Urban) Spaces through Form and Function". In: *Habitat International* 128 (Oct. 2022), p. 102641. ISSN: 01973975. DOI: `10.1016/j.habitatint.2022.102641`.

[AG20] Rachel Aldred and Anna Goodman. "Low Traffic Neighbourhoods, Car Use, and Active Travel: Evidence from the People and Places Survey of Outer London Active Travel Interventions". In: *Findings* (Sept. 10, 2020). ISSN: 2652-8800. DOI: `10.32866/001c.17128`.

[AGL81] Donald Appleyard, M. Sue Gerson, and Mark Lintell. *Livable Streets*. Berkeley: University of California Press, 1981. 364 pp. ISBN: 978-0-520-03689-5.

[Ald+21] Rachel Aldred et al. "Equity in New Active Travel Infrastructure: A Spatial Analysis of London's New Low Traffic Neighbourhoods". In: *Journal of Transport Geography* 96 (Oct. 2021), p. 103194. ISSN: 09666923. DOI: `10.1016/j.jtrangeo.2021.103194`.

[Ali+21] Liaqat Ali et al. "Dynamics of Transit Oriented Development, Role of Greenhouse Gases and Urban Environment: A Study for Management and Policy". In: *Sustainability* 13.5 (5 Jan. 2021), p. 2536. ISSN: 2071-1050. DOI: `10.3390/su13052536`.

[Alv22] Nazaret Alvarez. *00b115-Minute City: Human-Centred Planning in Action*. 3. EIT Urban Mobility, Nov. 2022, p. 66. URL: `https://www.eiturbanmobility.eu/%C2%B115-minute-city-human-centred-planning-in-action/` (visited on 12/02/2022).

[App21] Bruce Appleyard. *Livable Streets 2.0*. 1st edition. Elsevier, Mar. 22, 2021. 1696 pp.

[Bar11] Marc Barthélemy. "Spatial Networks". In: *Physics Reports* 499.1 (Feb. 1, 2011), pp. 1–101. ISSN: 0370-1573. DOI: `10.1016/j.physrep.2010.11.002`.

[Bar22] Marc Barthelemy. *Spatial Networks: A Complete Introduction : From Graph Theory and Statistical Physics to Real-World Applications*. Cham: Springer, 2022. ISBN: 978-3-030-94105-5. DOI: `10.1007/978-3-030-94106-2`.

[BB18] Melissa Bruntlett and Chris Bruntlett. *Building the Cycling City: The Dutch Blueprint for Urban Vitality*. Illustrated edition. Washington, DC: Island Press, Aug. 28, 2018. 240 pp. ISBN: 978-1-61091-879-4.

[BB21] Melissa Bruntlett and Chris Bruntlett. *Curbing Traffic: The Human Case for Fewer Cars in Our Lives*. Washington: Island Press, 2021. ISBN: 978-1-64283-165-8.

[BCL23] Filip Biljecki, Yoong Shin Chow, and Kay Lee. "Quality of Crowdsourced Geospatial Building Information: A Global Assessment of OpenStreetMap Attributes". In: *Building and Environment* 237 (June 1, 2023), p. 110295. ISSN: 0360-1323. DOI: `10.1016/j.buildenv.2023.110295`.

[Boe17] Geoff Boeing. “OSMnx: New Methods for Acquiring, Constructing, Analyzing, and Visualizing Complex Street Networks”. In: *Computers, Environment and Urban Systems* 65 (Sept. 1, 2017), pp. 126–139. ISSN: 0198-9715. DOI: 10.1016/j.compenvurbsys.2017.05.004.

[Boe19a] Geoff Boeing. “The Morphology and Circuity of Walkable and Drivable Street Networks”. In: *The Mathematics of Urban Morphology.* Ed. by Luca D'Acci. Modeling and Simulation in Science, Engineering and Technology. Cham: Springer International Publishing, 2019, pp. 271–287. ISBN: 978-3-030-12381-9. DOI: 10.1007/978-3-030-12381-9_12.

[Boe19b] Geoff Boeing. “Urban Spatial Order: Street Network Orientation, Configuration, and Entropy”. In: *Appl Netw Sci* 4.1 (Dec. 2019), p. 67. ISSN: 2364-8228. DOI: 10.1007/s41109-019-0189-1.

[Boe22] Geoff Boeing. “Street Network Models and Indicators for Every Urban Area in the World”. In: *Geogr. Anal.* 54.3 (2022), pp. 519–535. ISSN: 1538-4632. DOI: 10.1111/gean.12281.

[Bos+23] Joris Van den Bossche et al. *Geopandas/Geopandas: V0.13.2.* Version v0.13.2. Zenodo, June 2023. DOI: 10.5281/zenodo.8009629.

[Bra08] Ulrik Brandes. “On Variants of Shortest-Path Betweenness Centrality and Their Generic Computation”. In: *Social Networks* 30.2 (May 1, 2008), pp. 136–145. ISSN: 0378-8733. DOI: 10.1016/j.socnet.2007.11.001.

[BS20] Pankaj Bajracharya and Selima Sultana. “Rank-Size Distribution of Cities and Municipalities in Bangladesh”. In: *Sustainability* 12.11 (11 Jan. 2020), p. 4643. ISSN: 2071-1050. DOI: 10.3390/su12114643.

[Büt23] Carlson Moses Büth. *Superblockify.* Version 0.2.2. July 2023. URL: https://github.com/cbueth/Superblockify.

[CB20] Beata Calka and Elzbieta Bielecka. “GHS-POP Accuracy Assessment: Poland and Portugal Case Study”. In: *Remote Sens.* 12.7 (7 Jan. 2020), p. 1105. ISSN: 2072-4292. DOI: 10.3390/rs12071105.

[Cer59] Ildefons Cerdà i Sunyer. *Proyecto de Ensanche de la Ciudad y su puerto aprobado por el gobierno de S.M.* 1859. URL: http://www.ub.edu/visitavirtual/visitavirtualEH/index.php/ca/coneix-la-universitat-de-barcelona/la-ciutat-al-segle-xix/l-eixample-i-l-edifici-historic/170-planol-del-projecte-cerda (visited on 06/14/2023).

[Cha+17] Sarah Chapman et al. “The Impact of Urbanization and Climate Change on Urban Temperatures: A Systematic Review”. In: *Landscape Ecol* 32.10 (Oct. 1, 2017), pp. 1921–1935. ISSN: 1572-9761. DOI: 10.1007/s10980-017-0561-4.

[Che22] Xiaofei Chen. *Supergrid and Superblock: Lessons in Urban Structure from China and Japan.* London: Routledge, Oct. 3, 2022. 256 pp. ISBN: 978-1-00-303719-4. DOI: 10.4324/9781003037194.

[Cho+23] Kuan-Yeh Chou et al. “Analysis of Cycling Accessibility Using Detour Ratios – A Large-Scale Study Based on Crowdsourced GPS Data”. In: *Sustainable Cities and Society* 93 (June 1, 2023), p. 104500. ISSN: 2210-6707. DOI: 10.1016/j.scs.2023.104500.

[CLP06] Paolo Crucitti, Vito Latora, and Sergio Porta. “Centrality in Networks of Urban Streets”. In: *Chaos: An Interdisciplinary Journal of Nonlinear Science* 16.1 (Mar. 31, 2006), p. 015113. ISSN: 1054-1500. DOI: 10.1063/1.2150162.

[Cra22] Christina E. Crawford. “2. From Garden Cities to Urban Superblocks”. In: *2. From Garden Cities to Urban Superblocks.* Cornell University Press, Jan. 31, 2022, pp. 49–82. ISBN: 978-1-5017-5921-5. DOI: 10.1515/9781501759215-006.

[DB23] Veronica Davis and Tamika L Butler. *Inclusive Transportation: A Manifesto for Repairing Divided Communities*. Washington: Island Press, July 13, 2023. 176 pp. ISBN: 978-1-64283-209-9.

[Dib+19] Jacob Dibble et al. “On the Origin of Spaces: Morphometric Foundations of Urban Form Evolution”. In: *Environment and Planning B: Urban Analytics and City Science* 46.4 (May 2019), pp. 707–730. ISSN: 2399-8083, 2399-8091. DOI: 10.1177/2399808317725075.

[Eec04] Jan Eeckhout. “Gibrat’s Law for (All) Cities”. In: *American Economic Review* 94.5 (Nov. 1, 2004), pp. 1429–1451. ISSN: 0002-8282. DOI: 10.1257/0002828043052303.

[Egg22a] Sven Eggimann. “Expanding Urban Green Space with Superblocks”. In: *Land Use Policy* 117 (June 1, 2022), p. 106111. ISSN: 0264-8377. DOI: 10.1016/j.landusepol.2022.106111.

[Egg22b] Sven Eggimann. “The Potential of Implementing Superblocks for Multifunctional Street Use in Cities”. In: *Nat Sustain* 5.5 (5 May 2022), pp. 406–414. ISSN: 2398-9629. DOI: 10.1038/s41893-022-00855-2.

[ERL22] Hanae El Gouj, Christian Rincón-Acosta, and Claire Lagesse. “Urban Morphogenesis Analysis Based on Geohistorical Road Data”. In: *Appl Netw Sci* 7.1 (1 Dec. 2022), pp. 1–26. ISSN: 2364-8228. DOI: 10.1007/s41109-021-00440-0.

[Fle+20] Martin Fleischmann et al. “Morphological Tessellation as a Way of Partitioning Space: Improving Consistency in Urban Morphology at the Plot Scale”. In: *Computers, Environment and Urban Systems* 80 (Mar. 1, 2020), p. 101441. ISSN: 0198-9715. DOI: 10.1016/j.compenvurbsys.2019.101441.

[Fle+23] Martin Fleischmann et al. *Pysal/Momepy: Version v0.6.0*. Version v0.6.0. Zenodo, May 2023. DOI: 10.5281/zenodo.7884363.

[Fon+17] Cidália Costa Fonte et al. “Assessing VGI Data Quality”. In: *Ubiquity Press* (Sept. 11, 2017). DOI: 10.5334/bbf.g.

[Fos+23] Mogens Fosgerau et al. “Bikeability and the Induced Demand for Cycling”. In: *Proc. Natl. Acad. Sci.* 120.16 (Apr. 18, 2023), e2220515120. DOI: 10.1073/pnas.2220515120.

[FRP21] Martin Fleischmann, Ombretta Romice, and Sergio Porta. “Measuring Urban Form: Overcoming Terminological Inconsistencies for a Quantitative and Comprehensive Morphologic Analysis of Cities”. In: *Environment and Planning B: Urban Analytics and City Science* 48.8 (Oct. 2021), pp. 2133–2150. ISSN: 2399-8083, 2399-8091. DOI: 10.1177/2399808320910444.

[GA21] Anna Goodman and Rachel Aldred. “The Impact of Introducing a Low Traffic Neighbourhood on Street Crime, in Waltham Forest, London”. In: *Findings* (Feb. 16, 2021). DOI: 10.32866/001c.19414.

[Gem21] Gemeente Amsterdam, Verkeer en Openbare ruimte. *30 km/u in de stad*. Amsterdam.nl. Dec. 23, 2021. URL: https://www.amsterdam.nl/30km/ (visited on 06/02/2023).

[GH20] Xin Ge and Dongqing Han. “Sustainability-Oriented Configurational Analysis of the Street Network of China’s Superblocks: Beyond Marshall’s Model”. In: *Frontiers of Architectural Research* 9.4 (Dec. 1, 2020), pp. 858–871. ISSN: 2095-2635. DOI: 10.1016/j.foar.2020.07.001.

[Gib31] R. Gibrat. “Les Inegalits Economiques”. In: *Sirey* (1931). URL: https://cir.nii.ac.jp/crid/1573950399584830336.

[Gil+23] Sean Gillies et al. *Shapely*. Version 2.0.1. Zenodo, Jan. 2023. DOI: 10.5281/zenodo.7583915.

[Goo+21] Anna Goodman et al. "The Impact of 2020 Low Traffic Neighbourhoods on Fire Service Emergency Response Times, in London, UK". In: *Findings* (May 11, 2021). ISSN: 2652-8800. DOI: 10.32866/001c.23568.

[Gra23] Henry Grabar. *Paved Paradise: How Parking Explains the World.* New York: Penguin Press, May 9, 2023. 368 pp. ISBN: 978-1-984881-13-7.

[Grä23] Grätzl-Blattl. *Ein Langer Weg.* 2023. URL: https://graetzl-blattl.at/zeitung/pilotstudie-supergraetzl-volkertviertel (visited on 04/28/2023).

[GUA20] Anna Goodman, Scott Urban, and Rachel Aldred. "The Impact of Low Traffic Neighbourhoods and Other Active Travel Interventions on Vehicle Ownership: Findings from the Outer London Mini-Holland Programme". In: *Findings* (Dec. 9, 2020). ISSN: 2652-8800. DOI: 10.32866/001c.18200.

[Hor23] Ulrik Frees Horneman. "Enhedslisten i nyt udspil: Biler skal have mindre plads på københavnske veje". In: *TV 2 Kosmopol. Trafik* (June 6, 2023). URL: https://www.tv2kosmopol.dk/koebenhavn/enhedslisten-i-nyt-udspil-biler-skal-have-mindre-plads-paa-koebenhavnske-veje (visited on 06/14/2023).

[How98] E. Howard. *To-Morrow: A Peaceful Path to Real Reform.* London: Swan Sonnenschein & Co., Ltd., 1898. ISBN: 978-0-262-58002-1.

[HSS08] Aric A. Hagberg, Daniel A. Schult, and Pieter J. Swart. "Exploring Network Structure, Dynamics, and Function Using NetworkX". In: *Proc. 7th Python Sci. Conf.* Ed. by Gaël Varoquaux, Travis Vaught, and Jarrod Millman. Pasadena, CA USA, 2008, pp. 11–15.

[HZN15] Hartwig H. Hochmair, Dennis Zielstra, and Pascal Neis. "Assessing the Completeness of Bicycle Trail and Lane Features in OpenStreetMap for the United States". In: *Trans. GIS* 19.1 (2015), pp. 63–81. ISSN: 1467-9671. DOI: 10.1111/tgis.12081.

[Jac23] Sarah Jacob. "Amsterdam Makes a New Push to Keep Cars Out". In: *Bloomberg.com* (Apr. 4, 2023). URL: https://www.bloomberg.com/news/articles/2023-04-04/drowning-in-traffic-amsterdam-proposes-new-car-restrictions (visited on 06/02/2023).

[Jok+15] Jokar Arsanjani Jamal et al. *OpenStreetMap in GIScience Experiences, Research, and Applications.* 1st ed. 2015. Lecture Notes in Geoinformation and Cartography. Cham: Springer International Publishing, 2015. 324 pp. ISBN: 978-3-319-14280-7. DOI: 10.1007/978-3-319-14280-7.

[Kir+18] Alec Kirkley et al. "From the Betweenness Centrality in Street Networks to Structural Invariants in Random Planar Graphs". In: *Nat Commun* 9.1 (Dec. 2018), p. 2501. ISSN: 2041-1723. DOI: 10.1038/s41467-018-04978-z.

[Køb23] Københavns Kommune. *Principaftale om budget 2024 og 2025.* June 6, 2023. URL: https://www.kk.dk/politik/budget-og-regnskab/principaftale-om-budget-2024-og-2025 (visited on 06/14/2023).

[KR09] Lamia Kamal-Chaoui and Alexis Robert. *Competitive Cities and Climate Change.* Paris: OECD, Dec. 15, 2009. DOI: 10.1787/218830433146.

[Kra+16] F. Kraas et al. *Humanity on the Move: Unlocking the Transformative Power of Cities.* Berlin: WBGU - German Advisory Council on Global Change, Aug. 2016. ISBN: 978-3-936191-45-5. URL: http://www.wbgu.de/en/flagship-reports/fr-2016-urbanization/ (visited on 06/11/2023).

[Kre+04] Holger Krekel et al. *Pytest 7.4*. 2004. URL: `https://github.com/pytest-dev/pytest`.

[Kuf+22] Monika Kuffer et al. "The Missing Millions in Maps: Exploring Causes of Uncertainties in Global Gridded Population Datasets". In: *ISPRS Int. J. Geo-Inf.* 11.7 (7 July 2022), p. 403. ISSN: 2220-9964. DOI: `10.3390/ijgi11070403`.

[KV04] Samuel Kotz and Johan René Van Dorp. "The Triangular Distribution". In: *Beyond Beta: Other Continuous Families of Distributions with Bounded Support and Applications*. WORLD SCIENTIFIC, Dec. 2004, pp. 1–32. ISBN: 978-981-256-115-2. DOI: `10.1142/9789812701282_0001`.

[KVK23] Do Ngoc Khanh, Alvin C. G. Varquez, and Manabu Kanda. "Impact of Urbanization on Exposure to Extreme Warming in Megacities". In: *Heliyon* 9.4 (Apr. 1, 2023), e15511. ISSN: 2405-8440. DOI: `10.1016/j.heliyon.2023.e15511`.

[LA04] Chris Lattner and Vikram Adve. "LLVM: A Compilation Framework for Lifelong Program Analysis & Transformation". In: *Proc. 2004 Int. Symp. Code Gener. Optim. CGO04*. Palo Alto, California, Mar. 2004.

[Lag15] Claire Lagesse. "Lire les Lignes de la Ville". PhD thesis. Universite Paris Diderot-Paris VII, Sept. 25, 2015. URL: `https://shs.hal.science/tel-01245898` (visited on 06/15/2023).

[LAG21] Anthony A Laverty, Rachel Aldred, and Anna Goodman. "The Impact of Introducing Low Traffic Neighbourhoods on Road Traffic Injuries". In: *Findings* (Jan. 11, 2021). ISSN: 2652-8800. DOI: `10.32866/001c.18330`.

[Lam+23] Siu Kwan Lam et al. *Numba/Numba: Version 0.57.1*. Version 0.57.1. Zenodo, June 2023. DOI: `10.5281/zenodo.8087361`.

[LB14] Rémi Louf and Marc Barthelemy. "A Typology of Street Patterns". In: *J. R. Soc. Interface* 11.101 (Dec. 6, 2014), p. 20140924. DOI: `10.1098/rsif.2014.0924`.

[Łc] Langa Łukasz and contributors to Black. *Black: The Uncompromising Python Code Formatter*. Version 1.2.0. URL: `https://black.readthedocs.io/en/stable/`.

[Ley+18] Stefan Leyk et al. "Assessing the Accuracy of Multi-Temporal Built-up Land Layers across Rural-Urban Trajectories in the United States". In: *Remote Sensing of Environment* 204 (Jan. 1, 2018), pp. 898–917. ISSN: 0034-4257. DOI: `10.1016/j.rse.2017.08.035`.

[LM01] Vito Latora and Massimo Marchiori. "Efficient Behavior of Small-World Networks". In: *Phys. Rev. Lett.* 87.19 (Oct. 17, 2001), p. 198701. DOI: `10.1103/PhysRevLett.87.198701`.

[Mai22] Minjung Maing. "Superblock Transformation in Seoul Megacity: Effects of Block Densification on Urban Ventilation Patterns". In: *Landscape and Urban Planning* 222 (June 1, 2022), p. 104401. ISSN: 0169-2046. DOI: `10.1016/j.landurbplan.2022.104401`.

[Mar21] Robert Joseph Martin. *Points of Exchange: Spatial Strategies for the Transition Towards Sustainable Urban Mobilities*. Ph.d.-Serien for Det Tekniske Fakultet for IT Og Design, Aalborg Universitet. Aalborg Universitetsforlag, 2021. URL: `https://vbn.aau.dk/en/publications/points-of-exchange-spatial-strategies-for-the-transition-towards-`.

[Mas+15] A. Paolo Masucci et al. "On the Problem of Boundaries and Scaling for Urban Street Networks". In: *J. R. Soc. Interface* 12.111 (Oct. 6, 2015), p. 20150763. DOI: `10.1098/rsif.2015.0763`.

[Mon14] Charles Montgomery. *Happy City: Transforming Our Lives Through Urban Design*. Reprint edition. New York: Farrar, Straus and Giroux, Oct. 7, 2014. 368 pp. ISBN: 978-0-374-53488-2.

[Mor] Carlos Moreno. *Carlos Moreno: The 15-Minute City | TED Talk*. URL: https://www.ted.com/talks/carlos_moreno_the_15_minute_city (visited on 03/03/2023).

[Mor+21] Carlos Moreno et al. "Introducing the "15-Minute City": Sustainability, Resilience and Place Identity in Future Post-Pandemic Cities". In: *Smart Cities* 4.1 (Jan. 8, 2021), pp. 93–111. ISSN: 2624-6511. DOI: 10.3390/smartcities4010006.

[Mue+20] Natalie Mueller et al. "Changing the Urban Design of Cities for Health: The Superblock Model". In: *Environment International* 134 (Jan. 2020), p. 105132. ISSN: 01604120. DOI: 10.1016/j.envint.2019.105132.

[NBC23] Vinicius M Netto, Edgardo Brigatti, and Caio Cacholas. "From Urban Form to Information: Cellular Configurations in Different Spatial Cultures". In: *Environ. Plan. B Urban Anal. City Sci.* 50.1 (Jan. 1, 2023), pp. 146–161. ISSN: 2399-8083. DOI: 10.1177/23998083221107382.

[Nel22] Samuel Nello-Deakin. "Exploring Traffic Evaporation: Findings from Tactical Urbanism Interventions in Barcelona". In: *Case Studies on Transport Policy* 10.4 (Dec. 1, 2022), pp. 2430–2442. ISSN: 2213-624X. DOI: 10.1016/j.cstp.2022.11.003.

[Nie+19] Mark Nieuwenhuijsen et al. "Implementing Car-Free Cities: Rationale, Requirements, Barriers and Facilitators". In: *Integrating Human Health into Urban and Transport Planning*. Ed. by Mark Nieuwenhuijsen and Haneen Khreis. Cham: Springer International Publishing, 2019, pp. 199–219. ISBN: 978-3-319-74983-9. DOI: 10.1007/978-3-319-74983-9_11.

[Ope23] OpenStreetMap contributors. *OpenStreetMap*. 2023. URL: https://www.openstreetmap.org.

[OS12] Atsuyuki Okabe and Kōkichi Sugihara. "Network Voronoi Diagrams". In: *Spatial Analysis along Networks: Statistical and Computational Methods*. John Wiley & Sons, Ltd, 2012, pp. 81–100. ISBN: 978-1-119-96710-1. DOI: 10.1002/9781119967101.ch4.

[Par+23] I. P. Gustave S. Pariartha et al. "Compounding Effects of Urbanization, Climate Change and Sea-Level Rise on Monetary Projections of Flood Damage". In: *Journal of Hydrology* 620 (May 1, 2023), p. 129535. ISSN: 0022-1694. DOI: 10.1016/j.jhydrol.2023.129535.

[PP23] Martino Pesaresi and Panagiotis Politis. *GHS-BUILT-S R2023A - GHS Built-up Surface Grid, Derived from Sentinel2 Composite and Landsat, Multitemporal (1975-2030)*. European Commission, Joint Research Centre (JRC), 2023. DOI: 10.2905/9F06F36F-4B11-47EC-ABB0-4F8B7B1D72EA.

[Rip+20] William J Ripple et al. "World Scientists' Warning of a Climate Emergency". In: *BioScience* 70.1 (Jan. 1, 2020), pp. 8–12. ISSN: 0006-3568. DOI: 10.1093/biosci/biz088.

[Rip+22] William J Ripple et al. "World Scientists' Warning of a Climate Emergency 2022". In: *BioScience* 72.12 (Dec. 1, 2022), pp. 1149–1155. ISSN: 0006-3568. DOI: 10.1093/biosci/biac083.

[RR18] Hannah Ritchie and Max Roser. "Urbanization". In: *Our World in Data* (June 13, 2018). URL: https://ourworldindata.org/urbanization (visited on 06/02/2023).

[Rue19] Salvador Rueda. "Superblocks for the Design of New Cities and Renovation of Existing Ones: Barcelona's Case". In: *Integrating Human Health into Urban and Transport Planning: A Framework*. Ed. by Mark Nieuwenhuijsen and Haneen Khreis. Cham: Springer International Publishing, 2019, pp. 135–153. ISBN: 978-3-319-74983-9. DOI: 10.1007/978-3-319-74983-9_8.

[Sab+23] Arash Saboori et al. "Comparison of Life Cycle Greenhouse Gas Emissions and Energy Consumption between Complete Streets vs. Conventional Streets". In: *Pavement, Roadway, and Bridge Life Cycle Assessment 2020*. Red. by John Harvey et al. 1st ed. CRC Press, 2023. ISBN: 978-1-00-309227-8. DOI: 10.1201/9781003092278.

[Sat08] David Satterthwaite. “Climate Change and Urbanization: Effects and Implications for Urban Governance”. In: *U. N. Expert Group Meet. Popul. Distrib. Urban. Intern. Migr. Dev.* Vol. 24. United Nations – DESA New York, 2008, pp. 340–363.

[Sat09] David Satterthwaite. “The Implications of Population Growth and Urbanization for Climate Change”. In: *Environ. Urban.* 21.2 (Oct. 1, 2009), pp. 545–567. ISSN: 0956-2478. DOI: 10.1177/0956247809344361.

[SFM23] Marcello Schiavina, Sergio Freire, and Kytt MacManus. *GHS-POP R2023A - GHS Population Grid Multitemporal (1975-2030).* European Commission, Joint Research Centre (JRC), Apr. 25, 2023. DOI: 10.2905/2FF68A52-5B5B-4A22-8F40-C41DA8332CFE.

[Shp22] Ermal Shpuza. “The Shape and Size of Urban Blocks”. In: *Environment and Planning B: Urban Analytics and City Science* (May 17, 2022), p. 239980832210987. ISSN: 2399-8083, 2399-8091. DOI: 10.1177/23998083221098744.

[Sim21] John Simmerman. *Episode 78 • Season 2: Livable Streets 2.0 w/ Bruce Appleyard.* In collab. with Bruce Appleyard. June 1, 2021. URL: https://www.activetowns.org/2021/06/10/livable-streets-2-0/ (visited on 06/02/2023).

[SP23] Yacheng Song and Yueting Pang. “Measuring the Superblock Based on a Hierarchy Matrix of Geometry, Configuration, Network, and Area: The Case of Nanjing”. In: *Environ. Plan. B Urban Anal. City Sci.* 50.4 (May 1, 2023), pp. 1057–1071. ISSN: 2399-8083. DOI: 10.1177/23998083221133393.

[Spe13] Jeff Speck. *Walkable City: How Downtown Can Save America, One Step at a Time.* Reprint edition. New York: North Point Press, Nov. 12, 2013. 320 pp. ISBN: 978-0-86547-772-8.

[Spe18] Jeff Speck. *Walkable City Rules: 101 Steps to Making Better Places.* 3rd edition. Washington, DC: Island Press, Oct. 15, 2018. 312 pp. ISBN: 978-1-61091-898-5.

[Sta21] Stadt Wien. *Pilotstudie Supergrätzl - Ergebnisbericht Am Beispiel Volkertviertel.* GZ 367568. Vienna: Stadt Wien - Stadtentwicklung und Stadtplanung, Nov. 24, 2021, p. 58.

[Sta22] Statistisches Bundesamt (Destatis). *Städte (Alle Gemeinden mit Stadtrecht) nach Fläche, Bevölkerung und Bevölkerungsdichte am 31.12.2021.* 2022. URL: https://www.destatis.de/DE/Themen/Laender-Regionen/Regionales/Gemeindeverzeichnis/Administrativ/05-staedte.html (visited on 07/04/2023).

[Sus] Sustrans. *An Introductory Guide to Low Traffic Neighbourhood Design.* Sustrans. URL: https://www.sustrans.org.uk/for-professionals/infrastructure/an-introductory-guide-to-low-traffic-neighbourhood-design/ (visited on 10/24/2022).

[Sze+22] Michael Szell et al. “Growing Urban Bicycle Networks”. In: *Sci Rep* 12.1 (1 Apr. 26, 2022), p. 6765. ISSN: 2045-2322. DOI: 10.1038/s41598-022-10783-y.

[SZH21] Yacheng Song, Ye Zhang, and Dongqing Han. “Access Structure”. In: *Environ. Plan. B Urban Anal. City Sci.* 48.9 (Nov. 1, 2021), pp. 2808–2826. ISSN: 2399-8083. DOI: 10.1177/2399808320988560.

[Tra20] Transport for London. *Streetspace Guidance: Appendix Six (a): Supplementary Guidance on Low Traffic Neighbourhoods.* June 2020. URL: https://tfl.gov.uk/info-for/boroughs-and-communities/streetspace-funding (visited on 03/07/2023).

[VLD05] I. Vragović, E. Louis, and A. Díaz-Guilera. “Efficiency of Informational Transfer in Regular and Complex Networks”. In: *Phys. Rev. E* 71.3 (Mar. 18, 2005), p. 036122. DOI: 10.1103/PhysRevE.71.036122.

[VVS23] Ane Rahbek Vierø, Anastassia Vybornova, and Michael Szell. *BikeDNA: A Tool for Bicycle Infrastructure Data & Network Assessment*. Mar. 2, 2023. DOI: 10.48550/arXiv.2303.01223. preprint.

[Wan15] Jiaqiu Wang. "Resilience of Self-Organised and Top-Down Planned Cities—A Case Study on London and Beijing Street Networks". In: *PLOS ONE* 10.12 (Dec. 18, 2015), e0141736. ISSN: 1932-6203. DOI: 10.1371/journal.pone.0141736.

[Wil23] Ben Wilson. *Urban Jungle: Nature and the City from the Stone Age to the Climate Emergency*. JONATHAN CAPE & BH - TRADE, June 13, 2023. 320 pp. ISBN: 978-1-78733-314-7.

[Xin+22] Qian Xing et al. "Projections of Future Temperature-Related Cardiovascular Mortality under Climate Change, Urbanization and Population Aging in Beijing, China". In: *Environment International* 163 (May 1, 2022), p. 107231. ISSN: 0160-4120. DOI: 10.1016/j.envint.2022.107231.

[ZC] Tobias Zwick and Contributors to StreetComplete. *StreetComplete*. URL: https://github.com/streetcomplete/StreetComplete (visited on 06/15/2023).

[ZF23] S. Roderick Zhang and Bilal Farooq. "Interpretable and Actionable Vehicular Greenhouse Gas Emission Prediction at Road Link-Level". In: *Sustainable Cities and Society* 92 (May 1, 2023), p. 104493. ISSN: 2210-6707. DOI: 10.1016/j.scs.2023.104493.

[ZHN13] Dennis Zielstra, Hartwig H. Hochmair, and Pascal Neis. "Assessing the Effect of Data Imports on the Completeness of OpenStreetMap – A United States Case Study". In: *Trans. GIS* 17.3 (2013), pp. 315–334. ISSN: 1467-9671. DOI: 10.1111/tgis.12037.

A. Further Analysis Plots

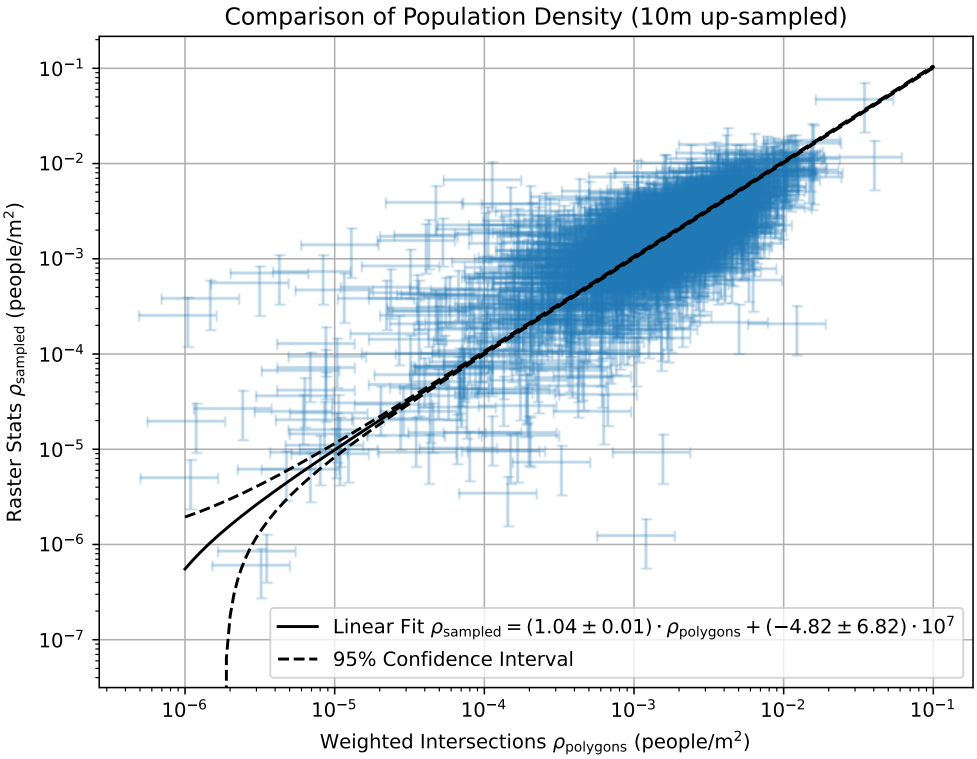

Figure A.1: Comparison of the cell population results from our result to using the **up-sampled** rasterstats approach, for the case study of La Crosse, Wisconsin, USA. Upsampling the GHSL raster by a factor of 10 in both spatial dimensions reduces the overestimation of the rasterstats approach.

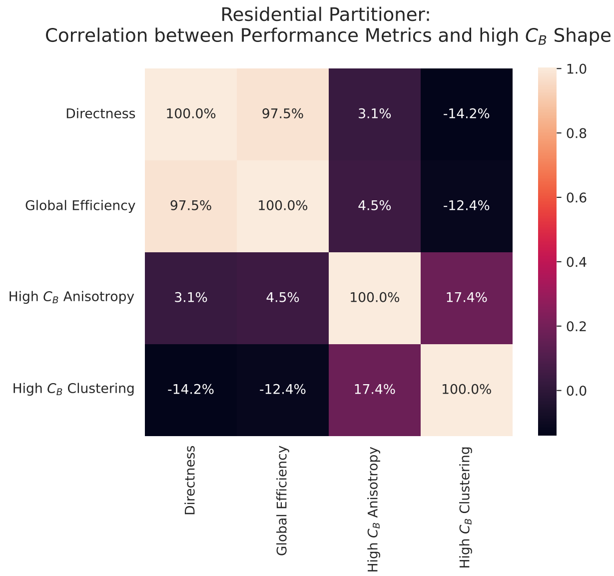

Figure A.2: Correlation matrix of the performance metrics and high C_B distribution shape for the residential partitioner. Per se, the performance metrics do not show a clear correlation with the high C_B distribution shape.

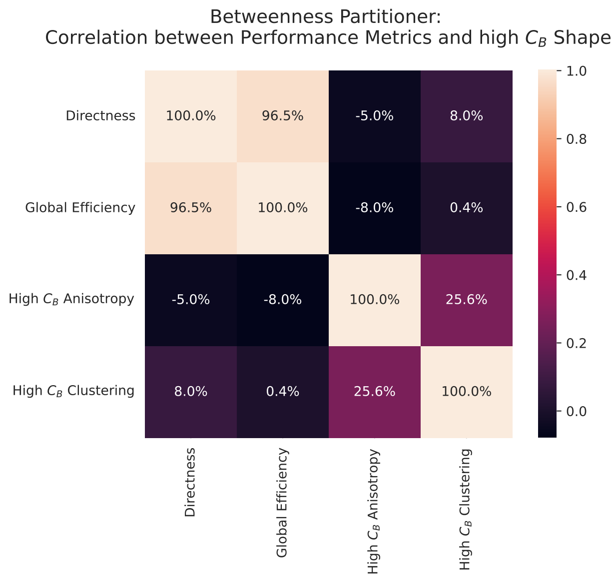

Figure A.3: Correlations between the performance metrics and high C_B distribution shape for the results of the betweenness partitioner. Correlations are qualitatively similar to the results of the residential partitioner (Fig. A.2).

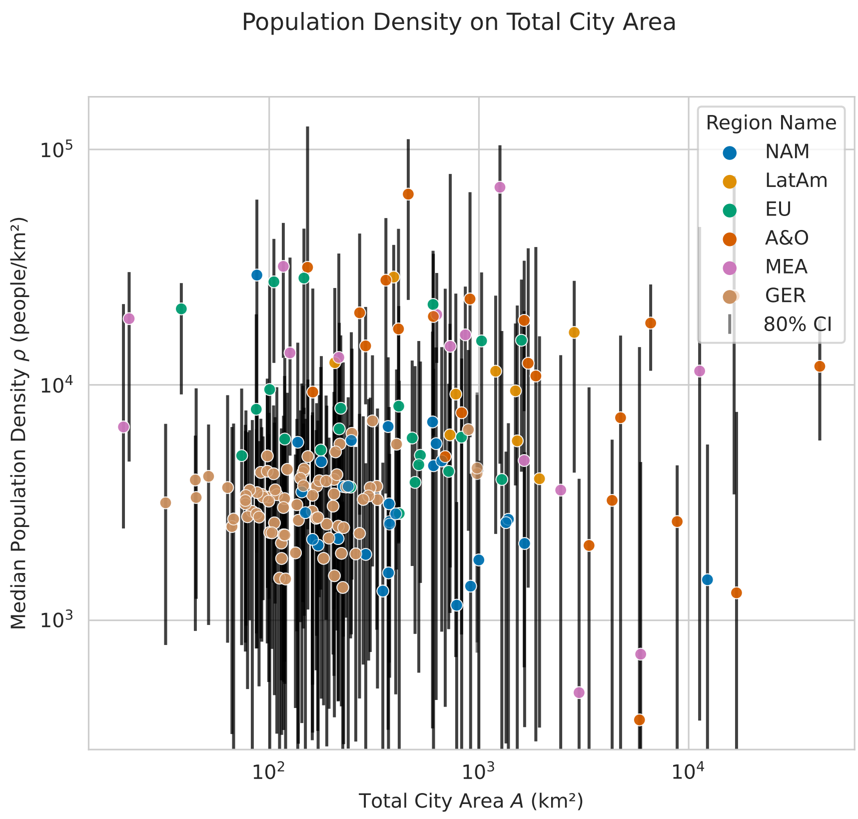

Figure A.4: Population density ρ by the total city area A for each of the 100 global cities. No clear trend can be observed.

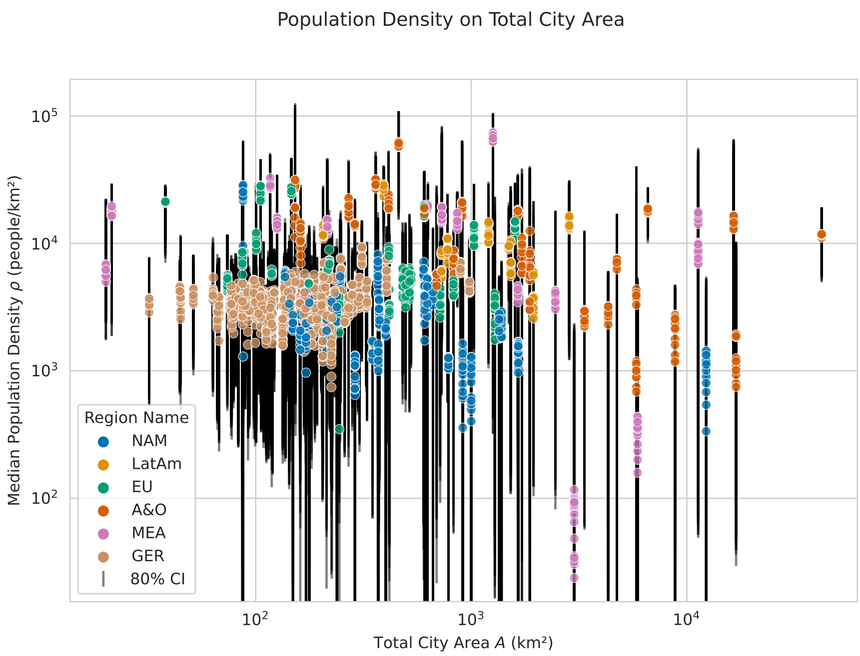

Figure A.5: Population density ρ by the total city area A for each of the 80 German cities. No clear trend can be observed.

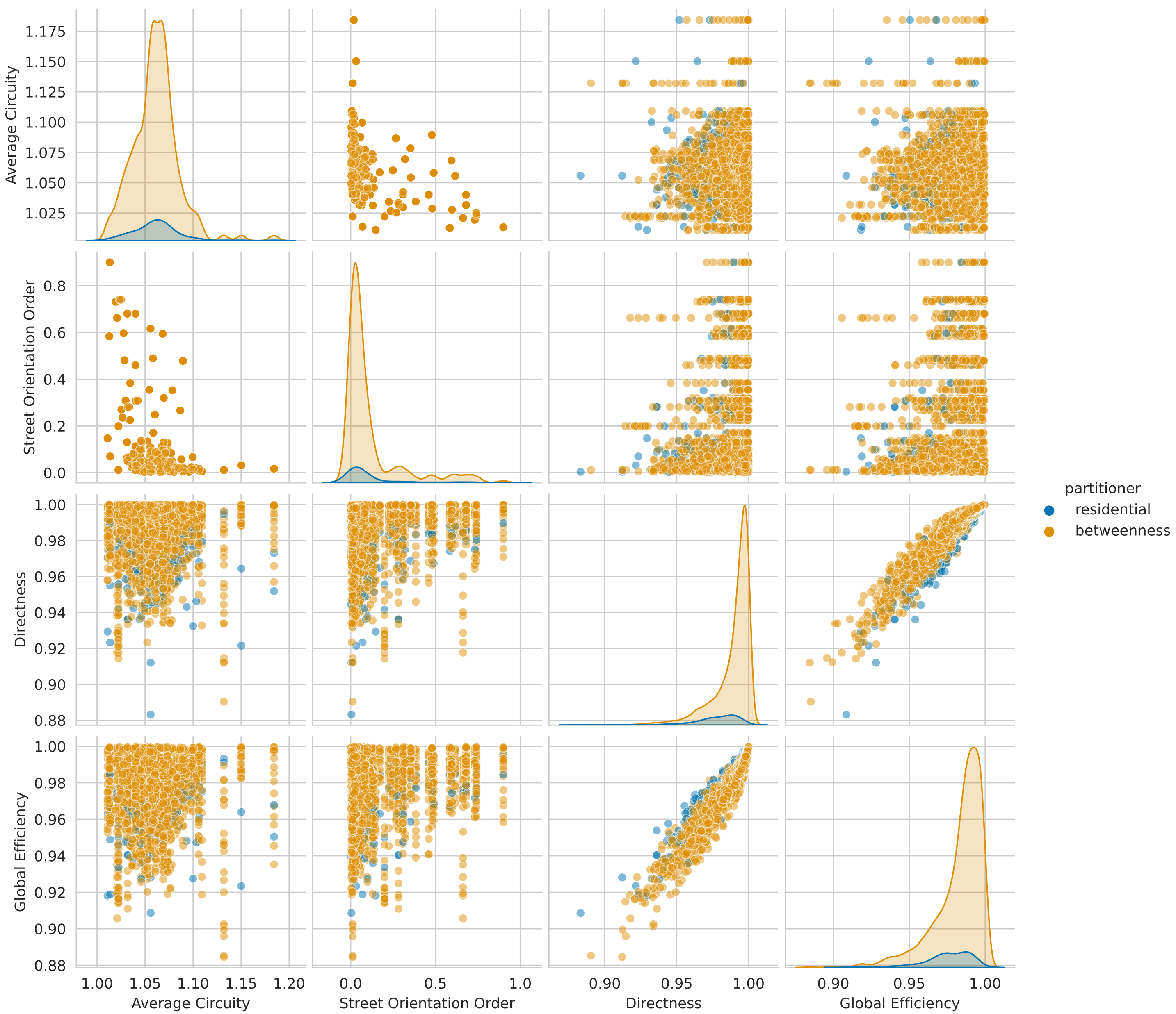

Figure A.6: Pairwise distribution plot of average circuity ς and street orientation order ϕ by the performance metrics for the residential and betweenness approach.

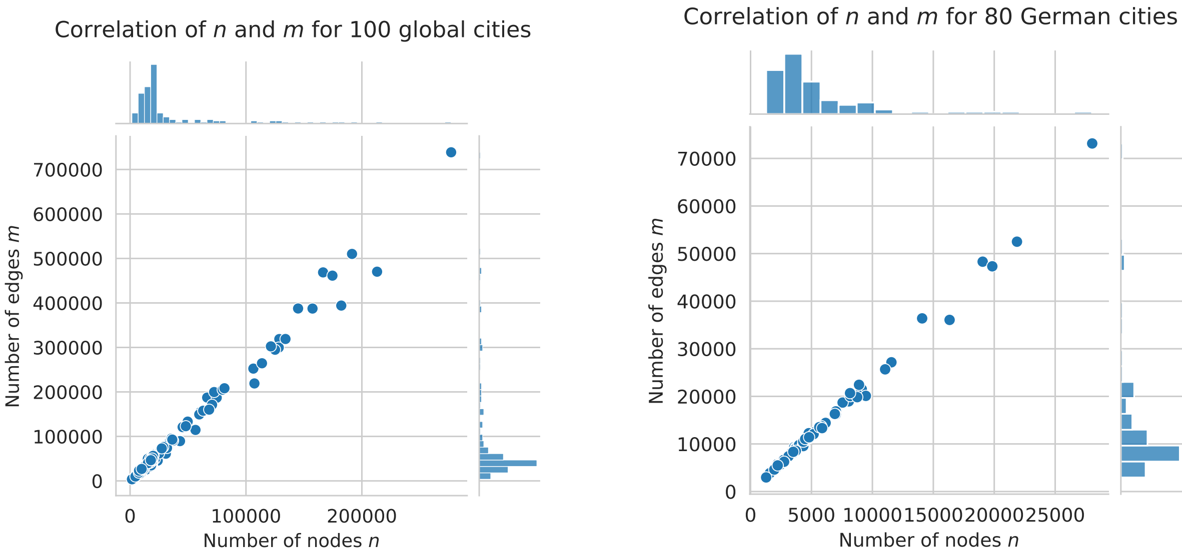

Figure A.7: The correlation between number of edges scales linearly with the number of nodes in both the global and the German list of cities.

B. Cities

Table 3: Overview of the first 100 city set used in this study, as chosen by [Boe19b]. For each city, general stats are listed: number of nodes n and number of edges m in the OSM graph, average node degree $\overline{k}$, total edge length L, average circuity ς, street orientation order ϕ, nominal value of the population approximation p_{GHSL} using [SFM23], city area A, and population density ρ. For the reduced graphs, the summarizing statistics are listed under the respective city, marked with "$\hookrightarrow$".

Region	City	n	m	$\overline{k}$	L 10^6m	ς	ϕ	p_{GHSL} (inh.)	A (km^2)	ρ $\left(\frac{10^3\text{inh.}}{\text{km}^2}\right)$
AO	**Bangkok**	182 218	394 089	4.33	34.19	1.06	0.092	12 342 851	1643	7.51
	$\hookrightarrow$	16 861	34 770	4.12	3.69	1.06	0.093	2 122 987	138	15.31
	Beijing	128 781	318 841	4.95	76.99	1.09	.266	24 149 290	16 913	1.43
	$\hookrightarrow$	17 414	41 891	4.81	13.99	1.08	0.230	3 431 286	3592	0.96
	Hanoi	157 409	387 387	4.92	42.53	1.06	0.004	7 412 688	3349	2.21
	$\hookrightarrow$	18 832	46 076	4.89	5.51	1.05	0.026	572 503	416	1.37
	Hong Kong	3012	5588	3.71	0.71	1.13	0.012	1 220 949	152	8.01
	Jakarta	106 363	252 393	4.75	18.26	1.06	0.171	11 342 187	6589	1.72
	$\hookrightarrow$	17 509	39 039	4.46	3.03	1.06	0.188	1 837 297	105	17.36
	Kabul	24 800	64 135	5.17	6.47	1.04	0.080	5 656 560	360	15.71
	$\hookrightarrow$	19 349	49 349	5.10	4.88	1.04	0.062	4 657 675	188	24.77
	Karachi	166 527	468 658	5.63	37.15	1.03	0.068	21 243 358	5827	3.65
	$\hookrightarrow$	18 154	48 954	5.39	5.88	1.05	0.272	702 146	646	1.09
	Kathmandu	19 269	48 251	5.01	4.98	1.15	0.032	3 008 734	413	7.28
	Kyoto	45 341	120 940	5.33	8.26	1.08	0.353	1 270 597	827	1.54
	$\hookrightarrow$	19 156	50 394	5.26	3.79	1.09	0.337	519 979	342	1.52
	Manila	60 498	154 096	5.09	13.92	1.05	0.032	13 751 861	906	15.17
	$\hookrightarrow$	17 881	43 218	4.83	4.56	1.04	0.013	4 570 738	198	23.04
	Melbourne	213 130	470 228	4.41	57.66	1.06	0.249	5 378 918	8816	0.61
	$\hookrightarrow$	18 483	38 867	4.21	4.73	1.04	0.312	423 726	360	1.18
	Mumbai	25 819	60 472	4.68	6.27	1.06	0.088	14 523 039	460	31.56
	$\hookrightarrow$	19 194	44 496	4.64	4.71	1.06	0.091	11 792 239	230	51.27
	New Delhi	11 423	28 464	4.98	2.43	1.07	0.060	1 203 942	161	7.46
	Osaka	49 712	133 235	5.36	8.34	1.03	0.236	2 388 944	288	8.29
	$\hookrightarrow$	16 194	40 295	4.98	3.02	1.03	0.180	992 783	103	9.63
	Phnom Penh	33 812	86 298	5.10	8.71	1.04	0.309	2 369 492	690	3.43
	$\hookrightarrow$	19 128	48 425	5.06	4.92	1.04	0.310	1 410 415	323	4.36
	Pyongyang	14 802	35 085	4.74	7.39	1.10	0.013	3 480 278	1867	1.86
	Seoul	66 528	187 328	5.63	14.08	1.04	0.009	9 645 141	606	15.91
	$\hookrightarrow$	16 187	41 680	5.15	3.72	1.05	0.022	2 189 138	166	13.18
	Shanghai	74 750	186 949	5.00	51.68	1.04	0.099	33 924 003	16 475	2.06
	$\hookrightarrow$	18 230	42 418	4.65	10.43	1.03	0.111	16 422 248	1005	16.33
	Singapore	23 835	45 596	3.83	5.80	1.08	0.005	5 959 450	1717	3.47
	$\hookrightarrow$	18 372	34 142	3.72	4.37	1.07	0.006	4 544 117	403	11.26
	Sydney	113 802	264 400	4.65	36.84	1.07	0.085	5 100 197	4315	1.18
	$\hookrightarrow$	17 692	38 426	4.34	5.76	1.07	0.126	660 591	567	1.16
	Taipei	11 985	28 123	4.69	3.34	1.07	0.129	2 542 878	269	9.42
	Tokyo	277 025	738 637	5.33	46.73	1.05	0.048	13 453 095	42 188	0.32
	$\hookrightarrow$	16 046	39 628	4.94	2.95	1.06	0.044	755 145	92	8.13
	Ulaanbaatar	31 833	79 263	4.98	12.68	1.07	0.029	1 876 392	4735	0.40
	$\hookrightarrow$	19 307	47 944	4.97	7.22	1.07	0.051	1 453 462	923	1.57
EU	**Amsterdam**	11 817	27 070	4.58	2.61	1.07	0.083	818 407	219	3.73
	Athens	8690	17 901	4.12	1.14	1.01	0.070	613 633	38	16.11
	Barcelona	13 439	25 229	3.75	2.49	1.05	0.099	2 463 690	146	16.82
	Berlin	28 040	73 144	5.22	10.62	1.04	0.011	3 524 738	890	3.96
	$\hookrightarrow$	19 050	48 300	5.07	6.84	1.03	0.009	2 656 218	464	5.71
	Budapest	24 051	63 171	5.25	7.95	1.03	0.051	1 835 722	525	3.49
	$\hookrightarrow$	19 239	50 096	5.21	6.15	1.03	0.055	1 544 233	320	4.81
	Copenhagen	7797	19 539	5.01	1.98	1.04	0.027	764 718	100	7.61
	Dublin	11 487	26 597	4.63	2.48	1.06	0.026	554 085	118	4.67
	Glasgow	16 234	38 201	4.71	3.65	1.08	0.045	582 972	176	3.31
	Helsinki	9615	20 827	4.33	2.54	1.06	0.011	640 938	717	0.89
	Kiev	9844	23 193	4.71	4.44	1.05	0.017	2 552 854	826	3.09
	Lisbon	10 100	20 647	4.09	1.84	1.07	0.020	564 066	86	6.50
	London	128 283	299 812	4.67	28.89	1.06	0.015	9 734 682	1595	6.10

Continued on next page

Table 3: Overview of the first 100 city set used in this study, as chosen by [Boe19b].

Region	City	n	m	$\overline{k}$	L (10^6m)	ς	ϕ	p_{GHSL} (inh.)	A (km^2)	ρ $\left(\frac{10^3\text{inh.}}{\text{km}^2}\right)$
	↪	18 558	42 377	4.57	3.38	1.05	0.043	1 670 052	125	13.31
	Madrid	30 844	61 149	3.97	6.10	1.05	0.020	3 797 206	604	6.28
	↪	19 016	36 180	3.81	3.84	1.05	0.022	2 455 449	208	11.75
	Moscow	17 311	35 875	4.14	8.05	1.05	0.006	12 023 201	1029	11.68
	Munich	14 083	36 387	5.17	4.65	1.04	0.078	1 552 833	310	5.00
	Oslo	8245	18 754	4.55	3.00	1.11	0.006	708 820	480	1.48
	Paris	9612	18 599	3.87	1.81	1.02	0.012	2 322 862	105	22.06
	Prague	21 466	49 395	4.60	5.76	1.06	0.049	1 327 193	495	2.68
	↪	19 462	44 367	4.56	5.20	1.06	0.052	1 268 356	370	3.42
	Reykjavik	5276	10 842	4.11	1.04	1.06	0.058	104 272	244	0.43
	Rome	43 079	89 459	4.15	11.20	1.07	0.005	2 706 949	1285	2.10
	↪	18 903	38 705	4.10	5.24	1.07	0.010	1 052 128	455	2.31
	Sarajevo	4362	9783	4.49	1.17	1.10	0.019	196 713	73	2.66
	Stockholm	13 710	31 749	4.63	3.52	1.09	0.006	1 022 888	215	4.74
	Venice (Mestre)	5922	12 134	4.10	1.33	1.07	0.055	256 643	416	0.62
	Vienna	16 090	35 907	4.46	4.53	1.04	0.051	1 932 893	414	4.66
	Warsaw	19 262	43 966	4.57	6.02	1.04	0.032	1 849 553	516	3.58
LatAm	**Bogota**	59 687	149 426	5.01	10.98	1.04	0.032	8 899 793	392	22.69
	↪	18 824	44 024	4.68	3.71	1.04	0.176	3 194 973	131	24.32
	Buenos Aires	17 843	37 539	4.21	3.99	1.01	0.147	2 711 340	205	13.20
	Caracas	16 456	35 950	4.37	5.72	1.18	0.018	2 668 989	775	3.44
	Havana	23 123	62 196	5.38	7.27	1.04	0.031	2 078 137	1944	1.07
	↪	19 477	52 806	5.42	6.32	1.04	0.032	1 863 787	602	3.09
	Lima	144 967	387 549	5.35	32.14	1.05	0.006	10 924 814	2847	3.84
	↪	18 127	45 384	5.01	4.03	1.04	0.084	1 951 204	169	11.48
	Mexico City	125 091	294 838	4.71	24.56	1.05	0.137	7 649 332	1493	5.12
	↪	17 799	37 052	4.16	3.14	1.03	0.229	1 137 806	132	8.61
	Port au Prince	15 218	37 641	4.95	4.77	1.11	0.016	1 481 683	727	2.04
	Rio de Janeiro	70 736	171 153	4.84	16.91	1.06	0.014	6 768 933	1201	5.63
	↪	17 873	42 827	4.79	4.10	1.04	0.017	1 690 587	243	6.94
	Sao Paulo	121 498	302 351	4.98	29.37	1.05	0.002	11 858 950	1523	7.79
	↪	19 100	47 153	4.94	5.31	1.07	0.005	1 565 644	299	5.23
MEA	**Baghdad**	72 520	199 676	5.51	19.04	1.03	0.065	6 338 692	861	7.36
	↪	16 735	42 286	5.05	4.37	1.04	0.028	2 064 143	181	11.34
	Beirut	3765	7445	3.95	0.56	1.02	0.200	354 208	21	16.49
	Cairo	134 086	318 976	4.76	24.00	1.05	0.043	9 149 031	3002	3.05
	↪	17 650	34 148	3.87	6.08	1.07	0.067	344 396	1262	0.27
	Cape Town	79 864	204 966	5.13	22.07	1.10	0.024	5 052 916	2454	2.06
	↪	18 004	44 566	4.95	5.95	1.09	0.052	926 442	646	1.43
	Casablanca	35 680	95 143	5.33	6.30	1.04	0.113	3 387 477	214	15.77
	↪	17 799	45 994	5.17	3.04	1.04	0.077	1 343 586	93	14.33
	Damascus	9087	21 521	4.74	2.24	1.07	0.049	2 160 242	116	18.51
	Dubai	56 428	114 581	4.06	16.05	1.07	0.028	3 122 371	5905	0.53
	↪	17 272	32 314	3.74	6.24	1.07	0.017	574 925	1185	0.49
	Istanbul	191 502	510 182	5.33	49.28	1.07	0.007	14 243 965	11 281	1.26
	↪	16 291	37 918	4.66	5.15	1.10	0.005	1 409 086	524	2.68
	Jerusalem	8210	16 299	3.97	1.93	1.11	0.009	1 253 649	125	9.97
	Johannesburg	81 413	208 226	5.12	25.52	1.09	0.020	6 409 611	1644	3.90
	↪	17 678	43 513	4.92	5.88	1.07	0.027	1 475 380	358	4.11
	Lagos	1591	3676	4.62	0.40	1.06	0.058	119 799	20	5.93
	Mogadishu	15 313	49 563	6.47	3.83	1.03	0.282	3 867 823	1259	3.07
	Nairobi	37 142	90 543	4.88	9.73	1.07	0.019	5 838 242	729	8.00
	↪	18 697	44 678	4.78	4.62	1.07	0.020	4 476 584	257	17.40
	Tehran	107 288	219 061	4.08	16.27	1.05	0.130	7 294 182	629	11.59
	↪	18 134	34 834	3.84	2.69	1.04	0.153	1 671 360	101	16.45
NAM	**Atlanta**	12 796	33 391	5.22	5.17	1.07	0.320	517 627	348	1.49
	Baltimore	12 590	32 117	5.10	3.82	1.03	0.225	628 695	238	2.64
	Boston	10 965	25 154	4.59	2.55	1.04	0.025	613 869	246	2.49
	Charlotte	31 864	73 916	4.64	10.74	1.07	0.002	829 529	783	1.06
	↪	19 108	45 151	4.73	6.87	1.06	0.007	531 272	475	1.12
	Chicago	28 662	76 092	5.31	10.39	1.01	0.900	2 640 668	607	4.35
	↪	19 084	49 787	5.22	6.90	1.01	0.901	1 706 294	367	4.65
	Cleveland	8955	24 638	5.50	3.77	1.03	0.481	365 347	213	1.71
	Dallas	36 422	92 865	5.10	13.31	1.04	0.308	1 472 292	998	1.47
	↪	18 454	46 899	5.08	6.49	1.03	0.236	686 120	388	1.77
	Denver	17 259	49 360	5.72	6.77	1.03	0.680	675 848	401	1.68

Continued on next page

Table 3: Overview of the first 100 city set used in this study, as chosen by [Boe19b].

Region	City	n	m	$\overline{k}$	L (10^6m)	ς	ϕ	p_{GHSL} (inh.)	A (km^2)	ρ $\left(\frac{10^3\text{inh.}}{\text{km}^2}\right)$
	Detroit	20 793	59 718	5.74	8.41	1.01	0.584	658 243	370	1.78
	↪	19 660	57 010	5.80	8.05	1.01	0.570	648 677	344	1.88
	Honolulu	6312	15 140	4.80	2.11	1.07	0.029	404 124	225	1.79
	Houston	63 086	157 686	5.00	21.70	1.04	0.460	2 780 403	1651	1.68
	↪	16 809	40 159	4.78	5.72	1.03	0.607	692 999	306	2.26
	Las Vegas	68 220	160 177	4.70	19.83	1.06	0.616	2 451 129	1381	1.77
	↪	17 734	41 709	4.70	5.99	1.05	0.689	857 744	348	2.46
	Los Angeles	174 591	461 349	5.28	77.18	1.05	0.355	10 131 722	12 294	0.82
	↪	18 167	45 855	5.05	11.09	1.07	0.399	621 824	2581	0.24
	Manhattan	4576	9852	4.31	1.18	1.02	0.662	1 658 451	87	18.99
	Miami	8535	22 733	5.33	2.49	1.02	0.740	401 627	143	2.81
	Minneapolis	7793	23 678	6.08	3.38	1.02	0.741	375 276	148	2.52
	Montreal	25 298	64 796	5.12	8.74	1.07	0.130	1 972 042	625	3.16
	↪	18 782	46 544	4.96	6.28	1.05	0.216	1 625 328	362	4.48
	New Orleans	15 390	40 012	5.20	4.64	1.03	0.131	366 732	912	0.40
	Orlando	7573	18 346	4.85	2.58	1.06	0.489	304 166	288	1.05
	Philadelphia	24 983	61 623	4.93	6.74	1.03	0.309	1 501 334	368	4.07
	↪	19 130	46 073	4.82	4.87	1.02	0.347	1 176 093	228	5.15
	Phoenix	48 087	123 004	5.12	16.77	1.07	0.594	1 872 464	1346	1.39
	↪	17 971	46 315	5.15	6.78	1.05	0.718	792 393	390	2.03
	Pittsburgh	9822	25 533	5.20	3.27	1.05	0.019	309 714	161	1.92
	Portland	20 349	57 325	5.63	6.82	1.04	0.680	685 184	374	1.83
	↪	19 904	56 248	5.65	6.68	1.04	0.689	671 514	306	2.19
	San Francisco	9585	26 649	5.56	3.10	1.03	0.281	823 489	600	1.37
	Seattle	19 088	50 335	5.27	5.55	1.03	0.597	710 391	373	1.90
	St Louis	8932	24 282	5.44	3.22	1.03	0.270	312 467	171	1.83
	Toronto	27 352	73 018	5.34	11.04	1.09	0.479	2 860 231	664	4.30
	↪	17 916	46 576	5.20	7.32	1.09	0.453	1 925 607	420	4.58
	Vancouver	7714	22 864	5.93	2.83	1.02	0.732	693 480	136	5.07
	Washington	9992	26 887	5.38	3.24	1.03	0.384	701 524	177	3.96

Table 4: Shorthand names for the regions of the german study cities in Table 5.

Shorthand	**City**
BW	Baden-Württemberg
BY	Bavaria (Free State)
BE	Berlin
BB	Brandenburg
HB	Bremen (Hanseatic City)
HH	Hamburg (Hanseatic City)
HE	Hesse
MV	Mecklenburg-Western Pomerania
NI	Lower Saxony
NW	North Rhine-Westphalia
RP	Rhineland-Palatinate
SL	Saarland
SN	Saxony (Free State)
ST	Saxony-Anhalt
SH	Schleswig-Holstein
TH	Thuringia (Free State)

Table 5: Overview of the 80 most populated German cities (*Großstädte* as by > 100 000 inhabitants) by 2021 census [Sta22]. For each city, general stats are listed: number of nodes n and number of edges m in the OSM graph, average node degree $\overline{k}$, total edge length L, average circuity ς, street orientation order ϕ, nominal value of the population approximation p_{GHSL} using [SFM23], city area A, and population density ρ. For the reduced graphs, the summarizing statistics are listed under the respective city, marked with "↪". This only pertains Berlin and Hamburg.

Reg.	City	n	m	$\overline{k}$	L 10^6m	ς	ϕ	p_{GHSL} (inh.)	A (km^2)	ρ $\left(\frac{10^3\text{inh.}}{\text{km}^2}\right)$
BW	**Freiburg im Breisgau**	3803	8821	4.64	1.14	1.07	0.043	252 070	152	1.65
	Heidelberg	2844	6666	4.69	0.82	1.07	0.124	154 854	108	1.42
	Heilbronn	2639	6599	5.00	0.79	1.07	0.112	116 836	99	1.17
	Karlsruhe	5200	12 410	4.77	1.61	1.07	0.038	321 957	173	1.86
	Mannheim	6160	14 423	4.68	1.60	1.07	0.028	331 411	144	2.29
	Pforzheim	2845	7068	4.97	0.89	1.07	0.031	114 279	97	1.17
	Reutlingen	2659	6696	5.04	0.80	1.08	0.013	121 992	86	1.40
	Stuttgart	9128	21 508	4.71	2.61	1.06	0.011	608 298	207	2.94
	Ulm	3451	8055	4.67	0.94	1.08	0.025	117 743	118	0.99
BY	**Augsburg**	4778	12 256	5.13	1.40	1.06	0.073	284 132	146	1.94
	Erlangen	2674	6491	4.85	0.80	1.07	0.115	126 349	77	1.64
	Fürth	2137	5048	4.72	0.66	1.06	0.023	147 272	63	2.33
	Ingolstadt	3592	9337	5.20	1.15	1.08	0.046	124 418	133	0.93
	Munich	14 083	36 387	5.17	4.65	1.04	0.078	1 552 833	310	5.00
	Nuremberg	8061	18 952	4.70	2.24	1.06	0.016	499 332	186	2.67
	Regensburg	2873	6761	4.71	0.91	1.06	0.080	151 635	80	1.88
	Würzburg	2814	6754	4.80	0.90	1.07	0.017	128 355	87	1.46
BE	**Berlin**	28 040	73 144	5.22	10.62	1.04	0.011	3 524 738	890	3.96
	↪	19 050	48 300	5.07	6.84	1.03	0.009	2 656 218	464	5.71
BB	**Potsdam**	2682	6638	4.95	0.99	1.07	0.033	197 204	188	1.05
HB	**Bremen**	8847	20 240	4.58	2.91	1.07	0.019	569 530	326	1.75
	Bremerhaven	2217	5791	5.22	0.82	1.06	0.086	113 689	93	1.22
HH	**Hamburg**	21 866	52 501	4.80	7.53	1.07	0.019	1 761 088	979	1.80
	↪	19 841	47 327	4.77	6.71	1.07	0.017	1 635 324	553	2.96
HE	**Darmstadt**	2482	6208	5.00	0.79	1.05	0.134	143 254	121	1.17
	Frankfurt am Main	9464	20 104	4.25	2.44	1.06	0.025	821 447	248	3.31
	Kassel	3941	9740	4.94	1.23	1.06	0.045	195 841	106	1.84
	Offenbach am Main	1582	3861	4.88	0.45	1.04	0.090	109 759	44	2.45
	Wiesbaden	4806	11 227	4.67	1.47	1.06	0.017	297 597	203	1.46
NI	**Braunschweig**	5175	12 065	4.66	1.59	1.08	0.084	231 285	192	1.20
	Göttingen	2586	5979	4.62	0.73	1.07	0.117	124 678	116	1.07
	Hanover (Hannover)	7556	18 695	4.95	2.44	1.06	0.061	536 017	203	2.63
	Hildesheim	2594	6132	4.73	0.74	1.08	0.050	108 481	92	1.18
	Oldenburg	3714	9247	4.98	1.27	1.08	0.016	149 219	103	1.45
	Osnabrück	3790	9125	4.82	1.33	1.06	0.009	148 963	119	1.24
	Salzgitter	2693	6308	4.68	1.06	1.08	0.034	95 014	224	0.42
	Wolfsburg	3896	9042	4.64	1.17	1.10	0.067	114 474	204	0.56
MV	**Rostock**	3832	8877	4.63	1.18	1.09	0.057	180 835	181	1.00
NW	**Aachen**	3838	9060	4.72	1.38	1.06	0.022	243 387	160	1.51
	Bergisch Gladbach	2456	5674	4.62	0.81	1.08	0.023	116 460	83	1.40
	Bielefeld	7005	16 843	4.81	2.60	1.07	0.005	333 409	258	1.29
	Bochum	6996	16 208	4.63	2.01	1.07	0.031	357 434	145	2.45
	Bonn	5804	13 743	4.74	1.62	1.06	0.033	298 244	141	2.11
	Bottrop	2594	6401	4.94	0.93	1.06	0.023	120 419	100	1.20
	Cologne (Köln)	16 336	36 066	4.42	4.30	1.05	0.013	1 171 662	404	2.89
	Dortmund	11 562	27 160	4.70	3.47	1.06	0.076	597 406	280	2.13
	Duisburg	8187	20 051	4.90	2.52	1.05	0.017	541 060	232	2.32
	Düsseldorf	8755	19 833	4.53	2.33	1.06	0.011	629 943	217	2.90
	Essen	11 046	25 677	4.65	2.94	1.06	0.012	566 901	210	2.70
	Gelsenkirchen	4400	10 687	4.86	1.36	1.05	0.069	268 021	104	2.55
	Gütersloh	3372	8165	4.84	1.13	1.06	0.045	89 440	112	0.80
	Hagen	3733	8802	4.72	1.32	1.09	0.023	192 985	160	1.20
	Hamm	4359	10 864	4.98	1.80	1.06	0.050	171 828	226	0.76
	Herne	2614	6204	4.75	0.75	1.06	0.028	164 314	51	3.20

Continued on next page

Table 5: Overview of the 80 most populated German cities by 2021 census [Sta22].

Reg.	City	n	m	$\overline{k}$	L (10^6m)	ς	ϕ	p_{GHSL} (inh.)	A (km^2)	ρ $\left(\frac{10^3\text{inh.}}{\text{km}^2}\right)$
	Krefeld	4333	10 578	4.88	1.49	1.06	0.083	228 622	137	1.66
	Leverkusen	3232	7498	4.64	0.95	1.06	0.019	151 995	78	1.93
	Moers	2895	7016	4.85	0.89	1.07	0.046	107 912	67	1.60
	Mönchengladbach	5641	13 527	4.80	1.75	1.06	0.006	267 545	170	1.57
	Mülheim an der Ruhr	3097	7097	4.58	0.93	1.06	0.006	173 668	91	1.90
	Münster	6918	16 314	4.72	2.46	1.07	0.037	341 446	303	1.13
	Neuss	3558	8193	4.61	0.98	1.08	0.016	169 732	99	1.71
	Oberhausen	3660	8894	4.86	1.09	1.06	0.012	210 994	77	2.74
	Paderborn	1949	4616	4.74	0.56	1.07	0.033	93 098	44	2.09
	Recklinghausen	2728	6638	4.87	0.87	1.06	0.109	118 133	66	1.78
	Remscheid	1281	2965	4.63	0.38	1.09	0.005	55 548	32	1.73
	Siegen	3140	7293	4.65	1.09	1.10	0.004	111 237	114	0.97
	Solingen	3121	7412	4.75	1.00	1.08	0.010	158 327	89	1.77
	Wuppertal	5872	13 333	4.54	1.81	1.08	0.019	349 787	168	2.08
RP	**Koblenz**	2792	6173	4.42	0.84	1.08	0.012	121 517	105	1.15
	Ludwigshafen am Rhein	3976	9764	4.91	0.93	1.05	0.047	146 645	77	1.89
	Mainz	4304	9901	4.60	1.06	1.07	0.031	192 033	97	1.96
	Trier	2752	6261	4.55	0.77	1.08	0.023	124 173	117	1.06
SL	**Saarbrücken**	4331	9555	4.41	1.33	1.08	0.003	185 580	167	1.11
SN	**Chemnitz**	4463	10 658	4.78	1.76	1.07	0.013	281 487	220	1.27
	Dresden	8166	20 675	5.06	2.90	1.05	0.014	604 470	328	1.84
	Leipzig	8903	22 427	5.04	2.94	1.05	0.048	587 300	297	1.97
ST	**Halle (Saale)**	4325	10 471	4.84	1.30	1.07	0.098	226 774	135	1.67
	Magdeburg	4483	11 032	4.92	1.59	1.07	0.098	239 762	201	1.19
SH	**Kiel**	3713	8561	4.61	1.17	1.06	0.008	236 948	118	2.00
	Lübeck	3508	8349	4.76	1.37	1.08	0.015	214 359	213	1.00
TH	**Erfurt**	4805	11 402	4.75	1.48	1.07	0.048	229 810	269	0.85
	Jena	2231	5489	4.92	0.73	1.09	0.017	96 349	114	0.84